The molecular sieves CoAlPO-36 and MnAlPO-36 are extremely versatile catalysts.

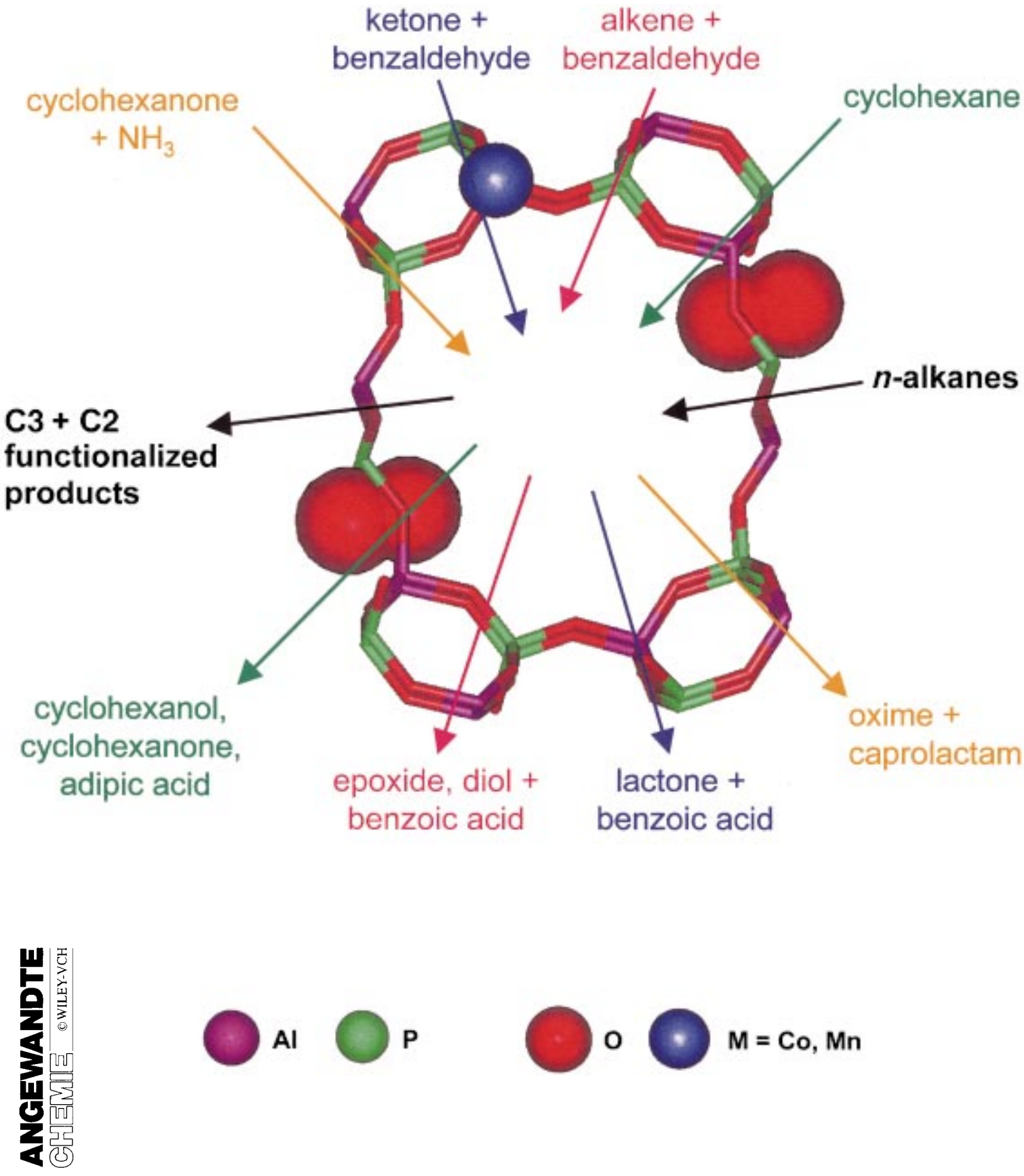

Design, Synthesis, and In Situ Characterization of New Solid Catalysts**

John Meurig Thomas*

Two distinct strategies exist for the design of solid catalysts. One adopts the reductionist approach, whereby the individual steps involved in overall catalytic conversion—the processes of adsorption, surface rearrangement, desorption, and transport of reactants and products to or from exterior surfaces—are analyzed in great detail so that the resulting information may be used to interpret the behavior of existing catalysts with a view to generating superior ones. The other focuses on the precise atomic architecture of the catalytically active site—its determination under operating conditions, its assembly and scope for its modification, the subtleties of its mode of action—which leads to the design of new catalysts capable of facilitating conversions that have hitherto proved either impossible or very difficult to effect. The present article deals exclusively with the second strategy, which is an integrated one. It seeks to demonstrate that, by adopting the principles and practices of solid-state chemistry (augmented by lessons derived from enzymology, and computational and organometallic chemistry) a wide range of new catalysts may be designed that, inter alia, effect regioselective, shape-selective, and enantioselective conversions, as well as producing high-performance catalysts for the isomerization and hydrogenation of alkenes. All the new catalysts described herein are either microporous or mesoporous solids. These have the dual advantages of possessing large surface areas and being amenable to delicate structural and compositional variation either during preparation or subsequently by anchoring on to their inner walls well-defined, isolated, and accessible molecular units that are heterogenized versions of homogeneous catalysts. The specific catalysts described are those designed for the following low-temperature reactions: the aerobic oxyfunctionalization of terminal groups in linear alkanes; low-temperature selective aerobic oxidation of cyclohexane; the radical-free (as well as free-radical) epoxidations of alkenes; Baeyer–Villiger oxidations of ketones to lactones; the preferential dehydrations of methanol to yield ethene and propene; and enantioselective allylic amination.

Keywords: catalysts · heterogeneous catalysis · microporosity · solid-state chemistry · synthetic methods

1. Introduction

It is clear that Karl Ziegler changed the world into which he was born. Polymers, in all their rich diversity of forms, nowadays profoundly influence our daily lives. But his scientific legacy in fields other than those of Ziegler catalysts and Ziegler–Natta polymers is also of high significance. For example, his "Aufbau method" of producing detergents, his demonstration of the reality of free-radical autoxidation reactions, as well as the elegance of his use of radical scavengers to terminate chain processes are all facets of his intellectual percipience and the penetrating power of his scientific work.

Listening to and reading the accounts of the early life, temperament, and religious conviction of Karl Ziegler, and recognizing the oft-repeated assertion that he viewed pure and applied research as a continuum, and that he also had unquenchable intellectual curiosity and an omnivorous scientific appetite, comparisons can be drawn between him and one of my scientific heros, Michael Faraday—who, like Ziegler, was of puritanical disposition. This is not the place to expatiate upon the admirable qualities of Faraday[1]—held by many to be one of the greatest ever Englishmen—except to note that, like Ziegler, he left the world a very different place from that which he himself had inherited. Political theorists and philosophers sometimes argue—and how right they are—that "interpreting the world" is secondary to the much more demanding task of changing it.[2]

[*] Prof. Dr. Sir J. M. Thomas
Davy–Faraday Research Laboratory
Royal Institution of Great Britain
London W1X4BS (UK)
Fax: (+44) 171-629-3569
E-mail: dawn@ri.ac.uk
and
Department of Materials Science, University of Cambridge
Cambridge CB23QY (UK)

[**] The majority of the contents of this article was presented at the Karl Ziegler Centenary Celebrations, Mülheim an der Ruhr, on 27 November, 1998. Other parts were included in the Linus Pauling Lecture at the California Institute of Technology, on March 30, 1999.

  1433-7851/99/3824-3589 $ 17.50+.50/0

2. The World Of Catalysis

Although the word catalysis was not coined until 1835 (by Berzelius)[6] the phenomenon itself was known to the ancients. Aristotle describes it in his treatise on meteorology, the Arab alchemist, Jabir, in the eighth century A.D., demonstrated how a mineral acid could catalyze the conversion of alcohol to ether, and it has been the backbone of the chemical industry for nearly two hundred years.

In designing and synthesizing new solid inorganic catalysts the aims are to maximize surface area, activity, selectivity, longevity, and durability. Unfortunately, few if any of the marvellous new tools, techniques, and avenues that are available to the organic chemist and molecular biologist—namely site-directed mutagenesis,[7, 8] chemically modified mutant enzymes,[9] the exploitation of non-natural amino acids in an expanded genetic code,[10] catalytic antibodies[11] (which turn to advantage the teeming multiplicity and subtleties of the immune system), design by directed (Darwinian) evolution[12, 13]—will ever be capable of being incorporated directly into the inorganic world, which is destined, almost by definition, to be impervious to the charms and advantages of animate life.

All is not lost, however, for there are real prospects, adumbrated in this review, that the technical virtuosity inherent in the development of a vast range of inorganic homogeneous catalysts, especially organometallic ones,[14, 15] may be simulated and extended by adroit design, synthesis, and manipulation of new inorganic solids. The key lies in producing materials with large surface areas, the surface composition, structure, and atomic architecture of which are incontrovertably characterized under operating conditions. Before we proceed to describe how this is done, it is first instructive to enumerate what the desiderata of these new, engineered heterogeneous catalysts are. These desiderata are shown in Table 1, the format of which owes much to the elegant animadversions of Cornils and Herrmann[15] on the "two cultures" that are so conspicuously ingrained in the minds of those who dwell on the strengths and weaknesses of homogeneous and heterogeneous catalysis.

Table 1. Desiderata for new engineered heterogeneous catalysts.

Apart from possessing high activity, high selectivity, long lifetimes, and durability, other desiderata are:

- the capability of operating under mild conditions that are environmentally and economically efficient
- freedom from restrictions imposed by diffusional considerations
- possession of isolated, well-defined (single site) active centers, the atomic architecture of which may be delicately modified
- capability of yielding a detailed mechanistic understanding of catalytic action (for example, by strategies such as that summarized in Figure 4).

Microporous and mesoporous solid catalysts are potentially, and in very many cases (as described in this article), capable of achieving all these desiderata.

At first sight, it would appear that, in seeking to create new, solids with large surface areas that are to be endowed with marked catalytic activity, the most propitious path to take is that which leads to the production of monodisperse particles of colloidal dimension. The dispersion D, defined as the fraction of the total number n of atoms in a particle that are at the surface (Figure 1), is clearly higher the smaller the value of n. Is it not sensible, therefore, if our aim is to maximize activity—given that we have chosen the right material for its intrinsic activity in the first instance—to work towards convenient, easy methods of producing highly comminuted solids, the diameter of the individual particles of which should be in the 10–20 Å diameter range? The answer is not a simple yes, because small particles have melting points that are far below those of their bulk analogues. This result is because the amplitudes of the motion of atoms at a surface far exceed

John Meurig Thomas is Professor of Chemistry and Former Director of the Davy Faraday Research Laboratory, The Royal Institution of Great Britain, London, and Master of Peterhouse and Honorary Research Fellow, Department of Materials Science, University of Cambridge. For nine years he was Head of the Department of Physical Chemistry, University of Cambridge and for twenty years prior to that he was at the University of Wales (Bangor and Aberystwyth), where he graduated (Swansea) in 1954. He is one of the founders of modern solid-state chemistry; and for his contributions to it, to surface and materials chemistry, and to heterogeneous catalysis he has received numerous national and international awards. These include the Davy Medal of the Royal Society, the Faraday Medal of the Royal Society of Chemistry, the Willard Gibbs Gold Medal of the American Chemical Society, the Messel Gold Medal of the Society of Chemical Industry, and the Semenov Centenary Medal of the Russian Academy of Sciences. Earlier this year he became the first recipient of the American Chemical Society Award for Creative Research in Homogeneous and Heterogeneous Catalysts for his develpment of in situ methods in catalysis and for laying the foundations of the molecular design of catalytically active centers. He is the author of over 850 publications, ten patents, and many books including (together with W. J. Thomas) Heterogeneous Catalyses: Principles and Practice, Wiley-VCH, Weinheim, ***1997****, and Michael Faraday and The Royal Institution: The Genius of Man and Place, Institute of Physics, Bristol,* ***1991****. His 1987 series of Royal Institution Christmas Lectures on Crystals was broadcast nationally by the BBC. He is the founding co-editor-in chief of Catalysis Letters, Topics in Catalysis*, and *Current Opinion in Solid State and Materials Science. He was knighted in 1991 for his services to chemistry and the popularization of science.*

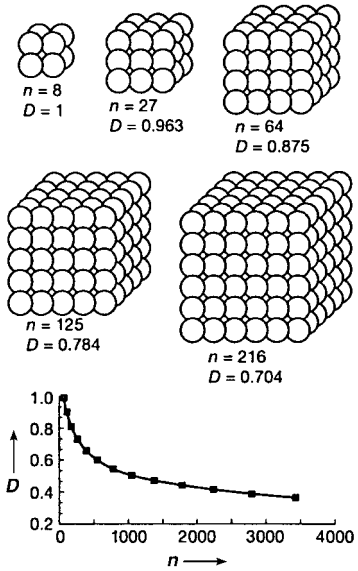

Figure 1. One way to increase the fraction D of surface-situated atoms in a crystal is to prepare it in nanoparticulate form. The smaller the particle size, the larger is this fraction (n = total number of atoms in the crystal).[16] Another method (see Figure 2) is by producing the crystal in such a porous state that D is close to unity even for micron-sized or even larger crystals.

those of atoms in the bulk.[17] The mobility of small particles is therefore large; consequently they are prone to coalesce and sinter, thereby greatly decreasing the total surface area. If, however, nanoparticles of diameter 10–20 Å can, by appropriate chemical strategies (see Figures 46 and 48), be securely anchored to the atoms of the substratum upon which they have been laid down, then indeed the answer to the question posed earlier is a resounding yes for so-called structure-insensitive reactions.

Although there are certain, high-performance inorganic catalysts (such as the bimetallic ones described in Section 7.6) that are good examples of nanocrystals, the way towards creating a versatile and large family of large-area, high-performance inorganic catalysts lies elsewhere, namely by harnessing the advantages of microporous and mesoporous solids.

3. Solids With Three-Dimensional Surfaces: The Expanding Realm Of The Microporous And Mesoporous

Highly microporous or mesoporous solids such as those that possess channels, cavities, or cages with diameters in the range of 4 to 14 Å (micro) and 15 to 150 Å (meso) offer the best means for designing or modifying new inorganic heterogeneous catalysts (Figure 2). As operating catalysts it is to be noted that they:

- permit free ingress of reactant and egress of product species that have cross-sections smaller than the diameter of the pores
- offer greater scope (especially mesoporous solids) for the grafting of organometallic moieties[18–23] on to the inner surfaces of the pores. This opens ready routes for the heterogenization of homogeneous catalysts, thus capitalizing on the advantages of high activity and single-site active centers of the homogeneous category, and the robustness and ease of separation that is a feature of the heterogeneous catalysts
- open up many new strategies for shape-selective, enantioselective, and regioselective conversions

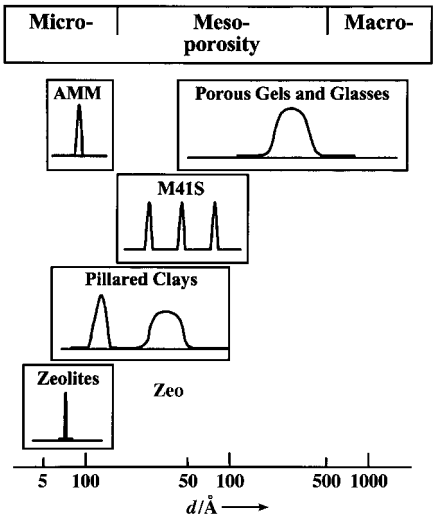

Figure 2. Solids may nowadays be routinely produced with (largely internal) surface areas that exceed 1000 $m^2 g^{-1}$. Some of these are microporous (aperture diameters from ca. 3 to 14 Å), some mesoporous (ca. 15 to 150 Å), and some macroporous. It is occasionally possible to produce solids with a bimodal pore-size distribution (of micro- and mesopores). AMM = amorphous microporous metallosilicate (W. F. Maier, I.-C. Tilgner, M. Wiedorn, H.-C. Ko, *Adv. Mater.* **1993**, *5*, 726; W. F. Maier, J. A. Martens, S. Klein, J. Heilmann, R. Parton, K. Vercruysse, P. A. Jacobs, *Angew. Chem.* **1996**, *108*, 222; *Angew. Chem. Int. Ed. Engl.* **1996**, *35*, 180); for M41S are MCM-41, MCM-48, and MCM-50 included (C. T. Kresge et al.;[52] J. C. Vartuli, J. S. Beck;[56] for pillared clays see J. M. Thomas in *Intercalation Chemistry* (Eds.: M. S. Whittingham, E. J. Jacobson), Academic Press, New York, **1982**, p. 56. (After Behrens[51])

Moreover, because they are, in essence, solids with three-dimensional surfaces, they greatly facilitate experimental procedures for their characterization. Thus, the full panoply of spectroscopic and diffraction (or other scattering) tools may be deployed[24, 25] to determine, often under in situ conditions, either the local or average structure of the solid catalyst itself, or the nature of the species undergoing conversion at its (three-dimensional) surface (Figure 3).

What is particularly convenient here is that, with this category of solid, the distinction between the model catalyst (tailored so as to facilitate retrieval, usually by the academically oriented researcher, of structural and compositional information) merges with the operational (real life) catalyst, engineered by the applied scientist so as to exhibit the best possible chemical performance.

Because of their relative ease of production and the wide range of compositional variation that they exhibit, it is possible to realize most of the catalytic desiderata enumerated in Table 1. Moreover, because the engineered catalysts described in this review have such well-defined, single-site active centers, it is also possible to synthesize soluble "fragments" of the catalysts in which the active site is placed in a

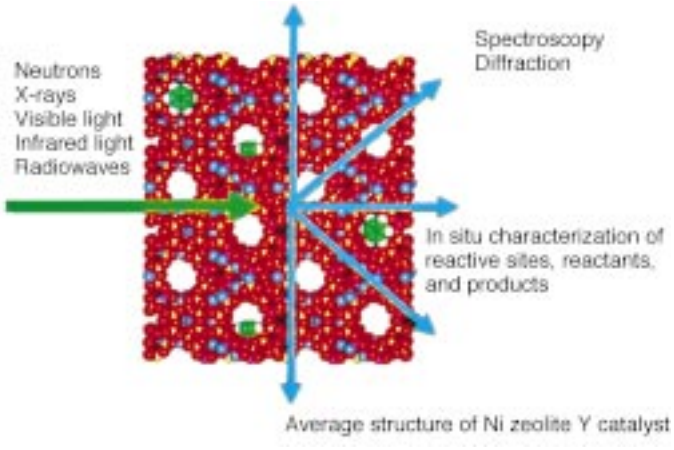

Figure 3. The detailed atomic structure of this rather complicated Ni^{2+}-ion-exchanged zeolite Y catalyst may be determined under operating conditions from a Rietveld refinement procedure of either the X-ray or neutron powder diffraction pattern. The precise atomic environment of the Ni^{2+} ions (that are the active sites for the catalytic conversion of acetylene to benzene)[26] may also be determined in situ by X-ray absorption spectroscopy. With catalysts such as this, which have three-dimensional surfaces, a wide range of both spectroscopic and diffraction methods may be used to retrieve structural and mechanistic information pertaining to the catalyst itself and the reactants that are catalytically converted at their (interior) surfaces. Specific examples are described later in the text. Red: oxygen; yellow: silicon; blue: nickel. For clarity, sodium ions are not shown.

well-defined, and controllable, atomic environment (Figure 4). This makes it possible to achieve an understanding of the factors that govern catalytic performance to a degree previously unequalled. It also paves the way to a deeper understanding of the determinants of catalytic promotion, poisoning, and inhibition.[28]

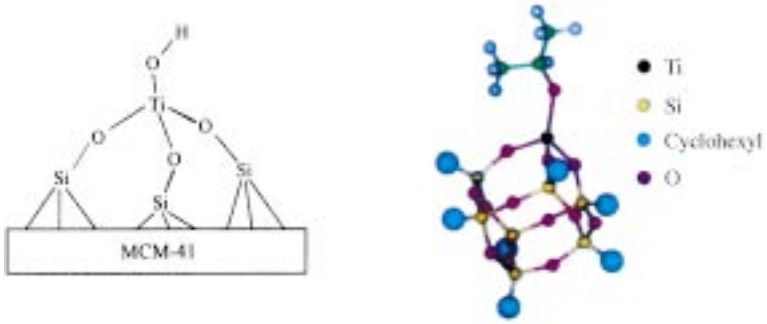

Figure 4. The in situ techniques described in this article and in ref. [27] yield the atomic architecture of active sites in heterogeneous catalysts, such as in the epoxidation of alkenes. The Ti^{IV} ions, with their pendant OH groups, are tripodally attached to the silica (or silica-germania) support (left). Titanosilsesquioxanes, such as that shown on the right, are soluble analogues of the active sites and are amenable to structural and mechanistic studies by the classical tools (NMR spectroscopy, spectrophotometry, etc.) used in studies of homogeneous catalysts.[28]

4. Rational Design Or Blind Chance: Is The Combinatorial Approach Destined To Be Invincible?

Any discussion of engineered catalysts, like any discussion of new generations of pharmaceutical or agrochemical products, nowadays tends to be dominated by the compelling immediacy of combinatorial methods[29] (first introduced by Hungarian workers in the early 1970s). The laborious methods of trial-and-error—which have served catalysis and many other fields of science so well over the last two centuries—must, it is argued, give way to more streamlined combinatorial methods of discovery. These new methods, which are an inherent feature in biological nature[30] especially in the immune system, and are used increasingly in drug design, consist essentially of three main components: 1) automated library syntheses of new candidate catalysts (using robots, for example) that are readily amenable, 2) miniaturization or microminiaturization, 3) high-throughput screening of catalytic performance. Taken altogether, these three features then lead to an ultra-rapid production of databases from which numerous key items of catalytic information pertaining, for example, to the best combination of elemental composition and atomic structure or architectures (for a given desired catalyst) may be extracted.

The first example of combinatorially prepared inorganic catalysts was reported by Hill and Gall, [31] who synthesized a library of various polyoxometalates for the aerobic oxidation of the mustard gas analogue tetrahydrothiophene from stock solutions that contained precursors such as Na_2WO_4, Na_2MoO_4, and Na_2HPO_4. Central to the combinatorial methodology is the development of an effective algorithm for the discovery of a new catalyst. This, in turn, requires a rapid and reliable method of screening (that is, of quantitatively recording the performance) of the library of assembled candidate catalysts.

It is timely to quote two highly relevant examples (highlighted on the front cover of *Angewandte Chemie*, Figure 5) of work done at Ziegler's laboratory in Mülheim. In both of these studies the enthalpy changes associated with the chemical reactions under investigation were used as a quantitative measure of catalytic activity for the purposes of rapid screening.

Maier and co-workers showed that thermal imaging is a very sensitive means of detecting activity in positional catalytic libraries that contain only about 200 μg of catalyst at each addressable position in the library.[32] Minute wells sunk into a slab of slate (chosen because of its low thermal reflectivity so as to minimize interference) were filled with sol–gel precursor solutions for so-called[33] amorphous mixed-metal oxides of different compositions, which were processed to yield an array of candidate catalysts (Figure 6). A thermal image of the whole array without substrate was stored and subsequently subtracted from the images of the array under operation. This procedure permitted Maier et al. to minimize the effect of different thermal emissivities of the catalyst wells, so that they could detect very small temperature differences associated with catalytic activity. This technique offers a fast, convenient parallel assay of quite a sizeable library of catalysts for the hydrogenation of 1-hexyne at 100 °C and for the oxidation of isooctane and toluene at 350 °C.

Reetz and co-workers[34] also demonstrated the power and utility of sensitive thermal imaging (infrared cameras and

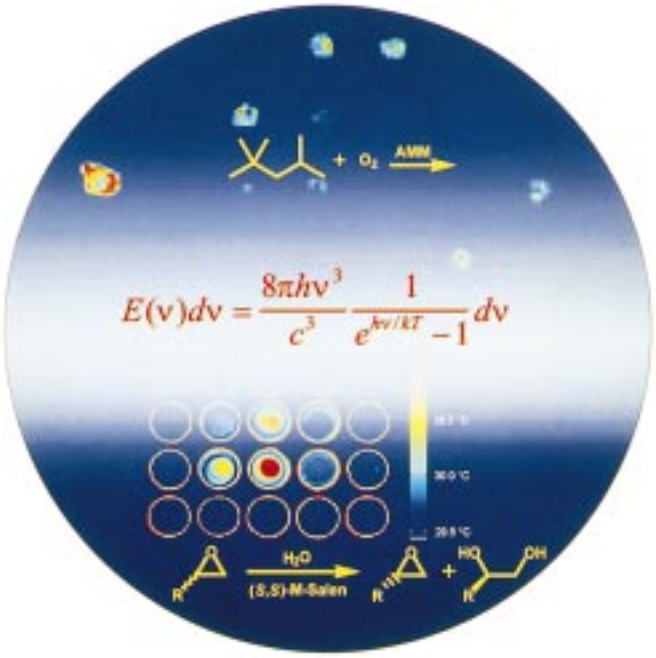

Figure 5. Visual portrayal of the combinatorial approach to the screening of a library of amorphous mixed-metal (AMM) oxides for the catalytic oxidation of isooctane[32] (top) and of enantioselective transition metal catalysts for the ring-opening hydrolysis of epoxides[34] (bottom) on the cover picture of Issue 19 of *Angewandte Chemie* in 1998. In each case, thermal imaging (implied here by the central equation) is used as a very sensitive means of detecting activity in addressable catalytic libraries.

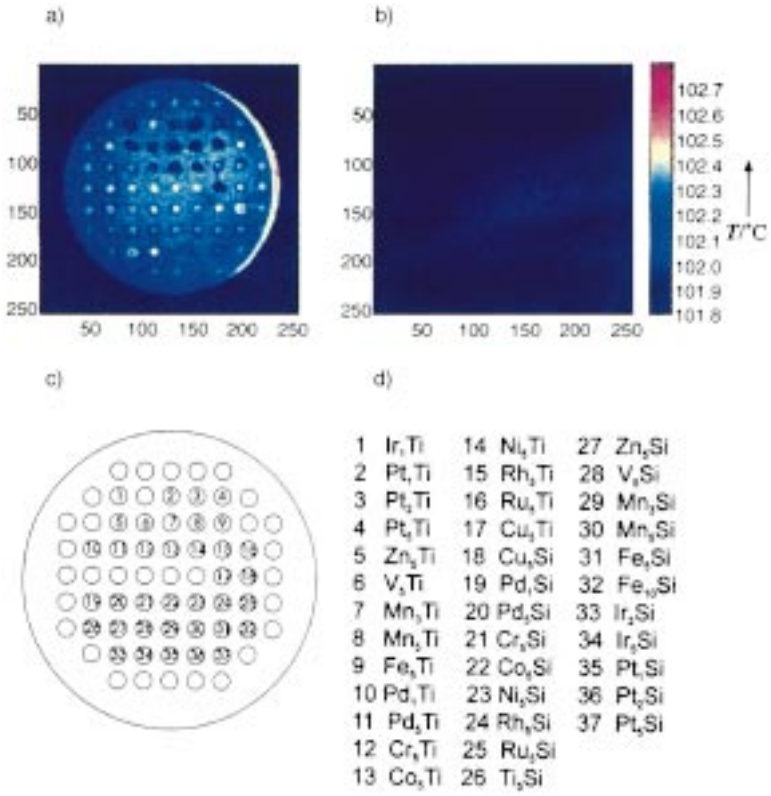

Figure 6. a) IR image of the library of catalysts without correction for emissivity; b) emissivity-corrected IR-thermographic image of the library of catalysts prior to the start of reaction (bar on right is the temperature key); c) deposition pattern of the library;[32] d) composition of the oxide catalyst spots of the library according to the AMM notation, which give the molar percentages of active metal and base metal oxides.

array detectors) to explore a library of homogeneous catalysts for the enantioselective acylation of a chiral alcohol (1-phenylethanol) that was catalyzed by immobilized lipase. They also demonstrated this approach in the enantioselective ring-opening of chiral epoxides with transition metal–salen catalysts. The array of reactants included the two different enantiomers of the substrate, for which the catalysts showed drastically different activities.

It is a relatively simple matter to devise high-throughput methods to probe catalytic selectivities as well as activities. Mallouk et al.[35] have done this in their quest for optimized alloy electrocatalysts for the electrochemical oxidation of methanol in a fuel cell; Senken[36] has done it for an array of solid catalysts on a porous support; and Weinberg et al.[37] in their high-throughput screening (and synthesis) of a combinatorial library of 120 different heterogeneous ternary alloy catalysts (based either on Rh–Pt–Cu, Rh–Pd–Cu, or Rh–Pd–Pt thin films) in the oxidation of CO by either O_2 or NO.

For solids, in which the performance (catalytic or otherwise) of the prepared composition and structure more-or-less instantaneously reaches their steady-state value at the instant of preparation, the combinatorial (blind chance) approach is a reliable means of making rapid progress in the quest for new materials. But when the catalytic performance (or other measured property) takes a substantial time before achieving its optimal value, or when it is a critical function of a time-dependent (crystallographic) structure, the combinatorial approach can be misleading at best, and unhelpful at worst (see Thomas[25] and Schlögl[38] for a selection of such examples). These deficiencies can be compounded if the solid catalysts prepared in the library of candidates exhibit varying degrees of structural abnormalities such as nonstoichiometry, antiphase boundaries, or crystallographic shear planes.[23]

In summary, therefore, it is assuredly the case that the combinatorial approach is here to stay. It will undoubtedly grow in importance, if only because it shortens the length of the cycle from synthesis to testing or re-designing and formulation. But it is not invincible. There remains immense scope for the traditional approaches that combine insight, inspiration, know-how, and various kinds of technical virtuosity.[39, 40] One only has to recall the emergence of the seminal developments of asymmetric catalysts (by Sharpless et al.[41] and others) using procedures based on straightforward and novel ligand variation around a transition metal ion center, to appreciate the power of conventional methods in homogeneous catalysis. The same can be said of numerous other designed catalysts such as the β-cyclodextrin-modified diphosphanes as ligands for supramolecular rhodium catalysts[42] and of the many examples cited by Cornils and Herrmann.[14] Likewise, in heterogeneous catalysis an eloquent illustration of the role of flair and imagination is seen in the

design[43–46] of powerful microporous catalysts (see Figures 7 and 8). Even in the field of designing new synthetic enzymes, it is not essential to opt only for biological routes such as mutagenesis. Dutton et al.[47] demonstrate the importance of flair coupled to rational design in their elegant work on so-called "maquette catalysts".

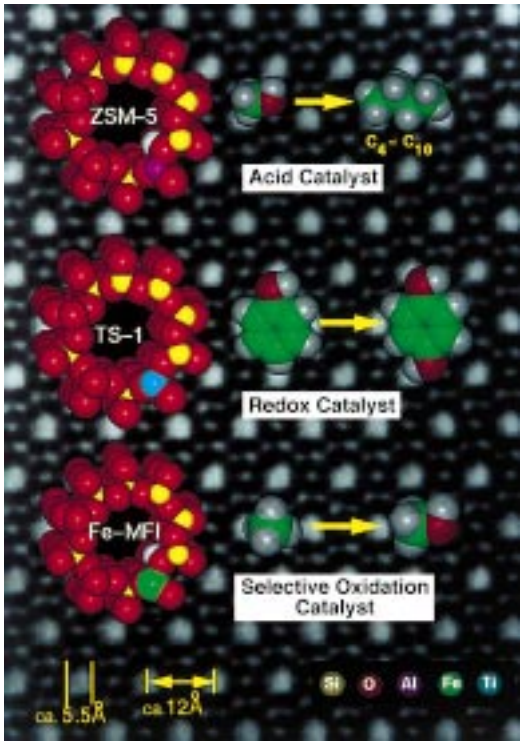

Figure 7. Superimposed on a high-resolution electron micrograph of silicalite, which has pores of diameter 5.5 Å, are computer graphic, scalar models of the pore openings of the catalysts ZSM-5[44] (top), TS-1[45] (middle), and Fe-MFI[25] (bottom) where, respectively, framework Si^{4+} ions have been isomorphously replaced by Al^{3+} (to produce a solid acid catalyst), Ti^{IV}, to produce a so-called "redox" catalyst (but which is better described, see Section 7.4.2, as a selective oxidation catalyst) and Fe^{3+}, which is promising as a catalyst for the conversion of methane into methanol.

The phenomenally successful, shape-selective, solid acid catalyst ZSM-5 arose largely from the work of Weisz and his co-workers, who were initially concerned with academic considerations relating to the acid-catalyzed dehydration of linear and branched alkanols inside the pores of model acid catalysts such as Ca^{2+} ion-exchanged zeolite A.[43, 44] It was premeditated action by researchers in the ENI Chem company,[45, 46] who focused on the aim of combining the inherent shape-selectivity of a pentasil structure (such as silicalite I, which is the pure siliceous end member of the aluminosilicate ZSM-5) and the well-known propensity of Ti^{IV} ions as an active center for selective oxidation (in the presence of H_2O_2), that led to the design of the versatile TS-1 catalyst for many commercially important selective oxidations. The same is essentially true of my own group's work described herein, and represented in part by the structures shown in Figure 8.[48]

5. Engineering Microporous And Mesoporous Catalysts

About one third of all the commonly encountered elements of the Periodic Table are nowadays capable of being incorporated into the framework structures (almost invariably in tetrahedral coordination) of the ever-growing families of micro- and mesoporous solids. In the case of microporous solids, also known as zeotypes or molecular sieves, the largest two sub-families are the aluminosilicates and aluminophosphates (known as AlPOs). These may be viewed as three-dimensional networks of corner-sharing SiO_4 and AlO_4 tetrahedra and of AlO_4 and PO_4 tetrahedra, respectively. Hetero atoms, which could be any of a wide range of di-, tri-, tetravalent, or higher value ions (typically Co^{2+}, Mg^{2+}, Mn^{2+}, B^{3+}, Ga^{3+}, Fe^{3+}, Ge^{4+}, Ti^{4+}, P^{5+}…), may be incorporated substitutionally at regular framework sites. And it is generally possible (indeed often it is the only satisfactory means) to incorporate these ions during the synthesis of the zeotype. Mesoporous solids, on the other hand, are generally easier to prepare in their pristine state (as SiO_2, TiO_2, Al_2O_3, GeO_2, SnO_2, ZrO_2, Nb_2O_5, and, quite recently, metal sulfides), and the heteroatoms which serve as the loci of catalytic action are grafted onto the inner surfaces of the mesopores after synthesis. For a summary of the various kinds of materials that fall into one of other (or both) of these two categories see refs. [25, 27, 49 – 58]. It is, however, not difficult to synthesize mesoporous solids, especially silica, with one of very many different types of heteroatom in the framework.[55, 58]

An indication of the burgeoning field of microporous solids (most of which display special catalytic activity and selectivity) may be gauged from the gallery of new materials[59–66] portrayed in Figure 8. Many of these are high-performance catalysts for such processes as skeletal isomerization of butenes[60] and the conversion of methanol to olefins.[62, 65]

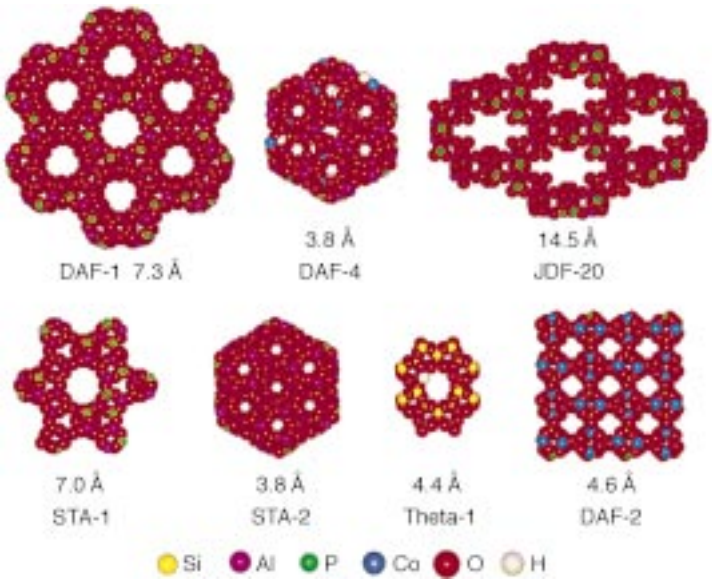

Figure 8. Projection models, to scale, of a selection of new microporous solids synthesized in recent years, usually with the aid of structure-directing templates (see Section 5). With the exception of DAF-2 and JDF-20, which tend to collapse when the template is driven away by calcining in air, all these new microporous solids are thermally robust solid catalysts.

Some, however, notably JDF-20 (Jilin-Davy-Faraday No. 20), which has the largest aperture so far recorded for a synthesized microcrystalline solid, is not particularly thermally stable. The structure collapses when the organic template used for its synthesis is driven off by thermal treatment.

In the family of mesoporous materials labeled M41S by their discoverers at the Mobil Oil Company,[52, 56] of which MCM-41 is a hexagonal mesoporous phase (and MCM-48 is a cubic phase[67]), experiment shows that, although there is good ordering of the hexagonal (or cubic) stacking of the channels themselves, comparatively little crystallographic order exists in the walls of the pores. Graphic representations of the nature of these mesoporous materials (which are also termed supramolecular-templated structures) are shown in Figure 9, and some typical high-resolution electron micrographs[68, 69] of such material are reproduced in Figure 10.

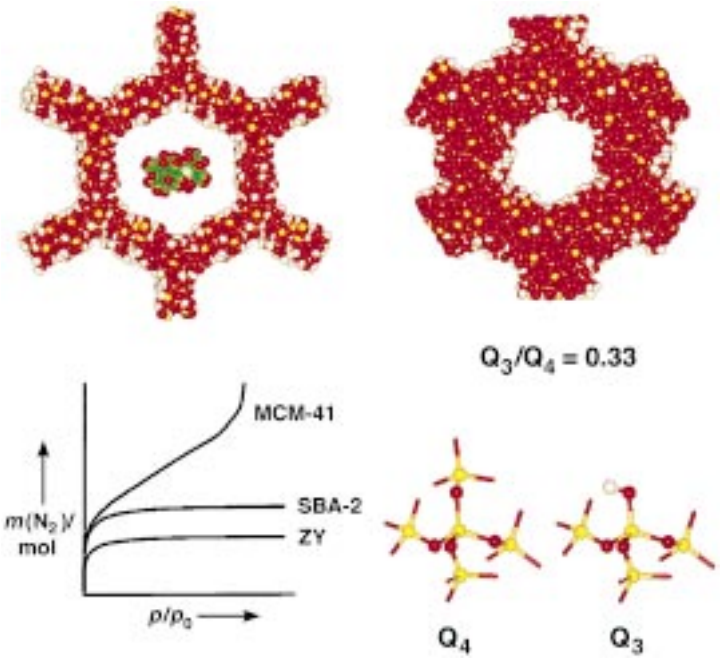

Figure 9. The MCM-41 mesoporous silicas depicted here have pore diameters of ca. 30 Å, and are easily capable of incorporating large organometallic species, such as multinuclear metal carbonylates, typically $[Ru_6C(CO)_{16}]$. Adsorption isotherms (of N_2 at 78 K) take up the shape shown in the top of the three plots (bottom left). For comparison adsorption isotherms for a zeolite Y (bottom of the three) and for SBA-2 (Santa Barbara No. 2), middle, are also shown. The top two structures are the energy-minimized ones computed by atom–atom procedures combined with molecular dynamics. (The computed ratio of Q_3/Q_4 of 0.33 for the structure at the top right is close to the value (0.40) determined from ^{29}Si MAS NMR spectroscopy).Q3 and Q4 are defined at the bottom right.

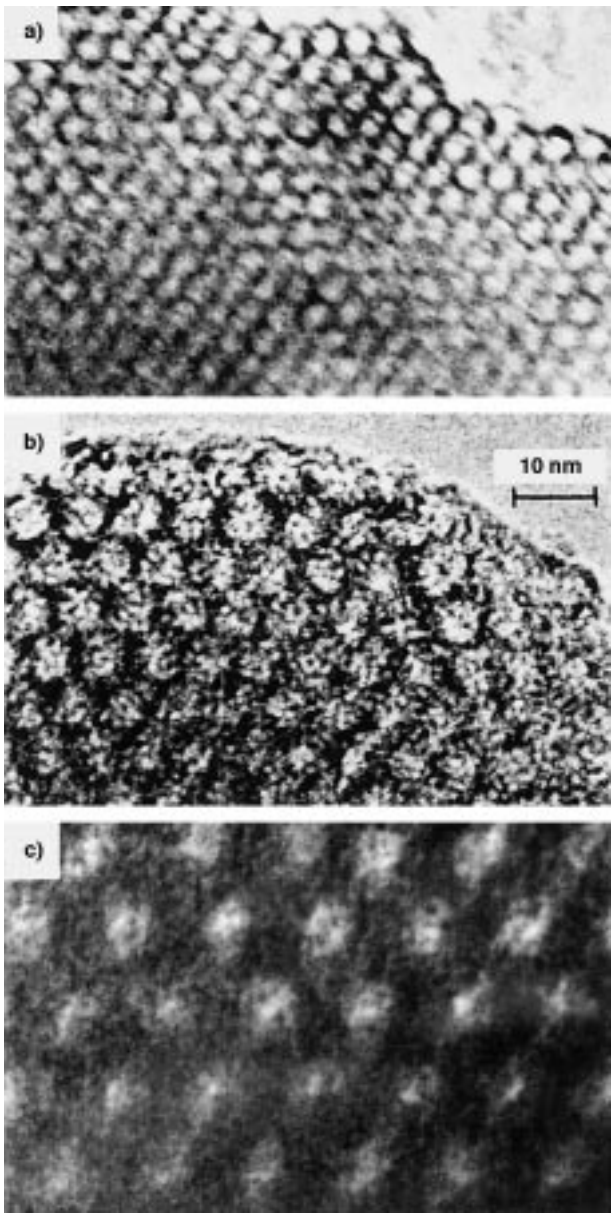

Figure 10. Depending upon the templates used, and the precise conditions of preparation, mesoporous silica belonging to the M41S family may exhibit pore diameters in excess of 100 Å and different thicknesses of pore walls.[68, 69] The inter-pore distances (center-to-center) shown here are 42, 68, and 122 Å. Well-defined cubic–hexagonal (ABC-AB), polytypic intergrowths are also frequently observed in certain types of mesoporous silica.[68]

In meeting the challenge of how to synthesize new microporous crystalline solids, two interrelated approaches may be pursued: 1) design by experiment based on intuition and accumulated chemical experience, and 2) design by computer modeling. Success in synthesizing new microporous catalysts using the first approach comes from an appropriate choice of constituents of the nutrient gel from which the templated solid crystallizes during hydrothermal treatment. Twenty years ago it became apparent that quaternized ammonium salts were ideal structure-directing template ions that favored production of the pentasil catalysts ZSM-5 and ZSM-11. In an extension of this strategy diisopropylamine was used[70, 71] to yield MAlPO-18 (M = Co, Mn, Zn, Mg, Mn…) when the acetate of the divalent ion was added to mixtures of $Al(OH)_3$ and H_3PO_4. Cyclohexylamine is the template of choice to produce MAlPO-44, and decamethonium ions for DAF-1, and so on. In the second approach a new procedure, of growing power and potential has evolved from the use of energy minimization methods[72–74]—to investigate the packing energies of organic amines (such as triethylammonium ions) within distinct AlPO structures—to one in which, for a given

target solid, an appropriate algorithm is used to build up, within the desired cavity of the target microporous catalyst, the template molecule to be used in its chemical synthesis (see Section 5.1).

We focus first on the design based on accumulated chemical intuition. To make explicit our aim we are setting out to "find" the most appropriate template that will yield a microporous acid catalyst such as CoAlPO (or SAPO), which, after driving away the template by calcination leaves active sites of the type that we can establish in quantitative terms, using in situ characterization by X-ray absorption, X-ray diffraction, and FT-IR spectroscopy. This Brønsted acid site is, in effect, a detachable proton bound to the framework oxygen atom that is adjacent to a Co^{II} ion that has isomorphously replaced Al^{III} in the framework. In effect, our aim is to synthesize both cobalt- and silicon-containing solid acids based on AlPO, in which the cavities are somewhat different from those in CoAlPO-18[70] and SAPO-18[75]. (In a SAPO catalyst the detachable proton is bound to an oxygen atom which is next to the framework Si^{IV} center which has isomorphously replaced the P^{V} center).

More will be said later (Section 7.5) about microporous solid acid catalysts, derived by replacing Al^{III} ions in the framework of a "targeted" AlPO with divalent ions such as Co^{II} or Mn^{II}. We shall also have more to say (see Section 7.1) about the microporous oxidation catalyst analogues that are produced by calcining the parent solid acid in O_2 so as to yield a neutral framework in which up to about 4 atoms per cent of the Al^{III} ions are isomorphously replaced by Co^{III}, Mn^{III}, or Fe^{III} ions.

5.1. Designing Templates for the Synthesis of Microporous Solids Using a De Novo Computer-Modeling Technique

De novo ligand design has been applied for some time in the search for biologically active materials—see refs. [76–82] for further details and applications. These techniques allow a molecule to be "grown" so as to fit accurately into a targeted space. The molecule is grown, in a computational sense, to promote favorable interactions between the substrate and the target cavity. But owing to the complex, and frequently ill-defined nature of biological active sites, a number of approximations are often made, for example, restricting the growth to linking units[79–81] and annealing dense arrangements of atoms into suitable molecules.[83] Template molecules required for the production of microporous inorganic solids are usually much simpler and smaller than those required in biological contexts. Furthermore, the target host (the microporous material) has many advantages over the organic cavity. Firstly, it is crystalline, and can therefore be readily described atomistically; even hypothetical structures can be defined in this way. Secondly, the frameworks possess reasonable rigidity so that conformational changes in the pore need not in general be considered. Finally, the interactions present in the templating of microporous materials are dominated by van der Waals interactions.[76, 84] Interactions involving charge and hydrogen bonding are less important in determining the final structure formed, although they are significant in the gel chemistry that is an essential precursor of the crystalline product.

We have recently developed a new code, ZEBEDDE[74] (*ze*olites *b*y *e*volutionary *de* novo *de*sign), to investigate the application of de novo techniques to designing templates for microporous materials. The target space (the framework) in which a molecule (the template) is to be grown is supplied by the user, along with a library of fragments from which the template is to be constructed. The template then grows by a number of randomly selected actions until a cost function, which measures the effective fit of the molecule in the framework, is satisfied. We exploit the crystalline nature of the framework, by allowing the symmetry of the template to be defined and for the growth to occur under periodic boundary conditions. The actions available allow 1) the addition of new atoms, by selecting molecular fragments from a library and bonding them to the existing template, 2) rotation of single or multiple fragments around the new bonds formed, 3) the displacement and rotation of the growing molecule within the framework, 4) the formation of rings from chains, 5) the optimization of the molecule using energy minimization, either in isolation or within the reference framework. Throughout these actions, the growth is controlled by the cost function and additional van der Waals overlap functions. Further details are given elsewhere.[74]

Our initial applications of this new methodology have proven to be fruitful, firstly in demonstrating the effectiveness of the method for generating previously identified templates and also in predicting a new template that has been shown independently to be an effective template for the targeted levyne framework.[62] We have considered a number of frameworks, which exhibit different topological features—cages, intersecting channels, pockets—in our evaluation of the method and we highlight a number of these applications here.

In our study of the levyne structure we first attempted to "reproduce" the relatively complex cyclic templates 1-amino-adamantane and *N*-methylquinuclidium used experimentally, to form the synthetic zeolite NU-3,[85] which is isotypic with levyne.[86] This was accomplished in two ways. First, by including adamantane and quinuclidine in the fragment library we could test whether our algorithms could successfully insert such large fragments into a confined region. Secondly, we wished to see if such complex fragments could be formed by our ring-formation strategy which converts chain molecules into rings, by bonding *n*th order neighbors if they are within a suitable distance ($n = 5$ forms 6-membered rings). Each of these approaches proved successful and close analogues of both experimental templates were generated (Figure 11). In addition a number of other cyclic templates were generated, of which 1,2-dimethylcyclohexane was considered to be an excellent candidate given its high binding energy.[72] Independent experimental work in this laboratory led us to use an amino analogue, 2-methylcyclohexylamine, to form a CoAlPO, designated DAF-4, which possesses the levyne structure (see below). Figure 12 illustrates how this template was generated by our code.

To test further the trustworthiness of our methodology, we attempted to grow templates for ZSM-5, which has a three-dimensional intersecting channel system. Again, the method

Figure 11. An overlay of the predicted position of the ZEBEDDE-constructed aminoquinuclidine analogue and the experimental (red)[87] position of the *N*-methylquinuclidinium template in the levyne cage. The cage is represented by the positions of the tetrahedral cations (Al, P, Co) of the framework. The oxygen atoms, which lie approximately midway between the verticles, are omitted for clarity. (From J. M. Thomas, D. W. Lewis, *Z. Phys. Chemie* **1996**, *197*, 537).

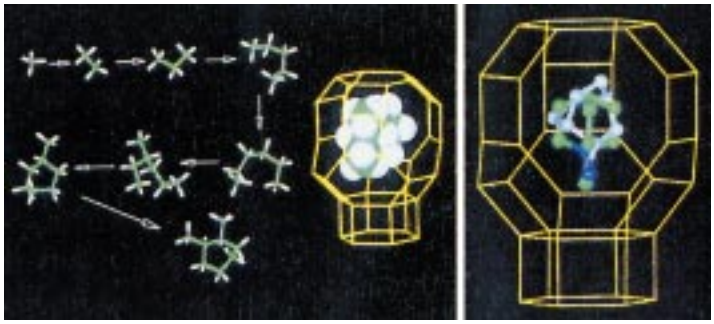

Figure 12. The growth process involved (in ZEBEDDE) in the formation of the 1,2-dimethylcyclohexane in the levyne structure. Starting from the methane seed, the alkyl chain grows inside the restricted void of the levyne structure. When an atom with a 5th order neighbor within a distance of 3 Å is selected (along with the ring formation action), methylcyclohexane is formed and further substitutions of this ring then occurs. The predicted position of the template in the levyne unit cell is shown on the right.

proved successful and generated a number of the variety of templates known to form this. Simulations of templating in this structure allowed us to validate the importance of specifying template symmetry within the host. Large templates, such as tetrapropylammonium, tend to be located at the channel intersections, and specifying the growth of one template at each intersection encouraged the formation of quaternary ammonium ions and similar templates (for example, tripropylamine). Similarly, if the symmetry were specified so as to favor a higher template concentration, then smaller, linear templates (such as *n*-diamines), are formed in the channels,. Further details of these simulations are given elsewhere.[74]

We have recently[88] been guided in the synthesis of a small-pore microporous material (known as DAF-5[89]) using the computationally designed template ZEBEDDE. Our aim was to synthesize an aluminophosphate-based material processing a chabazite structure (CHA) that would crystallize out of a nutrient phase containing an appropriate template (structure-directing) organic cation. We judged[88] that the following features would be crucial in our strategy: a) the selected template would form a CHA framework quickly and in a phase-pure form; b) the template would be present at a concentration of one molecule per unit cell and must fully occupy the CHA cage; c) the charge on the template could be varied to accommodate a range of metall ion (for example, Co^{II}) concentrations in the framework and thus allow a degree of control over the catalytic behavior arising from the presence of these constituents.

We performed a number of simulations using seeds from C_1 (methane) to C_4 (*n*-butane).[89, 90] Bicyclohexane, another molecule generated by our code, was more rigid. Pursuing our principles of rational design (described in detail in ref. [89]), we identified 4-piperidinopiperidine as a suitable candidate for initial evaluation of templates based on the cyclohexane motif; the commercial availability of this material is also important. The generation of 4-piperidinopiperidine from an ethane seed within the CHA structure[91] is illustrated in Figure 13a, and Figure 13b depicts the energy-minimized geometry of the molecule in a siliceous unit cell of chabazite.

Preparations with a typical gel composition of $0.2\,CoO:0.9\,Al_2O_3:15\,P_2O_5:30\,H_2O:2.0\,C_{10}H_{20}N_2$ yielded a single blue crystalline phase, designated DAF-5. Its X-ray powder diffraction pattern could be readily indexed with the auto-indexing program TREOR[92] to a hexagonal unit

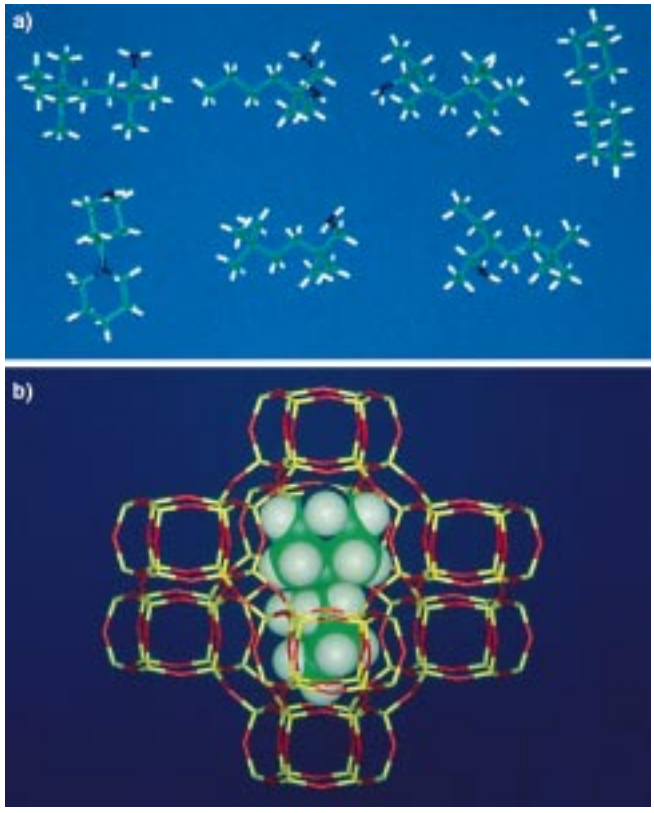

Figure 13. a) Generation of the 4-piperidinopiperidine template molecule (starting from a substituted ethane seed) with the ZEBEDDE code to yield a new chabazite CoAlPO structure known as DAF-5; b) energy-minimized position of the 4-piperidinopiperidine inside the chabazitic cage (From D. W. Lewis, G. Sankar, J. M. Thomas, C. R. A. Catlow, J. K. Wyles, D. J. Willock, *Angew. Chem.* **1997**, *109*, 2791; *Angew. Chem. Int. Ed. Engl.* **1997**, *36*, 2675).

cell, very similar to that of the mineral chabazite. Although high-resolution X-ray (synchrotron-based) powder diffractograms proved invaluable in refining the positions of atoms in the AlPO-framework of DAF-5, only micro-single crystal ($30 \times 30 \times 30$ μm specimen size) diffraction, again using synchrotron radiation,[93, 94] was sufficiently powerful to determine the structure of the disordered template (4-piperidinopiperidine) within the individual chabazite cages (Figure 14). More details pertaining to the application of computer modeling to the mechanisms of synthesis of microporous catalytic materials have been published elsewhere.[95]

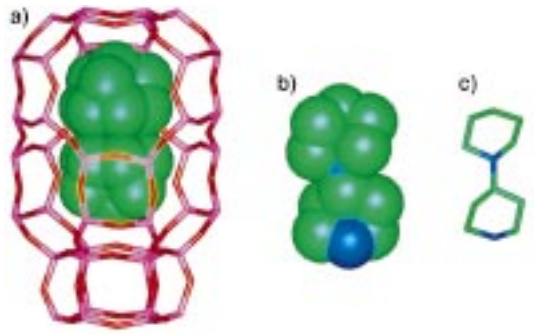

Figure 14. a) Graphical representation of the structure of DAF-5 derived from a single crystal diffraction study. For clarity only one of the cages is shown that contains all possible conformations of the occluded template molecule, 4-piperidinopiperidine. One of the possible conformations of the latter is also shown using ball (b) and stick (c) representations, the carbon atoms being green, the nitrogen atoms blue.

6. Characterizing The Architecture Of Engineered Catalysts

Ultimate success in the design of solid oxide catalysts as well as other covalently bonded or heterogenized organometallic catalysts predicates knowledge of precisely what structure or architecture it is that has to be targeted. This, in turn, demands the greatest possible precision in determining, under operating conditions, the structure of the catalyst in general and of that of the active site in particular. It follows ineluctably that there is an exigent need for in situ methods of characterizing solid catalysts if one is to succeed in engineering desired, well-defined active sites at the surfaces of large-area (porous) solids.

Demonstrably, only those interrogating probes, such as high energy photons or neutrons that are capable of penetrating through the walls of a catalytic reactor and into the cavernous recesses of the interior of micro- and mesoporous catalysts, will, in the final analysis, prove adequate to meet the demanding needs of in situ characterization of commercially viable reactors. In laboratory studies of model catalysts considerable insights may be gained through the use of noninvasive techniques such as infra-red and (laser) Raman spectroscopy, not least because such techniques, such as those described in Section 6.2, may be deployed under in situ conditions. This does not, however, mean that all ex situ methods are secondary (at best) or worthless (at worst). On the contrary, there are a number of ex situ methods, especially those based on electron beams, which are invaluable for the elucidation of the structure of catalysts. We, therefore, illustrate in the next section the principles and merits of such methods, before focusing on in situ methods.

6.1. Ex Situ Methods

6.1.1. Electron Microscopy

The single most remarkable attribute of the electron microscope is its versatility.[96] It can identify new (or hitherto established) phases by diffraction or from high-resolution electron microscopic (that is real-space) images, and simultaneously yield X-ray emission or electron-energy loss spectroscopy (EELS).[97, 98] Information pertaining to chemical bonding and oxidation states in a spatially resolved fashion[99] may also be retrieved through its agency.

The characterization of the ultrastructure of zeolitic and related (catalytically significant) solids by electron microscopy was pioneered in the early 1980s at the University of Cambridge[100–105] and subsequently extended by the research groups of Terasaki,[106, 107] Treacy,[108] Bovin,[109] and others.[110] A measure of the power of the high-resolution (transmission) electron microscopic (HR(T)EM) images for microporous and mesoporous siliceous catalysts is seen in Figures 7 and 10. Images of this quality, such as that shown in Figure 15, permit precise details of surface structure, of crystallographic (polytypic and other) intergrowths, to be determined.[107, 111] New types of structures and correctivities among mesoporous variants (such as SB-2 and STAC-1) have been identified by HREM by Zhou and his co-workers.[68, 112]

Recent advances in detector technology (of charge-coupled devices (CCD) and image plates in particular) permit the recording of HREM images with far lower electron dose than

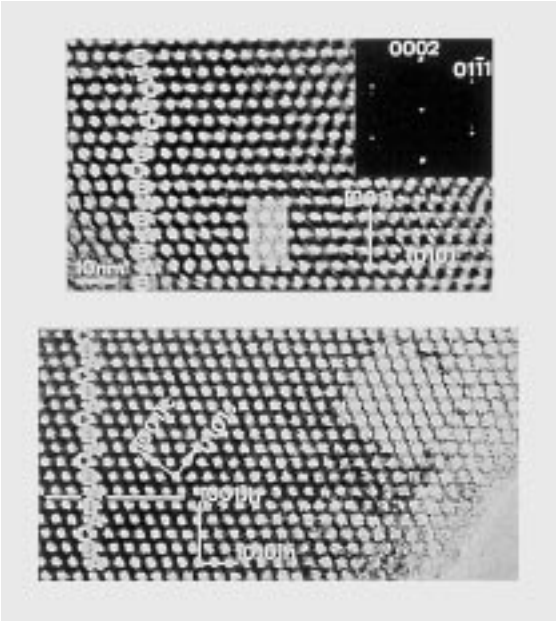

Figure 15. High-resolution electron micrographs with accompanying diffraction pattern (top right) and computed images of the new mesoporous silica known as STAC-1 (St. Andrews and Cambridge). Well-defined cubic (ABC stacking) and hexagonal (AB) polytypic intergrowths are frequently present in such preparations.[68]

for film recording.[113, 114] This means that it is much easier to treat the digital data of electron-diffraction patterns and HREM images (in the manner pioneered by Klug[115] and Henderson[116]) quantitatively. Indeed, the era of electron crystallography, which has been so conspicuously successful in virus research,[115, 117] is now a demonstrated success in the determination of the structure of zeolitic solids, thanks to the work of Gonzalez-Calbet and Vallet-Regi.[118] Figure 16 illustrates the kind of information that may be obtained.

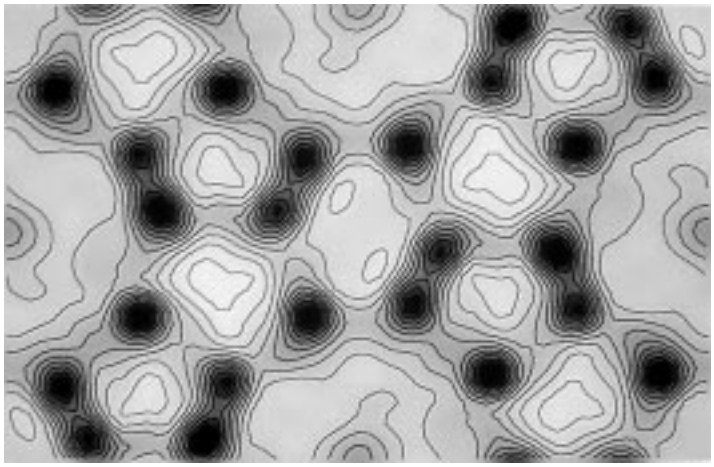

Figure 16. Typical illustration of the quality of the electron-density map for a zeolitic solid that may be derived by the application of electron crystallography.[118, 119]

Very recently, Wagner, Terasaki, and Davis[119] at Tohoku University, Japan, used electron crystallography to obtain the three-dimensional structure (and to refine it) of a new large-pore, high-silica molecular sieve that contains an occluded organic structure-directing agent. Alas, such is the exceptionally rapid beam damage suffered by AlPO-based molecular sieves (see refs. [120, 121]) during electron microscopic examination that it is not yet possible to solve their structures even with electron crystallography aided by the most sensitive detector system. But this situation will soon change. Those microporous solids that are sufficiently beam-stable, such as SSZ-48,[119] have their structures solved by applying direct methods to a three-dimensional electron diffraction data set collected from submicron-sized crystals that are too small for single crystal X-ray analysis.

Recently, largely through the pioneering work of structural biologists such as Baumeister and colleagues, information about the three-dimensional spatial organization (for example, minute metallic particles interspersed within a supporting matrix) has been obtained by electron tomography, which is a general method for 3D reconstruction of a specimen from a series of projection images, that is, from a tilt series. A powerful feature of electron tomography is that individual objects may be investigated in situ to reveal structural detail in three dimensions. The resolution finally achieved is, of course, governed by the number of images recorded and is, typically, about 200 for a specimen of 1000 Å thickness to achieve a spatial resolution of 15 Å.

6.1.2. Scanning Transmission Electron Microscopy (STEM) and the use of Rutherford Scattering for Z-Contrast Imaging

Images in the scanning transmission electron microscope are formed by rastering a focused probe over the specimen and at each point in the raster detecting either transmitted electrons to form a bright-field (BF) image or scattered electrons to form a dark-field (DF) image. The simple diagram of Figure 17 illustrates[110] the detector geometry

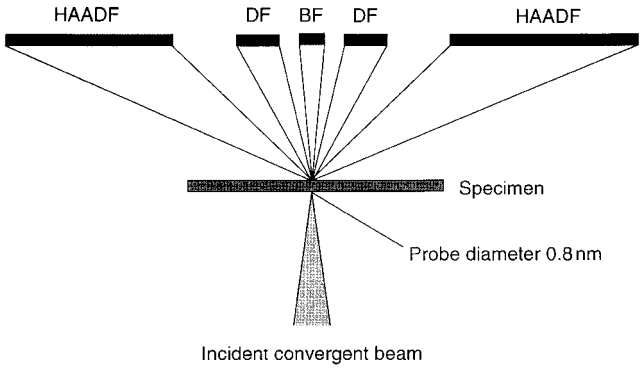

Figure 17. Schematic diagram illustrating the geometry of the detectors in a STEM. Typical values for the detector collection angles are BF picture 0 – 19 mrad, DF picture 10 – 50 mrad, HAADF picture 80 – 200 mrad.[69]

found in the STEM. Conventional DF images are recorded using an annular detector placed around the BF detector. Such images are formed from electrons that have been scattered to relatively small angles. Electrons scattered to low angles are predominantly coherent and thus both BF and DF images will show phase contrast (diffraction contrast) and are thus prone to contrast reversals with changes in specimen thickness or defocus. Electrons scattered to high angles are predominantly incoherent and images formed using a high-angle annular dark field (HAADF) detector[122] do not show the contrast changes associated with coherent scattering. Further, electrons scattered at such high angles must have been scattered from close to the nucleus of the atom and thus the cross-section for HAADF scattering approaches the unscreened Rutherford cross-section which is strongly dependent on the atomic number Z: in fact it is proportional to Z^2.[123, 124] Thus an image formed with a HAADF detector is very sensitive to changes in specimen composition and is thus an ideal way to image small nanoparticles with moderate or high atomic number on a support with a low atomic number. The power of the STEM is that BF and HAADF images can be acquired concurrently with other chemically sensitive signals such as X-ray emission, as shown below.

Figure 18 shows images recorded in the BF and HAADF modes of a mesoporous (MCM-41) silica that encapsulates catalytically active bimetallic particles of composition Pd_6Ru_6 (prepared[69,125] from the mixed metal cluster carbonylate $[Ru_6Pd_6(CO)_{24}]^{2-}$). The nanoparticles stand out (by Z-contrast) very clear on the siliceous (low Z) background. From the "element maps", recorded from the X-ray (K-emission) images of Pd and Ru, it seems that the bimetallic nanoparticles retain their 1:1 stoichiometry.

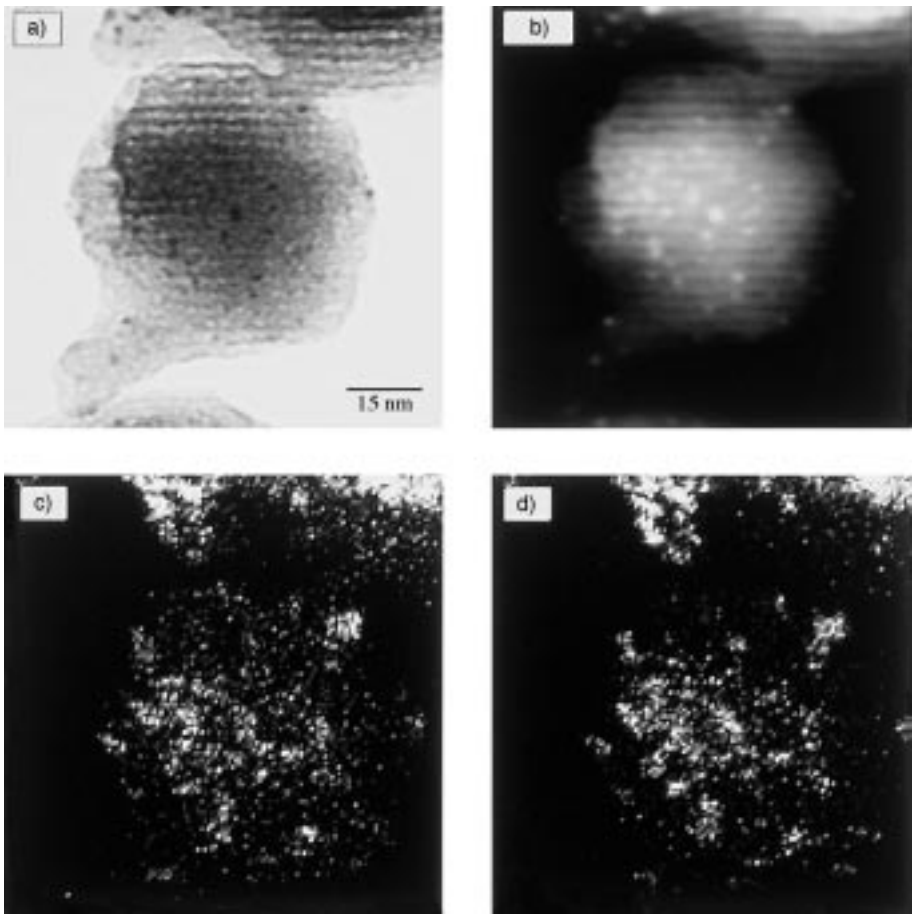

Figure 18. a) BF and b) HAADF images of mesoporous MCM-41 silica in which particles of Pd_6Ru_6 are encapsulated (top). The corresponding electron-stimulated X-ray emission images below show the spatial distribution of the Pd (c) and Ru (d).[69]

6.1.3. Environmental Cells in an Electron Microscope

In certain circumstances gas–solid reactions (both catalytic and stoichiometric) may be probed directly on the atomic scale using an appropriate chemical microreactor (environmental cell, ECELL) attached to the column of a high-resolution transmission electron microscope. Many designs for achieving this end have been described, but few can surpass the system evolved by Gai and Boyes.[126–128] The ECELL is fully integrated and permanently mounted inside the EHREM. A variety of accessories are added to aid simultaneous structural and compositional analyses of the reactor contents. In the EHREM, structures and chemistries of unknown phases are revealed by imaging, electron diffraction, and chemical analyses (with a sensitivity of $\leq 10^{-20}$ g of sample) whilst the sample is immersed in gas atmospheres at elevated temperatures (but still maintaining structural and compositional capabilities of a normal HREM operating in a vacuum). Detection of characteristic X-rays emitted by the interactions between the electron beam and the sample (namely, electron-stimulated X-ray spectroscopy) provides compositional information about the sample. The short wavelength of electrons (for example, 0.00251 nm at 200 keV) permits atomic-scale resolution. A conventional chemical reactor-type gas manifold system enables the inlet of gas mixtures into the reactor so that the flow rates and exchange gases can be controlled. The gas manifold system permits operation under vacuum as well as under gas environments. A heat source (furnace) and temperature control system allow the sample to be heated. With this method one may study reactions at elevated gas pressures and at temperatures between $-196\,^{\circ}C$ and $+1000\,^{\circ}C$. A low light-level television camera and a video recorder system connected to the EHREM allow real-time (time-resolved) dynamic events to be recorded. Low-dose imaging techniques minimize any invasive beam damage and none is detected in Gai's experiments. Blank experiments (without the beam) are also performed to confirm in situ data (with the beam switched on for a few seconds only to record the final state of the material).

The development of in situ electron microscopy provides direct and unparalleled insights into the dynamic evolution of structural changes. The ECELL has proved invaluable in elucidating the nature of the vanadyl pyrophosphate-catalyzed conversion of butane to maleic anhydride. As yet no microporous or mesoporous catalyst has proved amenable to study by this method, primarily because of the sensitivity of the beam.

6.1.4. High-Resolution Solid-State NMR Spectroscopy

It has long been appreciated[129–131] that magic-angle-spinning (MAS) NMR spectroscopy and many other variants of the resonance technique are ideally suited for the determination of crucial structural details pertaining to active sites in siliceous solids, aluminosilicates, and aluminophosphates. The convenient values of the relative isotopic abundances and magnetogyric ratios of ^{29}Si, ^{27}Al, ^{31}P, and ^{17}O make NMR spectroscopy an ideal technique to probe the architecture of a wide range of porous catalysts, and the corresponding properties of ^{13}C, ^{15}N, ^{1}H, and ^{2}H isotopes offer great scope for probing the nature of bound and catalytically implicated guest organic species undergoing conversion at the internal surfaces of the porous catalyst. Multiple-quantum solid-state NMR spectroscopy is an especially powerful means of locating cation locations inside solid catalysts.

When a new microporous solid is prepared, one of the best procedures for establishing its structure (after certifying by X-ray powder diffractometry that it is structurally unique) is to record the high-resolution MAS NMR spectrum in its pure siliceous form. It was shown[132] early on that the number of discrete ^{29}Si peaks in the spectrum is exactly the same as the number of crystallographically distinct sites occupied by

silicon in the structure. Moreover, the precise magnitude of the ^{29}Si chemical shift yields (by an equation established by Thomas et al.[133]) the value of the so-called T-O-T angle, where T is the tetrahedral site occupied by one silicon atom and joined, through an oxygen atom, to another. This approach has been put to good effect by the group of the Spanish worker Camblor[134] to establish the structure of several new microporous silicas in a family designated ITQ.

Lippmaa, a pioneer[135] of solid-state NMR spectroscopy, and his co-workers, have recently shown[136] how great insight into the acid strengths of these important microporous catalysts may be gained by monitoring the changes in "spinning side-band" intensities and shape (for the ^{1}H nucleus) as a function of temperature for a series of acid zeolites (H-Y, H-Mordenite, and H-ZSM-5). There is a clear difference in behavior between a proton attached to a surface oxygen atom that bridges tetrahedrally coordinated Si^{4+} and Al^{3+} ions and that which is attached to a Si^{4+} ion (Figure 19). Dipolar interaction is prominent in the latter case, and this is what gives rise to the changing profiles of the spinning side bands, attributable to bridging (acidic) hydroxyl groups, as a function of temperature.

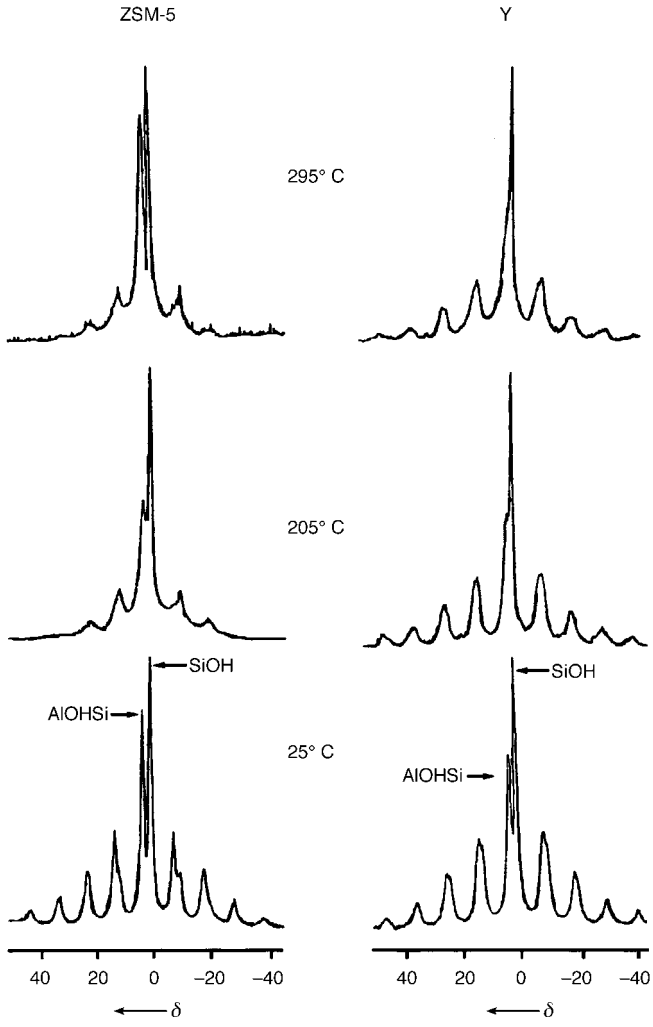

Figure 19. Insights into the acid strengths of a zeolitic catalyst ZSM-5 (left) and Y (right) may be gleaned by monitoring changes in intensities and shape of "spinning side bands" (for the ^{1}H nucleus) as a function of temperature.[137]

Although solid-state NMR spectroscopy is not ideally suited as an in situ technique for commercial-scale catalysts (operating at extremes of pressure and temperature) several successful attempts have been made, especially by Haw and co-workers,[138] to probe quantitatively the acidity (and alleged degree of superacidity) of zeolitic catalysts.

6.2. In Situ Methods

Insofar as retrieval of quantitative values of bond distances and angles are concerned, there are only three truly viable ways of attacking the structure of a solid catalyst operating under the severest commercial conditions—pressure as high as 100 bar, temperatures close to 700 °C—and they involve either neutrons or X-rays as the primary probing radiation (see Figure 3).[**]

Such are the fundamental aspects of the physics of neutron scattering that it is quite feasible to employ a beam of neutrons that can penetrate container walls or reaction cells made of stainless steel and yet be sensitive to very light atoms (^{1}H, ^{2}H, ^{12}C, etc.) at the site of catalytic reaction. High-energy (and high-flux) X-ray beams, such as those in a synchrotron radiation source, are likewise capable of reaching the solid catalyst inside a high-pressure, high-temperature cell, even when there are sturdy walls to the container. But with X-rays, in contrast to the situation that applies to neutrons, the walls of a metallic container have to be rather thin to avoid serious attenuation of the primary beam intensity.

6.2.1. Neutron Scattering

The availability of powerful sources of neutrons (either from a nuclear reactor or from a spallation proton source) makes it possible to conduct both spectroscopic (inelastic) and diffraction (elastic) measurements to high precision on catalysts undergoing chemical conversions. So far, however, very few genuine in situ measurements of operating catalysts have been completed. (One of these used[139] inelastic neutron scattering to determine the nature of hydrogen bound to a large-area MoS_2 hydrodesulfurization catalyst). But neutron diffraction studies of zeolitic solids at low and room temperatures have opened the way to important future possibilities.

Provided a catalyst is monophasic and well ordered, its atomic structure can be determined by neutron diffraction, even if it exists as a microcrystalline powder. This situation exists for many catalysts, especially zeolitic ones, and consid-

[**] There are a number of other powerful techniques, notably IR and Raman spectroscopy, Mössbauer and positron emission spectroscopy, ellipsometry, nuclear reactions, temporal analysis of products and luminescence life times, that can yield valuable information about catalysts operating close to industrially relevant conditions, but none of these enable the atomic architecture of active sites to be determined. For fuller discussions of many of these techniques, see ref. [23], pp. 232-241, and the special issue on in situ characterization of catalysts, in *Topics in Catalysis* **1999**, *8*. See in particular the paper by H. Knözinger and G. Mestl on Raman-based methods (p. 45).

erable progress has been made recently in arriving at the details of framework structure and location of exchangeable cations, and of model catalytic reactants sorbed within intrazeolite cavities. The method used for this purpose is the Rietveld neutron powder profile procedure. It was devized for analyzing complex diffraction patterns by curve-fitting techniques in which the least-squares refinement minimizes the difference between the observed and calculated profiles, rather than individual reflections. For neutron diffraction patterns, it can normally be assumed that the reflections have a Gaussian distribution, and that the calculated intensity at each point on the profile is obtained by summing the contribution from the Gaussian functions that overlap at that point. Besides the conventional parameters in the least-squares refinement (atomic coordinates and temperature factors of the individual atoms), additional parameters are required: the lattice parameters, which determine the positions of the reflections, a correction factor for setting the zero point of the detector, and three parameters that describe the variation of the half-width of the Gaussian distribution with scattering angle. Rietveld refinement procedures have been used to great effect in the study of uniform heterogeneous catalysts. Figure 20 illustrates[140] the kind of information that

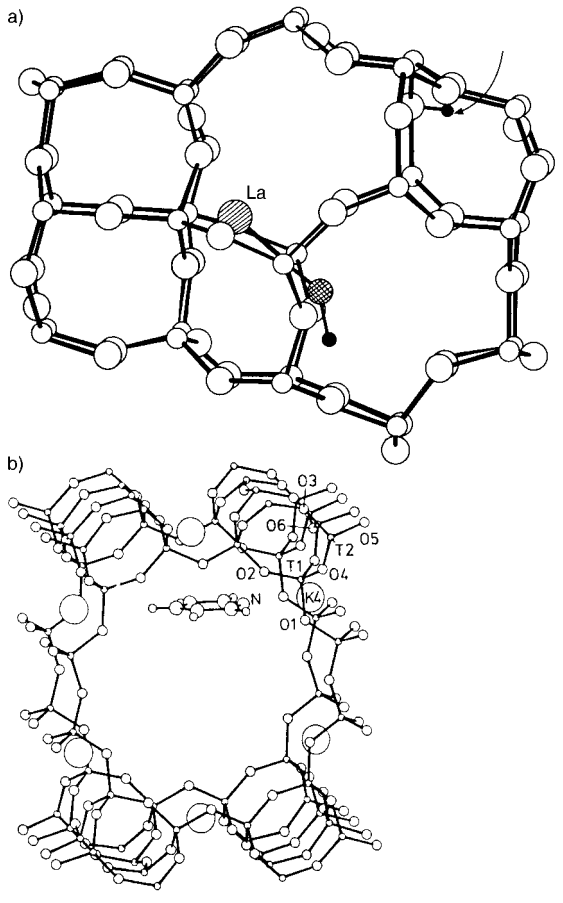

Figure 20. a) This picture of the catalytically active site, known in atomic detail, of La^{3+} exchanged zeolite Y was derived by Rietveld profile analysis of the neutron powder diffractogram.[141] b) The location of the pyridine in the catalyst potassium zeolite-L, as determined by neutron diffraction. The nitrogen atom of the pyridine forms a Lewis acid–base complex with the potassium ion, whilst the aromatic ring experiences short-range interaction with the aluminosilicate framework.[142]

can be derived by Rietveld analysis. No less an achievement than determining the precise structural detail of the active site in La^{3+}-ion-exchanged zeolite Y (an important cracking catalyst) is seen here. Here is the direct proof (previously only inferred) that La^{3+} ions in zeolite Y polarize their hydration shells so much that $(LaOH)^{2+}$ ions together with "free" protons, loosely attached to a framework oxygen atom are formed.[141, 142]

In a collaboration with W. I. F., David and his associates at the Rutherford–Appleton Laboratory, Dr. John Turner, Richard Catlow, and members of my group at the Royal Institution have made significant progress in reaching the goal of following the course of the cyclotrimerization[26] of acetylene at a Ni^{2+}-ion-exchanged Y catalyst surface.

6.2.2. Partial Radial Distribution Functions and the Isotopic Substitution Method

Consider an atom designated α at the origin and ask what is the average number of β-type atoms that occupy a spherical shell of radius r and thickness dr at an instant of time. That number is given by Equation (1). Here $\rho_\beta = N_\beta/V$, and N_β is the number of β species contained in the sample of volume V. It follows from the definition of $g_{\alpha\beta}(\boldsymbol{r})$, the partial radial distribution function in Equation (1), that the value of the integral [Eq. (2)] is the so-called running coordination number, that is, the average number of β atoms within a sphere or radius r_s for the chosen α atom.

$$\mathrm{d}n_\alpha^\beta = 4\pi\rho_\beta g_{\alpha\beta}(\boldsymbol{r})\boldsymbol{r}^2\,\mathrm{d}r \tag{1}$$

$$4\pi\rho_\beta \int_0^{r_s} g_{\alpha\beta}(\boldsymbol{r})\boldsymbol{r}^2\,\mathrm{d}r \tag{2}$$

If neutrons are incident on a solid containing several nuclear species the intensity of the scattered neutrons, $I(\boldsymbol{k})$ is given by Equation (3) with $C_\alpha = N_\alpha/N$. Here $\boldsymbol{r}_i(\alpha)$ denotes the position of the ith nucleus of α-type characterized by a neutron scattering length b_α and $\boldsymbol{k}$ is the scattering vector whose modulus k for elastic scattering (that is, $|\boldsymbol{k}_0| = |\boldsymbol{k}_1|$) is given by Equation (4), where θ is half the scattering angle and

$$\begin{aligned} I(\boldsymbol{k}) &= \sum_\alpha \sum_\beta b_\alpha b_\alpha \langle \sum_{i(\alpha)} \sum_{i(\beta)} \mathrm{e}^{i\boldsymbol{k}(\boldsymbol{r}_i(\beta)-\boldsymbol{r}_i(\alpha))}\rangle \\ &= N\,[\sum_\alpha c_\alpha b_\alpha^2 + \sum_\beta c_\alpha c_\beta b_\alpha b_\beta [S_{\alpha\beta}(\boldsymbol{k}) - 1]] \end{aligned} \tag{3}$$

$$k = 4\pi \sin\theta/\lambda_0 \tag{4}$$

λ_0 is the wavelength of the incident neutrons. The angular brackets show that an ensemble average has been taken, and $S_{\alpha\beta}(\boldsymbol{k})$ are the partial structure factors. Each $S_{\alpha\beta}(\boldsymbol{k})$ can be inverted to yield $g_{\alpha\beta}(\boldsymbol{r})$ through a Fourier transformation [Eq. (5)].

$$g_{\alpha\beta}(\boldsymbol{r}) = 1 + \frac{V}{2\pi^2 N r}\int \mathrm{d}k\,(S_{\alpha\beta}(\boldsymbol{k}) - 1)\,k \sin kr \tag{5}$$

Aided by the above background theory we now turn to the supreme advantages of replacing natural nickel (^{nat}Ni) atoms by the isotope ^{62}Ni. There is an enormous difference in neutron scattering lengths between these two species. In going

from ^{nat}Ni to ^{62}Ni the change (Δb) in scattering length is 18.9 fm, even larger than the substantial change (10.4 fm) in going from ^{1}H to ^{2}H.[143] Enderby has shown (Figure 21) that great insight into the nature of the hydration of

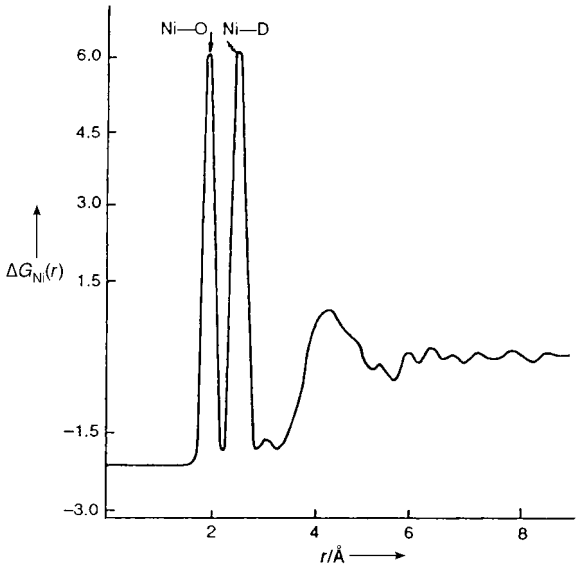

Figure 21. The hydration of Ni^{2+} ions may be studied precisely by neutron scattering as demonstrated by Enderby[143] if ^{62}Ni isotopes are used in place of natural Ni, and if D_2O is employed in place of H_2O. Here the first-order difference function $\Delta G_{Ni}(r)$ (in 10^{-2} barns str^{-1} for a 1.46 molal solution of $^{62}NiCl_2$ in D_2O is shown (see text).

Ni^{2+} ions in water (D_2O) is achieved in this way (see also Figure 22 and Table 2).[143] One sees that the geometry of the complex formed between the Ni^{2+} ions and water may be

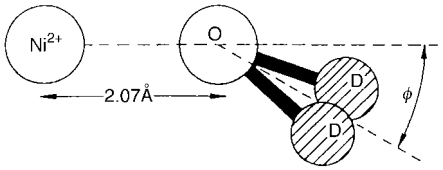

Figure 22. Neutron scattering also permits the determination of the instantaneous angle ϕ defined here, and also yields hydration numbers as a function of concentration (see Table 2).[143]

Table 2. Illustrative values of hydration numbers n_{Ni} of Ni^{2+} ions in D_2O (from Enderby[143]).

Electrolyte	Molality	n_{Ni}
$NiCl_2$	4.41	5.82
	3.05	5.82
	0.50	5.92
$Ni(ClO_4)_2$	3.80	5.82

accurately worked out. Proceeding in a rather similar fashion, Turner et al.[144] have achieved initial success in their ultimate goal to follow the course of cyclotrimerization in atomic detail, by assembling the appropriate partial structure factors around the ionic active sites in NiNaY catalysts. Figure 23 shows the results obtained for the bond distances in the complex formed between C_2D_2 and the active site, the first step in the catalytic process. With a special cell already assembled and tested[145] for operation in a pressure range of 10^{-6} mbar to 12 bar and temperatures from the cryogenic extreme up to 700 (with gold seals) or up to 1000 °C (with platinum seals), much can be expected from this powerful in situ technique in the future.

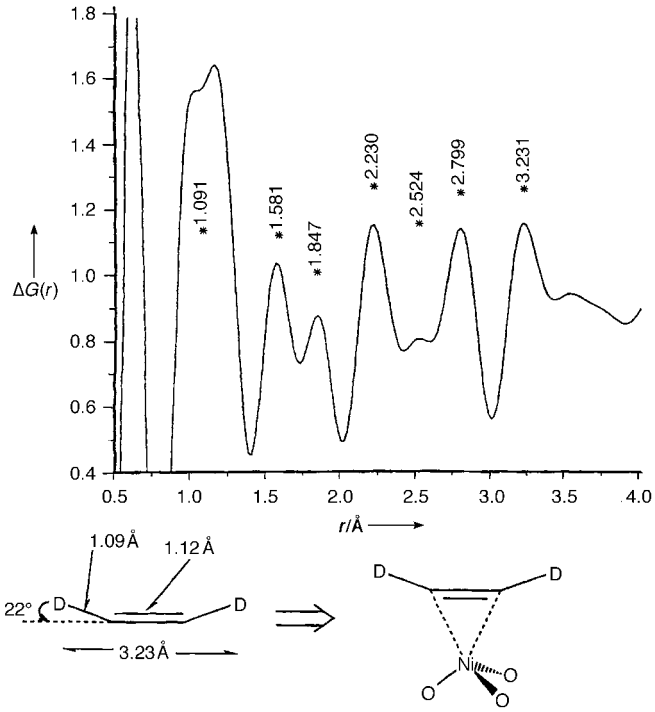

Figure 23. $\Delta G(r)$ plotted versus distance for the $Na^{62}NiY$ zeolite + C_2D_2 system. Bottom left is an interpretative drawing showing the distortion of the acetylene molecule when bound to the active site. Bottom right, the classical Dewar-Chatt-Duncanson picture of bound acetylene.

6.2.3. Combined X-Ray Absorption Spectroscopy and X-Ray Diffraction

There are numerous techniques now available for in situ studies of solid catalysts. They have been discussed at length in a recent monograph[23] and updated in a recent review.[146] We shall concentrate here only on those in situ techniques that utilize synchrotron radiation. A particularly powerful combination of techniques for micro- and mesoporous catalysts is that of X-ray absorption spectroscopy (XRA) and X-ray diffraction (XRD).[147–150] From the former, information pertaining to the immediate atomic environment of the absorbing atom (which is selected to be at, or close to, the active site) is extracted from the pre-edge, near-edge, and extended-edge fine structure (respectively abbreviated as PEXRA, XANES, and EXAFS). From the latter (XRD), information about the overall structural integrity and other aspects of long-range order within the phase in question is obtained. Between them, therefore, we achieve insights into the architecture of both the active site itself and the average picture of the solid in which the active site is situated.

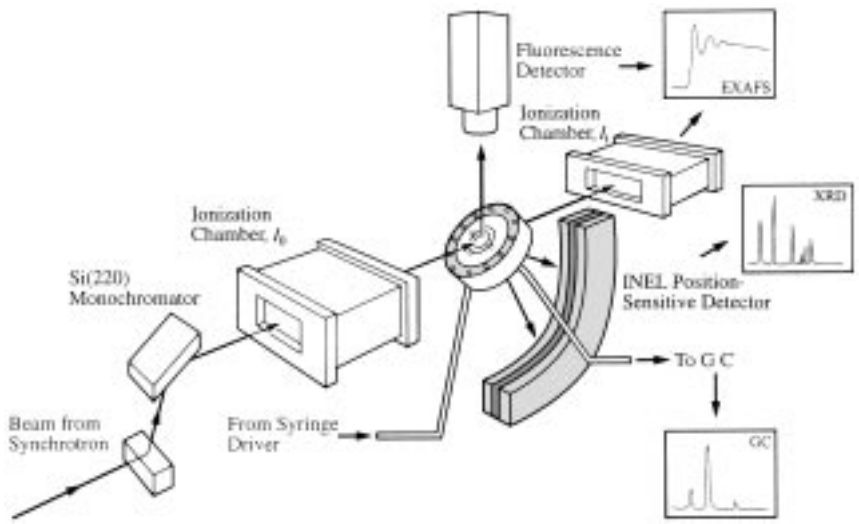

Figure 24. Schematic representation of the set-up used for the in situ parallel recording of X-ray absorption (XRA) spectra and X-ray diffraction (XRD) of solid catalysts in contact with either liquid or gaseous reactants. The fluorescence detector makes it possible to probe absorption edges of elements present at the ppm level in the catalyst (see also refs. [146, 151]).

Figure 24 shows the deployment of the XRA/XRD combination for in situ studies of either solid–liquid or solid–gas heterogeneous catalytic systems.[25, 151] The GC/MS analytical facility ensures that measurements of catalytic performance are conducted strictly in parallel with those of the nature of the active site.

6.2.4. X-Ray-Based in situ Studies of the Crystallization of Microporous Catalysts

Combined XRA-XRD measurements may be made in a time-resolved fashion using the set-up shown in Figure 25 to chart the growth of framework-substituted microporous AlPO catalysts such as CoAlPO-5 and CoAlPO-18. With a capillary reaction vessel housed in an appropriately designed furnace, both XRD patterns as well as richly detailed X-ray absorption spectra are obtainable (see Figure 7 of ref. [149]). The pre-edge X-ray absorption spectra,

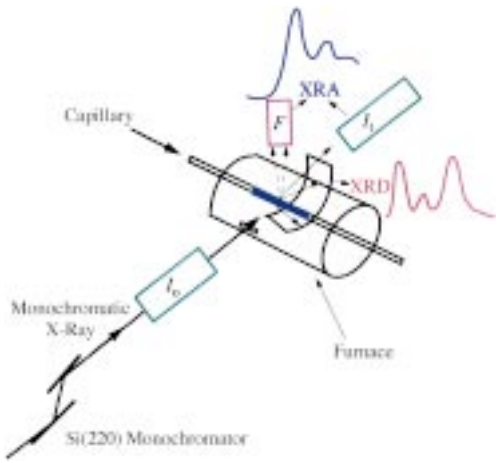

Figure 25. Schematic representation of the set-up used by Sankar et al.[149] for the combined XRD/XAS in situ measurements used to follow crystallization of molecular sieve catalysts from liquids and gels.

and also the XANES and EXAFS information (taken in conjunction with the XRD results), unmistakably reveal[149] that, prior to the onset of crystallization, octahedral Co^{II} ions in the precursor (templated) gel become tetrahedrally coordinated. With this technique one may record the appearance and disappearance of transitory phases during the course of the crystal growth in the phase that ultimately predominates.

Energy-dispersive X-ray diffraction techniques (EDXRD, Table 3) may be readily applied to study the development of crystalline phases during the synthesis of microporous material. One convenient arrangement, which uses three separate detectors set at different values of θ so as to cover a wide range of d-spacings is shown in Figure 26a. The time-resolved diffractograms in Figure 26b shows the

Table 3. The rudiments of energy dispersive X-ray diffraction (see Figure 26).[149]

$\lambda = hc/E$
$n\lambda = 2d\sin\theta$
$E/n = hc/(2d\sin\theta)$

- The detector angle 2θ was kept fixed at typicaly 1.5°; calibrated with a radioactive source and a silicon standard; the *wavelength is varied* as opposed to conventional XRD where wavelength is fixed and 2θ varied.
- *White radiation* permits simultaneous measurement over a wide range of energies (or d-spacing); the measurement range is dependent on the detector angle.
- The high intensity of X-rays allows the beam to pass through the stainless steel in situ hydrothermal cell, PTFE liner, and sample.
- The *time-resolved technique* typically used 1–2 min per scan.
- Poor resolution and intensity variation contribute towards the ED-XRD data being unsuitable for Rietveld refinement since structure factors are currently unobtainable.

sudden transition (at ca. 100 min) from an amorphous precursor gel to a crystalline zeolite (type A).

Normalized sigmoidal plots for the development of crystalline zeolite A at a series of fixed temperatures (Figure 27) all obey Avrami–Erofeev kinetics in which α (the fraction of crystalline product) is given by Equation (6), which, in turn, yields Equation (7). A plot of $-\ln(1-\alpha)^{1/n}$ versus $(t-t_o)$, where t is the time at which the data were collected after the

$$\alpha = 1 - e^{(-kt)^n} \quad (6)$$

$$-\ln(1-\alpha)^{1/n} = kt \quad (7)$$

start of the measurement procedure and t_o is the induction period (see Figure 27), that is, the time at which the X-ray reflections begin to appear, is indeed linear for $n = 4$. The gradient of the linear plot yields the rate coefficient k, which was determined over a range of temperatures. The resulting Arrhenius plot gave an activation energy of approximately 58 ± 3 kJ mol^{-1}, a value that accords well with the 60 kJ mol^{-1} computed for condensation reactions for Si-O-Si linkages in silicate systems.

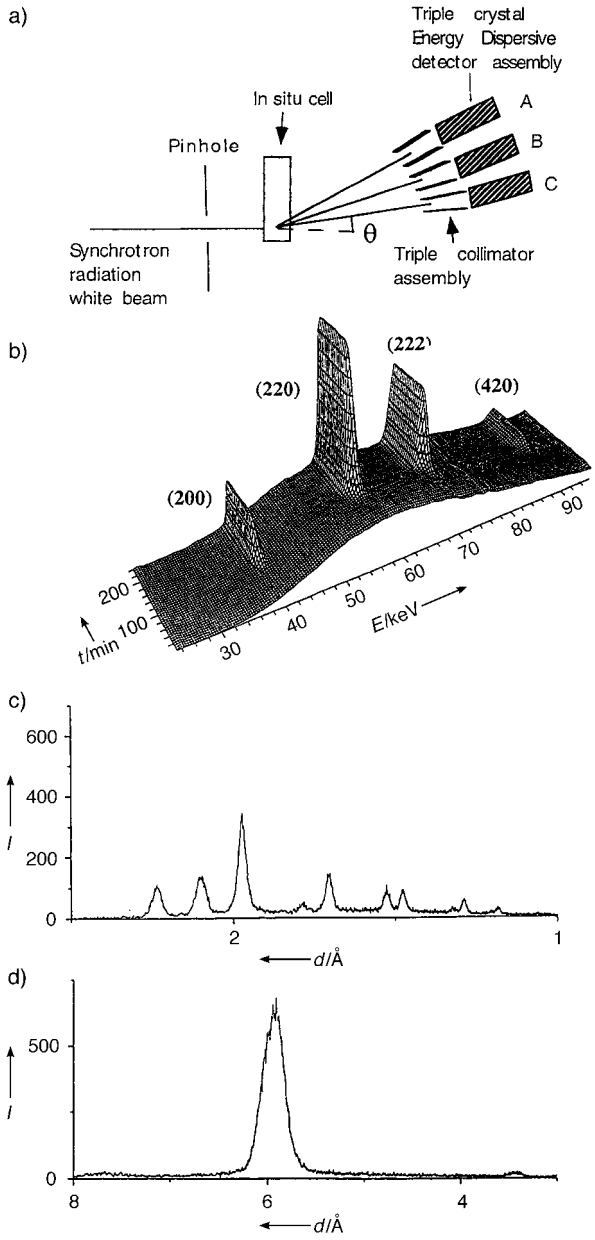

Figure 26. a) Set-up used for energy-dispersive X-ray diffraction (EDXRD) in situ measurements of the kinetics of crystallization of microporous materials. A bank of three detectors, each at fixed values of θ, ensures that a wide range of d-spacings is explored (c and d). b) A typical stacked, time-resolved EDXRD plot for zeolite A synthesized at 367 K.[149]

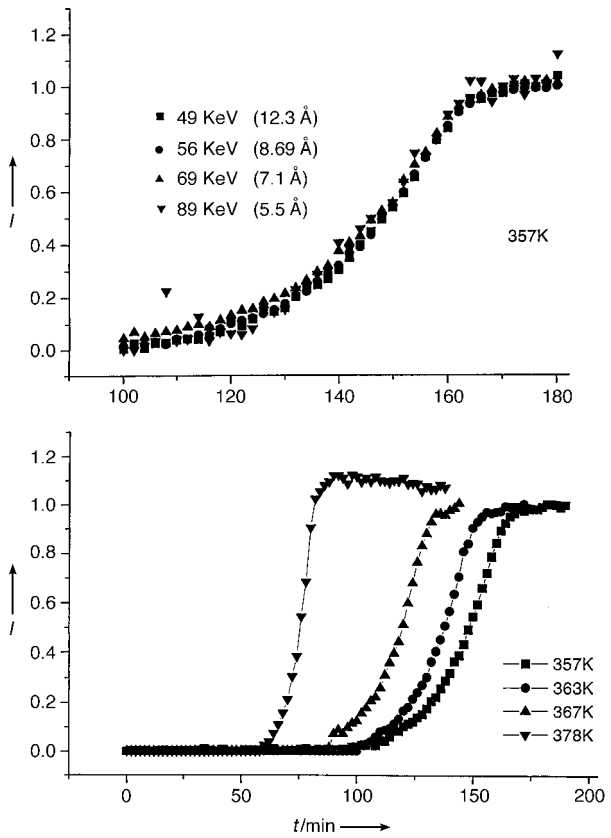

Figure 27. (Top) Normalized (against the intensity of the final data point) sigmoidal curves for zeolites synthesized at 357 K. Four strong reflections (at 12.3, 8.7, 7.1, and 5.5 Å) at four temperatures (bottom) were chosen so as to compare the rate at which the crystalline phase is formed. Since all four curves superimpose, we infer that the crystal growth is uniform.[149] In the bottom graph the temperature-dependence of the induction period t_0 can be seen.

- epoxidation of alkenes using either alkylhydroperoxides or molecular oxygen
- methanol to light-olefin conversion (preferentially to ethene and propene)
- hydrogenation of alkenes
- regioselective and enantioselective allylic amination.

All the catalysts that we have designed for these reactions are either microporous or mesoporous. Moreover the nature of the active site for each category of catalyst has been incontrovertibly established by the techniques described in Section 6.

7. Selected Case Histories

Equipped with all the information outlined above, we are now well placed to describe the atomic architecture of porous catalysts that have been engineered by my colleagues and me for the following types of reaction:

- selective oxidation of linear alkanes by molecular oxygen
- selective oxidation of cyclohexane (to cyclohexanone and cyclohexanol) using molecular oxygen or sacrificial oxidants
- Baeyer–Villiger conversions of ketones to lactones

7.1. Molecular-Sieve Catalysts for the Selective Oxidation of Linear Alkanes by Molecular Oxygen[152–154]

Terminally oxidized hydrocarbons are of considerable interest as potential feedstocks for the chemical and pharmaceutical industry, but selective oxidation of only the terminal methyl groups in alkanes remains a challenging task. It is accomplished with high efficiency and selectivity by some enzymes, but inorganic catalysts, while inferior in overall performance under benign conditions, offer significant advantages from a processing standpoint.[154] Controlled partial

oxidation is easier to achieve with "sacrificial" oxidants, such as hydrogen peroxide,[155] alkyl hydroperoxides, or iodosylbenzene,[156] than with molecular oxygen or air. These sacrificial oxidants, themselves the product of oxidation reactions, have been used in catalytic systems involving tailored transition metal complexes in either a homogeneous state,[157–159] encapsulated in molecular sieves,[160–162] or anchored to the inner surfaces of porous siliceous supports.[163] Here we report the design and performance of two aluminophosphate molecular sieves containing isolated, four-coordinated Co^{III} or Mn^{III} ions that are substituted into the framework and act, in concert with the surrounding framework structure, as regioselective catalysts for the oxidation of linear alkanes by molecular oxygen. The catalysts operate at temperatures between 373 and 403 K through a classical free-radical chain-autoxidation mechanism. They are thus able to use molecular oxygen as an oxidant, which, in combination with their good overall performance, raises the prospect of using this type of selective inorganic catalyst for industrial oxidation processes.

Cobalt(II) is one of the transition metal ions that, when occupying a small percentage of the framework (tetrahedral) sites in a molecular sieve, may be raised[164–166] to a higher oxidation state (Co^{III}) while remaining within the framework and act as active sites for the catalytic oxidation of cyclohexane [167] and other alkanes in air.[168] By taking advantage of this fact and choosing a molecular sieve that allows only end-on entry of the linear alkanes into the cavities containing the active sites (compare ref. [169]) we have been able to design effective catalysts that favor functionalization by oxygen at the terminal CH_3 and penultimate CH_2 groups and operate with air as the oxidant. (In conventional autoxidation of *n*-alkanes under homogeneous conditions and in the absence of steric constraints the regioselectivity is governed by the relative bond-dissociation energies. That is, whereas the bond-dissociation energies decrease from primary to secondary to tertiary carbon atoms, the corresponding selectivities increase).

We selected the molecular sieve known as aluminophosphate (AlPO) number 18 (idealized formula $Al_{24}P_{24}O_{96}$), which has pores similar to the zeotypic analogue of the aluminosilicate mineral chabazite. A few atom per cent of various divalent metal ions may be readily accommodated into the tetrahedral sites of this material's framework as isomorphous replacements for Al^{III} ions. This is done by templated hydrothermal syntheses as outlined in Section 5.

In this process the redox ions (Co^{II} or Mn^{II}) are raised to their triply charged states during calcination in O_2. In the course of the partial oxidations the transition metal ions, which replace some 4 atom % of the Al^{III} ions, eventually return to their 2+ states, and the catalyst changes color from green to blue (for $Co^{III} \rightarrow Co^{II}$) and blue →white (for $Mn^{III} \rightarrow Mn^{II}$). Combined in situ extended X-ray absorption spectroscopy and X-ray powder diffraction (Figure 28) show that the oxidation of the ion during calcination is accompanied by only minor structural changes, and these measurements yield quantitative structural information about the environment of the active Co^{III}- and Mn^{III}-centers.

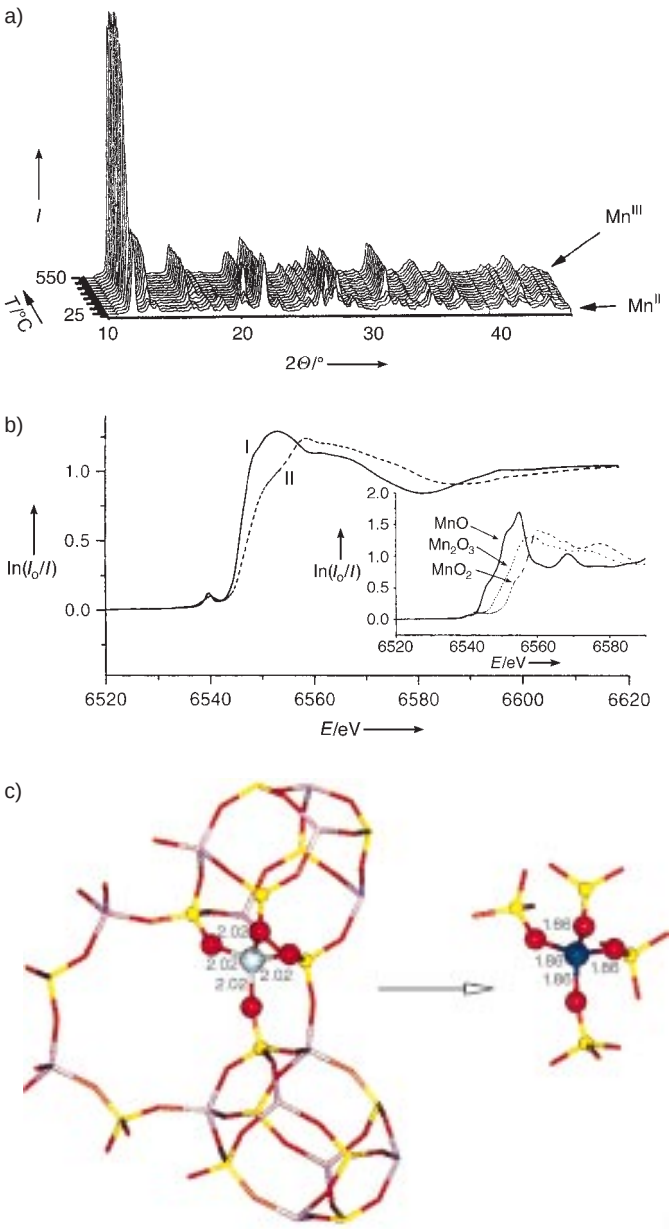

Figure 28. a) Stacked plots of X-ray diffractograms (recorded during calcination), showing that the integrity of the framework structure remains intact when Mn^{II} framework ions are oxidized to their Mn^{III} state. No exsolution occurs even after several oxidation–reduction cycles. b) X-ray absorption near-edge spectra of the Mn K-edge for MnAlPO-18 samples. The solid line (I) represents the as-prepared state, the dashed curve (II) the calcined state. For comparison the inset shows the corresponding information for three (model) oxides of manganese. c) The spatially-averaged EXAFS-derived structure around Mn^{II} (left) and Mn^{III} ions (right) in the AlPO-18 framework. (red: oxygen; yellow: aluminium; purple: phosphorous; gray: Mn^{II}; and blue: Mn^{III}; distances in Å).[153]

Measurements of the shifts in the K-edges and of the extended X-ray absorption fine structure of the Co and Mn ions show that these ions in the as-prepared (templated) form of CoAlPO-18 and MnAlPO-18 may be completely converted in dry air or O_2 into the Co^{III} or Mn^{III} states, respectively. For reasons that are not yet clearly understood, only a fraction of the Co^{II} or Mn^{II} ions isomorphously incorporated into the AlPO-36, AlPO-11 and AlPO-5 structures are convertible

into the +3 oxidation state by similar treatment in O_2 or dry air.[165] (In MAlPO-36 the fraction is ≈0.45, in MAlPO-11, ≈0.30, and in MAlPO-5, ≈0.20, where M = Co or Mn, all these values being deduced from changes in Co-O and Mn-O distances.)

The catalytic performance of the CoAlPO-18, MnAlPO-18, MgAlPO-18, CoAlPO-36, MnAlPO-36, MgAlPO-36, CoAlPO-11, and CoAlPO-5 molecular sieves was tested for the selective oxidation of *n*-pentane, *n*-hexane, and *n*-octane. Full details are described elsewhere, but the salient results are shown (for *n*-octane) in Figure 29. The overall performance of CoAlPO-18 and MnAlPO-18 is superior to that of all previously reported inorganic catalysts for the regioselective oxidation of linear alkanes, even though the latter use sacrificial oxidants, not air or O_2. An exception is the catalyst developed by Tolman et al.,[169] which uses a gas mixture of H_2 and O_2 to generate H_2O_2 in situ over finely divided Pd/Fe bimetallic particles.

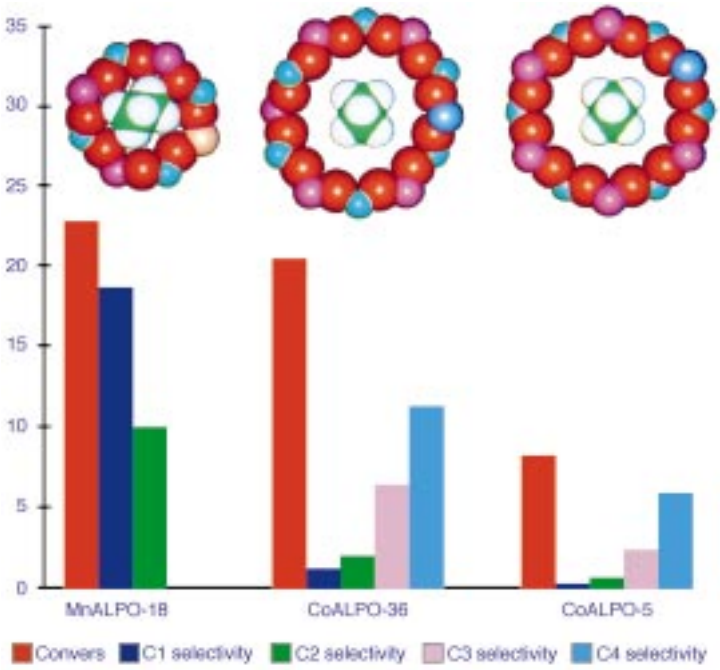

Figure 29. In the aerobic oxidation of *n*-octane (and other linear alkanes), terminal attack leading to oxyfunctionalization is much more favored in Mn (of Co) AlPO-18, than in Mn/CoAlPO-36, or in Mn/CoAlPO-5.[152, 153] The vertical axis shows the product quantities in mmol.

Given the pore dimensions and the fact that, under reaction conditions, the framework transition metal ions are all in their +3 state, it is unsurprising that CoAlPO-18 and MnAlPO-18 show the greatest activity—twice as active (in both *n*-hexane and *n*-octane oxidation) as a CoAlPO-11 catalyst. Our catalysts also show a high degree of regioselectivity: about 65.5% of the oxidation products of *n*-hexane after 24 h are the result of oxyfunctionalization at the terminal methyl group for MnAlPO-18 (61.5% for CoAlPO-18). As much as 31.7% (36.1% for CoAlPO-18) consist of 2-hexanol and 2-hexanone; there is no sign of attack at C_3 in hexane or at C_4 in the oxidation of *n*-octane.

It is well known[170] that the oxidation of alkanes by transition metals generally involves the participation of free radicals. We believe, for three reasons, that the overall selective oxidations of all the alkanes reported here, including that of cyclohexane, are no exceptions. Because of the small aperture of the AlPO-18 structure, it is easier to test the role of free radicals using the AlPO-36 structure, which has apertures large enough to allow alkylhydroperoxide radicals and radical scavengers to enter their interior surfaces (see Figure 33). First there is an induction period in the yield versus time plots (typified by that for *n*-hexane, using CoAlPO-36 as the catalyst, Figure 30), and this period is

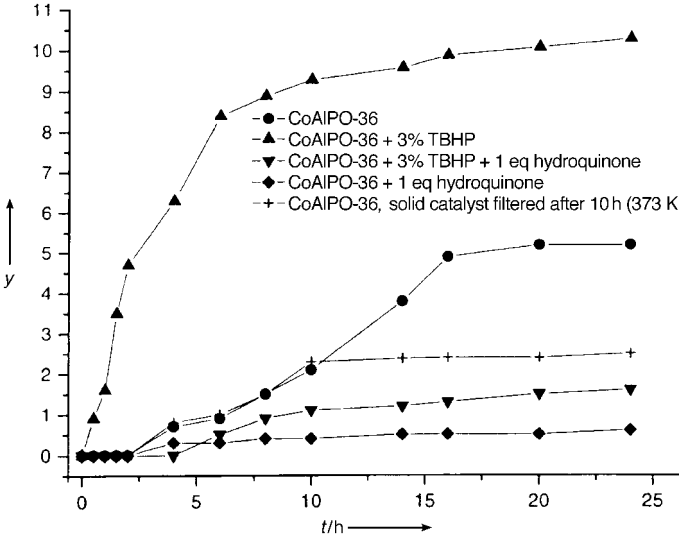

Figure 30. Kinetics of oxidation of *n*-hexane (conversion *y* in mol%) in air using CoAlPO-36 in the presence (▲) and absence (●) of a radical initiator. The addition of the free-radical initiator greatly reduces the initial induction period, accelerates the rate of the catalytic reaction, and gives rise to enhanced activity (the product selectivity is not affected). Addition of small amounts of hydroquinone (free-radical scavenger) completely suppresses the reaction (▼, ◆), which suggests the participation of free radicals in the catalytic process. In an identical experiment, the solid catalyst was filtered off from the reaction mixture (when hot) after 10 h, and the reaction was continued for a further period of 14 h (+). No increase in conversion was observed, indicating that the leached out metal ions (if any) are not responsible for the observed activity. In addition this experiment rules out the possibility of any gas-phase radical reactions. The resulting filtrate was independently analyzed for free or dissolved metal ions and only traces (<3ppb) were detected.[153]

greatly diminished by the prior addition of traces of free-radical initiators such as *tert*-butylhydroperoxide (TBHP). Second, addition of small quantities of hydroquinone, a free-radical scavenger, greatly hinders the oxidation (see curves plotted with ◆ and ▼ in Figure 30). Third, in the oxidation of cyclohexane (the peroxide of which is easier to analyze than that of *n*-alkanes) under identical conditions over a range of Co^{III}- and Mn^{III}AlPO catalysts, the presence of cyclohexyl peroxide (which subsequently decomposes to cyclohexanol and cyclohexanone) has been directly detected[171].

Although the precise mechanism of the oxidation of the alkanes involving CoAlPO and MnAlPO catalysts and dioxygen is not clear—as in the case of cytochrome P450[172] and other enzymatic reactions—there is little doubt that catalytic autoxidation dominates here. It is certain that framework-isolated Co^{II} or Mn^{II} ions present initially in the

freshly prepared sieve are vital for catalysis when converted into the Co^{III} or Mn^{III} state. It is likely that scope for expansion of the coordination shell of the transition metal ion (as with the Mn^{III} ion in the superoxide dismutase[173]) is a significant factor in facilitating the reaction. Divalent ions that cannot be raised to higher oxidation states, such as Mg^{II}, are totally inactive as oxidation catalysts. Experiments using MgAlPO-18 and MgAlPO-36 as catalysts (for the oxidation of *n*-octane under the conditions of Figure 29 at 373 K) showed no activity. This fact also rules out the possibility that free radicals produced solely in the gas phase are significant in the autoxidation. Moreover, introduction of acetonitrile (known to coordinate Co^{II} ions) before the admission of air poisons the CoAlPO-18 catalyst.

Overall conversions in the oxidations reported here have to be kept to a low level (≈7%) to avoid leaching of the transition metals by polar products (that is, carboxylic acids). However, they are comparable[161] to those in industrially significant oxidations of cyclohexane, and superior to what has been achieved to date using other inorganic catalysts.[153] The rates of reaction are rather slow, which reflects the diffusional requirements that have to be overcome when liquid reactants and products compete with one another and with solvated molecular oxygen for access to the sub-surface active site. It is possible that further enhancement of the catalytic performance may be achieved by optimizing such variables as the concentrations of Co^{III} or Mn^{III} ions substituted into the chabazite cages, the crystallite size, and the surface area. Moreover, by using a high-pressure flow system optimized with respect to contact time and oxygen pressure a higher yield of desirable products should be facilitated. It is also likely that other transition metal ions may serve equally well or better as selective oxidation catalysts. The regioselectivity of the oxidation is already remarkable, and may be understood from a computer simulation that determines the lowest energy state adopted by the alkane inside the chabazite cavity of the AlPO-18 framework (Figure 31).[174] A bound hexane (or any other linear alkane) molecule, gains easy access to the active sites and its end becomes slightly bent (shown by molecular dynamics calculations). This selectively favors oxidation at the terminal and penultimate carbon atoms.

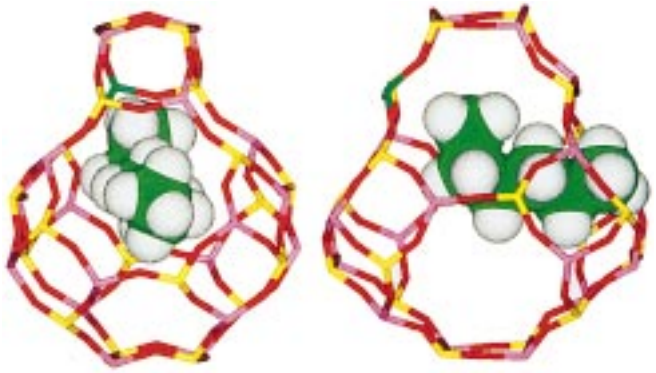

Figure 31. Energy-minimized configuration (two views) adopted by *n*-hexane at 0 K inside an AlPO-18 framework. This configuration was derived from a calculation that combines Monte Carlo molecular dynamics and docking procedures.[153] The framework composition was assumed to be SiO_2, for which more reliable potentials are available than for $AlPO_4$. Note that the terminal methyl group is significantly closer to a tetrahedral framework site than either C_2 or C_3, the respective distances being 3.53 Å (C_1), 3.75 Å (C_2), and 4.03 Å (C_3). The implication here is that Co^{III} (or Mn^{III}) ions in the framework of the AlPO-18 cage, along with intracage O_2, exert a greater influence on C_1 than on other carbon atoms in the hexane backbone.[153]

7.2. Designing Catalysts for the Selective Oxidation of Cyclohexane

The conversion of cyclohexane into cyclohexanol is one of the principal target reactions in the broad field of selective oxidation of alkanes since the latter compound is used as a feedstock in several industrial processes including the production of nylon from ε-caprolactam and adipic acid. Cyclohexane is expected to retain its dominant position as the feedstock of choice for adipic acid manufacture in the coming decade.

The conventional process is a thermal one, taking place at 125 to 165 °C and at pressures from 8 to 15 bar. It is accepted that the oxidation involves free radicals (facilitated by catalysts of Mn or Co salts) and intermediates such as cyclohexylhydroperoxide, which is selectively (and catalytically) decomposed to yield the alcohol and the ketone. It is prudent to limit the conversion to a maximum of about 10 %, to avoid build-up of other, unwanted products. Homogeneous catalytic oxidation of cyclohexane with cobalt acetate—the most popular industrial catalyst—suffers from the generation of by-products such as alkyl acetates, other ketones, cyclohexanediyl diacetate, and alkyl chlorides. (The precise structure of the active cobalt acetate catalyst remains unclear.) To confer greater stability upon the homogeneous Co^{III} acetate catalyst it is also necessary to employ, for reasons that are not entirely understood, either acetic acid or trifluoroacetic acid (or trichloroacetic acid) as solvent for the reactant mixture, Bromides are also often used as promoters.

With the aim of arriving at a cleaner, more efficient catalytic system for the production of cyclohexanone from cyclohexane, and also of gaining deeper insights into the nature of the catalytically active centers by in situ EXAFS studies, we designed[175] a new catalyst that entails harnessing the advantages of homogeneous organometallic catalysis on the one hand and of a large-area, well-defined (MCM-41) mesoporous silica support on the other.

Although there is still considerable debate[14,20,176,257] about the mechanism of the oxidation of cyclohexane in the presence of Co^{III}, Mn^{III}, and Ce^{IV} salts in acetic acid, our point of departure in this work is the earlier observation that several oxo-centered trimeric cobalt(III) acetates (coordinated with pyridine)[177] exhibit much greater activity in selectively oxidizing the tertiary C-H bond in adamantane than their dimeric analogues.

The apertures of the MCM-41 samples prepared by us are close to 30 Å and readily permit ingress of the monohydroxy-cobalt complexes $[Co_3(\mu_3\text{-}O)(OAc)_3(\mu_2\text{-}OH)(py)_3]PF_6$ to substitute the hydroxyl group for other ligands,[178] which we selected for immobilization inside the channels of the

MCM-41 mesoporous silica. It is possible to employ various routes to effect immobilization: anchoring to the surface directly or using surfaces functionalized with, for example, alkylcarboxylic acids. Each of these routes yields a catalyst for the selective oxidation of cyclohexane to cyclohexanone. However, distinct differences are observed in their respective turnover frequencies (TOFs), life times, and selectivities (see Table 4). The catalysis was effected in an essentially solvent-free fashion: the sacrificial oxidant *tert*-butylhydroperoxide (TBHP) and the reactant cyclohexane form a miscible liquid and each is consumed to yield cyclohexanone, cyclohexanol, other minor amounts of by-products (dicyclohexyl ether, dicyclohexylperoxide, and *tert*-butylcyclohexylperoxide), and *tert*-butyl alcohol (from TBHP).

In our first attempt at immobilization we reacted the monohydroxy cobalt complex with partially dehydrated siliceous MCM-41. The EXAFS spectrum after immobilization showed that there was virtually no change in the structure of the complex, which indicated either substitution of the bridging hydroxide ligand by a surface silanol group or physisorption brought about by interaction of the surface with the cationic cluster. Catalytic tests (Table 4) showed that 7.6% of the available cyclohexane was converted with a selectivity of about 89% into cyclohexanol and cyclohexanone after 24 h. The catalyst life time, however, was less than 48 h. This limited life time is most likely a result of the mobility of the cobalt clusters on the surface, giving rise to cluster–cluster and other unfavorable interactions at the interior surface, as well as some leaching indicated by slight discoloration of the solution.

Working on the principle that immobilization at a carboxyl-functionalized surface (that is envisaging the replacement of the bridging hydroxyl ligand by a carboxyl group) may produce a potentially more-stable catalyst, we proceeded to functionalize the MCM-41 surfaces with a 3-bromopropyltrichlorosilane tether, which we then derivatized by reaction with glycine. The virtual lack of solubility of glycine in solvents other than water means that the efficiency of the reaction between the amine part of the glycine and the bromoalkyl group could be expected to be low owing to the interaction of water with the amine. However, this would as a side-effect provide a means to ensure a high dispersion of the cobalt complex, which might aid stability (and, hence, longevity) by reducing possible interactions between cobalt clusters. Additionally, the nonderivatized bromoalkyl groups might act as a potential promoter echoing the use of bromide in commercial processes.

Catalytic tests established that after an initial TOF of around 352 mol cyclohexane per mol of catalyst per hour, a steady TOF of around 216 could be sustained for at least four days. The true heterogeneity of the catalyst was also examined by separating it by filtration and establishing that the filtrate displayed no further activity under the same reaction conditions. Additionally, no leaching could be detected (within experimental error) when comparing the elemental analysis results of the catalyst before and after reaction. No induction period could be observed (at a time resolution of 5 min); after an initial exponential behavior, the catalyst continued to produce cyclohexanone essentially in a linear fashion. At the outset more cyclohexanol than cyclohexanone is produced, but after about six hours cyclohexanone production is predominant, an equilibrium between cyclohexanol generation and consumption to form the ketone being reached after about 12 h (Figure 32).

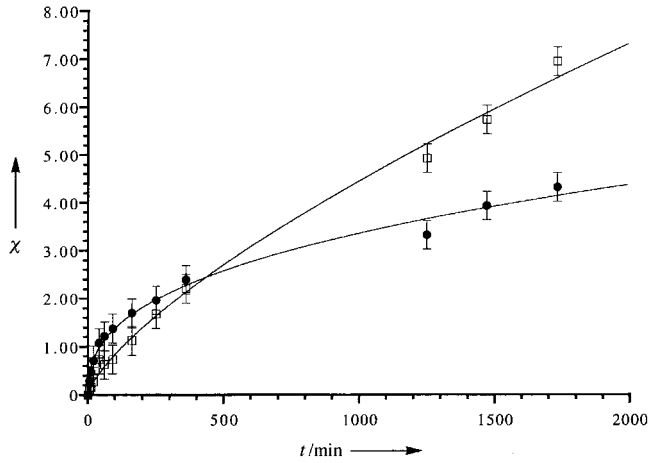

Figure 32. Plot of the of formation of cyclohexanol (●) and cyclohexanone (□) from cyclohexane against time with 150 mg of catalyst.[175] x is the percentage conversion.

Additionally, in situ X-ray absorption spectroscopy using synchrotron radiation enabled the detailed atomic environment of the active cobalt complex to be determined both prior to and during the course of the solid–liquid heterogeneous catalysis at realistic temperatures under continuous flow using a novel liquid/solid cell. A combination of in situ X-ray absorption spectroscopy and ex situ ^{29}Si MAS NMR spectroscopy yielded precise quantitative information of the heterogenized trimeric oxo-centered cobalt catalyst (see Figure 3 of ref. [175]).

The recent isolation[179–181] and characterization of a new series of multinuclear cobalt acetates provides further oppor-

Table 4. Catalytic performance in cyclohexane oxidation of the $[Co_3(\mu_3\text{-}O)(OAc)_5(\mu_2\text{-}OH)(py)_3]PF_6$ complex (see text) anchored to MCM-41 silica.[175]

Catalyst support	Co [wt%]	Si:Co	t [h]	Conversion [%][a]	TOF[b]	Selectivity [%][c]	Cyclohexanone: Cyclohexanol	Lifetime [h]
nonderivatized	0.376	210	4	3.7	89	85	0.6	< 48
MCM-41, glycine-functionalized through bromoalkyl tethers	0.201	300	24	11.9	230	89	1.5	
	0.201	300	96	38.1	216	95	3.3	

[a] 9.5 mL cyclohexane, 10 mL TBHP, and 0.5 mL mesitylene (internal standard) at 70 °C are required for 150 mg of catalyst. [b] In mol cyclohexane per mol catalyst per hour (Note: mol of catalyst refers to moles of the complex). [c] Based on cyclohexanone and cyclohexanol. [d] The experiment was stopped after four days.

tunities of improving anchored, heterogeneous, selective-oxidation catalysts for the conversion of cyclohexane into the corresponding alcohol and ketone.

7.2.1. From Sacrificial Oxidants to Selective Oxidation by Molecular Oxygen

As useful as alkylhydroperoxides are for the selective oxidation of cyclohexane (and for the conversions of alkenes into epoxides—see Section 7.4.2), it would be so much better if a solid catalyst were developed that effected such conversions using molecular oxygen or dry air. Such catalysts have been developed both in these laboratories and also at the National Chemical Laboratory in Pune (India).

Raja and Ratnasamy[182] showed how a solid catalyst comprising of transition metal complexes of a phthalocyanine or porphyrin (where some of the peripheral hydrogen atoms were replaced by electron-withdrawing groups) exhibited high stability and activity in the conversion of cyclohexane into the ketone and alcohol in the temperature range of 20 to 80 °C and a pressure of up to 60 bar. The performance of the catalyst is greatly improved if it is encapsulated in an aluminosilicate molecular sieve. Similar catalysts were developed[183] by them for the preparation of adipic acid from cyclohexane.

We have taken advantage in our studies of the convenient fact that a certain aluminophosphate (AlPO) molecular sieve containing isolated, four-coordinated Co^{III} or Mn^{III} ions that are substituted into the framework acts, in concert with the surrounding framework structure, as highly selective catalysts for the oxidation of cyclohexane to (predominantly) cyclohexanone and cyclohexanol in O_2 or air (see Section 7.1). One of the best AlPO molecular sieve catalysts to use for this purpose is CoAlPO-36 (the structure of which was determined[184] by stochastic methods). The results,[185] summarized in Figures 33 and 34, are compared with those for other (previously reported) CoAlPO structures.

Very recently[186] we prepared a very powerful selective oxidation catalyst for cyclohexane, again based on an AlPO structure, but this time with Fe^{III} ions (replacing Al^{III}) in four-coordinated sites in the framework. The conditions under which the oxidation ensues are benign: 403 K and 15 bar of dry air. The results (Figure 35) are vastly superior to those obtained with the cobalt-substituted analogue. (It is believed that, in this particular molecular-sieve structure, very few Co^{II} sites in the framework can be oxidized to the Co^{III} state, in marked contrast to the situation with Fe^{II} and Fe^{III} states). Incontrovertible evidence has been cited earlier for the free-radical (autoxidation) nature of the catalyzed selective oxidation of cyclohexane (see Figure 30 and the discussion of regioselective oxidations of alkanes in molecular-sieve catalysts in Section 7.1).

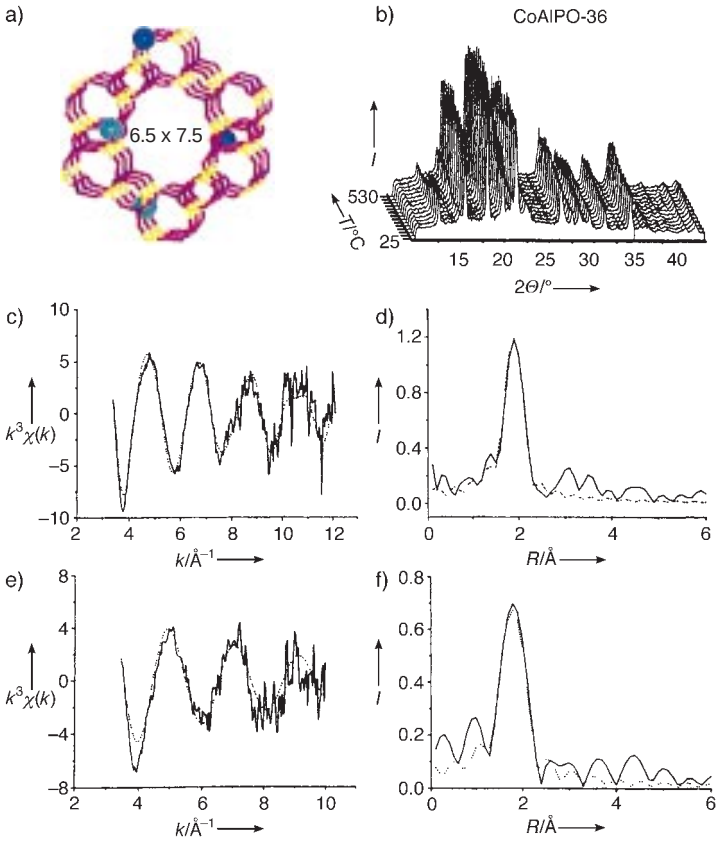

Figure 33. a) Computer graphic representation of the AlPO-36 structure in which cobalt ions have replaced some of the Al^{III} framework sites. After calcination in O_2, about 50% remain in the Co^{II} state (blue). b) XRD patterns of CoAlPO-36 catalysts recorded in situ during calcination in O_2 using combined XRD/XAS. The corresponding Co K-edge EXAFS data, recorded at room temperature and after calcination at 550 °C are shown in (c) and (e), respectively. The associated Fourier transforms (FT) are shown in (d) and (f). Solid line: experimental; dashed line: calculated.[185]

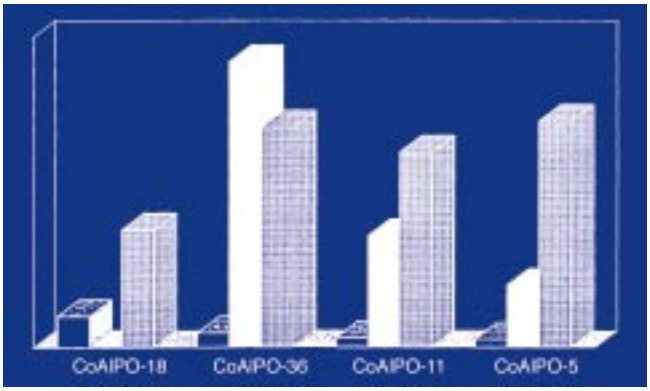

Figure 34. Bar-chart representation of the fraction of oxidized cobalt (dark), pore dimension (hatched), and catalytic activity (as % conversion; white) of CoAlPO-5, CoAlPO-11, CoAlPO-36, and CoAlPO-18 catalysts in the oxidation of cyclohexane in air (1.5 MPa) at 373 K.[185]

7.3. Baeyer–Villiger Oxidations with a Difference: The Facile Conversion of Ketones into Lactones

A century ago Baeyer and Villiger[187] reported the conversion of cyclic ketones into lactones using a peroxyacid as oxidant. For this purpose they used the most powerful oxidant then known, peroxomonosulfuric acid H_2SO_5, otherwise known as Caro's acid,. As has been explained in a recent admirable review,[188] Baeyer-Villiger oxidations are of major

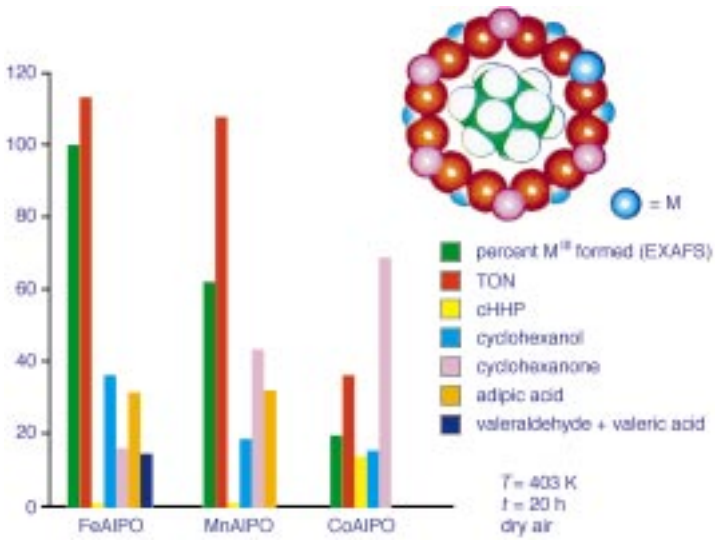

Figure 35. In the aerobic oxidation of cyclohexane, framework-substituted Fe^{III} ions yield more effective catalysts than Mn^{III} or Co^{III} ions for the same (AlPO-5) structure. TON = turnover number and cHHP = cyclohexylhydroperoxide.

synthetic interest in organic chemistry, with applications spanning such diverse areas as antibiotics, steroids, and many aspects of agrochemistry.

The peracids used for the first half-century or so of Baeyer–Villiger oxidations are now increasingly frowned upon (when not banned) because of environmental and other reasons, notably safety. The withdrawal from the market of 90 % H_2O_2 (which was the replacement for the original Caro's acid)—because of its highly explosive properties—has prompted greater use of lower grade peracids, and stimulated the search for effective catalysts (including enzymatic ones) that would enable Baeyer–Villiger reactions to be carried out with molecular oxygen.

Several heterogeneous catalytic systems based on hydrotalcites[189] or heteropolyoxometalates[190] have been used to effect Baeyer–Villiger oxidations. We argued, taking into account the redox properties[191] and pore dimensions of a range of metal ion substituted AlPOs, that Mn^{III}- and Co^{III}-substituted AlPO-36, as well as CoAlPO-18 and MnAlPO-18 (for smaller reactants), would be prime candidates as new Baeyer–Villiger catalysts. This is indeed the case; but these catalysts work under the so-called Mukaiyama conditions[192], whereby aldehydes are used sacrificially to create the desired peracid in situ (within the pores of the molecular sieve). This active peroxyacid then converts the cyclic ketone into the lactone outside the catalyst (Table 5).

The Mukaiyama conditions used by us and others are of considerable interest in that they offer attractive alternatives to the use of environmentally less acceptable oxidants such as CrO_3, $KMnO_4$, $Pb(OAc)_4$, RuO_4, Ag_2O, and $Co(acac)_3$ (many of which function stoichiometrically, at least in partial oxidations of alkenes, rather than catalytically).[193] H_2O_2 in the presence of an appropriate catalyst (for example, methyltrioxorhenium [194]) is also a good oxidant for the conversion of olefins into epoxides and cyclic ketones into lactones (Scheme 1[188]).

We have identified three different structures of potential catalysts that contain small amounts (up to 4 atom %) of either manganese or cobalt redox cations. The catalysts we have used are CoAlPO-36, MnAlPO-36, CoAlPO-5, MnAlPO-5, CoAlPO-18, and MnAlPO-18. The structure[195] of aluminum phosphate no. 36 (IZA structure code ATS) has well-defined, oval shaped channels (6.5×7.5 Å; see Figure 33), which, by appropriate preparative means (as descri-

Table 5. Baeyer–Villiger oxidation of ketones (Mukaiyama's conditions).[a]

Entry	Substrate	Catalyst	Pore size [Å]	T [K]	t [h]	TOF [h^{-1}][b]	Conv. [%]	Lactone selectivity [%]
1	cyclohexanone	CoAlPO-36	6.5×7.5	323	6	250	71	98[a]
2	cyclohexanone	CoAlPO-5	7.3×7.3	323	6	204	60	80[a]
3	cyclohexanone	MnAlPO-36[c]	6.5×7.5	323	6	257	78	98[a]
4	cyclohexanone	MnAlPO-5	7.3×7.3	323	6	207	64	82[a]
5	cyclohexanone	MgAlPO-36	6.5×7.5	323	6	[d]	20	64[a]
6	cyclohexanone	CoAlPO-18	3.8×3.8	323	6	[d]	22	62[a]
7	cyclohexanone	No catalyst	—	323	6	—	20	65[a]
8	cyclohexanone	CoAlPO-18[e]	3.8×3.8	323	6	166	48	72[a]
9	cyclopentanone	CoAlPO-36	6.5×7.5	323	6	238	58	92[b]
10	cyclopentanone	CoAlPO-5	7.3×7.3	323	6	185	46	76[b]
11	cyclopentanone	MnAlPO-36	6.5×7.5	323	6	246	61	94[b]
12	cyclopentanone	MnAlPO-5	7.3×7.3	323	6	187	50	77[b]
13	adamantan-2-one	CoAlPO-36	6.5×7.5	353	5	220	80	99
14	adamantan-2-one	MnAlPO-36	6.5×7.5	353	5	224	87	99
15	2-methylcyclohexanone	CoAlPO-36	6.5×7.5	323	6	201	65	86
16	2-methylcyclohexanone	MnAlPO-36	6.5×7.5	323	6	208	72	89

[a] Reaction conditions: substrate ca. 20 g; catalyst ca. 0.15 g; substrate:benzaldehyde = 1:3 (molar); O_2 (air) = 30 bar; Products: ε-caprolactone from cyclohexanone; δ-valerolactone from cyclopentanone. [b] TOF = moles of ketone converted per hour per mole of metal (Co, Mn) in the catalyst. [c] After the reaction the catalyst was filtered off, washed thoroughly with methanol, and calcined at 550 °C for 12 h. It was then re-used twice without significant loss of catalytic activity. The reaction mixture (after 6 h) was also analyzed by ICP (and AAS) and only trace amounts (< 2 ppb) of metal were detected. In a separate experiment, the solid catalyst (entry 3) was filtered off from the reaction mixture (at 323 K) after 2 h (conv. = 29 %) and the reaction was continued for a further 4 h (conv. after 6 h = 33 %) with the resulting filtrate (which also had trace amounts (< 2 ppb) of metal). No substantial increase in conversion was observed, clearly showing that the reactions are heterogeneously catalyzed. [d] The TOF have not been calculated in these cases, as the conversions obtained here are noncatalytic. [e] Hexanal was used instead of benzaldehyde.

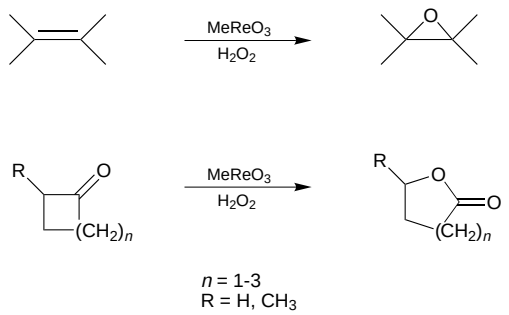

Scheme 1. Example of oxidation with H_2O_2/$MeReO_3$.

bed in Section 5), may be lined with a substantial number of either cobalt or manganese ions substituted in the framework in place of Al^{III} ions. Similarly, two other types of materials, AlPO-5 (AFI) and AlPO-18 (AEI) with pore dimensions of 7.3 and 3.8 Å, respectively, were synthesized with specific metal ions having identical concentrations. By calcining the freshly prepared MAlPOs samples (M = Co or Mn) in oxygen at 550 °C, the substituted ions may be converted[195] into their +3 oxidation states, to a degree that is dependent on the structure: the trend in the concentration of the +3 state in the three structures is AlPO-18 > AlPO-36 > AlPO-5.

Although the mechanistic details of the aerobic oxidation of ketones to lactones reported here still require elucidation, preliminary studies point to the fact that the active centers in the redox catalysts are the Co^{III} (or Mn^{III}) ions that line the micropores. We know for several reasons that the higher conversions are effected by the higher valence framework-substituted ions in the molecular sieve catalysts. Firstly, AlPO-36 analogues substituted with divalent ions, such as Mg^{2+} (or Zn^{2+}), that are not raised to higher oxidation states upon calcination in O_2 yield conversions not significantly different from those of the Mukaiyama sacrificial oxidations with benzaldehyde alone (see Table 5, entries 5 and 7). Secondly, in a parallel experiment using the smaller pore CoAlPO-18 (or MnAlPO-18), where all the transition metal ions are in the +3 oxidation state, and the diameter of micropores is 3.8 Å, no catalytic conversion of cyclohexanone into ε-caprolactone occurs when benzaldehyde is used as a sacrificial oxidant (Table 5, entry 6) because the latter is too large to gain access to the active site. (In addition, this clearly rules out the possibility of autoxidation by surface or transition metal impurities. It also constitutes proof that we are not dealing with homogeneous catalysis.) To substantiate that the autoxidation of the aldehyde is shape-selective, we used the straight chain *n*-hexanal, which is small enough to enter the 3.8 Å cages of the CoAlPO-18 catalyst as a sacrificial oxidant. The Baeyer–Villiger conversion of cyclohexanone into ε-caprolactone (Table 5, entry 8) freely ensues because the hexanal gains ready access to the framework active sites and forms the peroxyacid. Thus, large-pore CoAlPO-36 (or MnAlPO-36) and CoAlPO-5 (or MnAlPO-5) catalysts offer easy access to bulky sacrificial oxidants (such as benzaldehyde), and oxidize a number of ketones, including adamantan-2-one, to their corresponding lactones with very high selectivity.

The implications are clear: the aldehyde is first converted by O_2 at the active sites into the corresponding peroxyacid inside the micropores, and this peroxy acid, in the manner first outlined by Criegee[188, 196]—involving its initial nucleophilic attack at the carbonyl carbon atom—leads to the production of the lactone.[**] In addition, as in our study of the selective oxidation of cyclohexane,[167] there appears to be a clear trend in the dependence of catalytic activity on the combination of the pore-dimension of the molecular sieve and the framework-substituted ion: the ATS structure shows higher conversion and selectivity compared to AFI, and Mn^{III}-containing catalysts are slightly more active than their Co^{III} analogues. This agrees well with our estimation of the fraction of the metal ions that undergoes redox reaction.[191]

7.4. Epoxidation of Alkenes

The liquid-phase epoxidation of alkenes proceeds in the presence of hydroperoxides with catalytic systems that contain titanium(IV) ions (heterogeneously) or molybdenum(VI) ions (homogeneously). Thus the Shell process using Ti/SiO_2 and ethylbenzene hydroperoxide produces propylene oxide on an annual scale of more than one million tons of propylene oxide worldwide from propylene.[197] The ARCO HALCON process, on the other hand,[198] is carried out homogeneously using complexes of Mo or W.

Whereas the use of alkylhydroperoxides (in association with an appropriate catalyst) currently dominates the industrial scene, there have recently been attempts made to epoxidize alkenes using molecular oxygen. We begin this section, therefore, with a summarized account of our successful use of molecular-sieve catalysts for doing just that.

7.4.1. Epoxidation using Molecular Oxygen

As with the Baeyer–Villiger reactions described in Section 7.3, the center-piece of our heterogeneous catalyst is the aluminum phosphate molecular sieve AlPO-36, in which, as before, up to 4 atom % of Al^{III} sites have been isomorphously replaced by either Co^{III} or Mn^{III} ions. Again, as with the Baeyer-Villiger-Mukaiyama conditions outlined above, we exploit the easy autoxidation of aldehydes to promote the in situ formation of peroxy acids.[199]

By extending our earlier work on the design of redox molecular sieve catalysts for the aerobic terminal oxidation of linear alkanes (Section 7.1 above), for the selective oxidation of cyclohexane (Section 7.2), and for the Baeyer–Villiger oxidation of ketones to lactones (Section 7.3), we have achieved good conversions and selectivities for the epoxidation of cyclohexene and other alkenes using framework-substituted metal ions (M) in microporous alumina phosphate MAlPO-36 (M = Mn or Co) catalysts.[200]

[**] For the sake of completeness, it ought to be mentioned that the transition metal in the framework may itself be directly implicated in the Baeyer–Villiger reaction by, for example, catalyzing the addition of the peroxy species to the C=O group or by the formation of metal–peroxo species. In addition, the transition metal could also influence the second step of the Creigee mechanism.[196] I am grateful to Dr. Markus Dugal for drawing my attention to these possibilities.

Details of the synthesis (and structure) of the Mn^{II}- and Co^{II}-containing AlPO-36 molecular sieves have been given earlier (ref. [185]). Briefly, the Mn^{II} (or Co^{II}) ion is introduced to the template-containing precursor gel from which small crystals of phase-pure product appear. Upon calcination in O_2 at about 550 °C, the organic template (tetrapropylammonium hydroxide) is entirely gasified, leaving the oval-shaped cages (6.5 × 7.5 Å) of the resulting catalyst empty. X-ray absorption spectroscopy shows that, after calcination in O_2, some fifty per cent of the Mn^{II} (or Co^{II}) originally present (isomorphously substituting for Al^{III}) are converted into the Mn^{III} (Co^{III}) oxidation state, but that all these transition metal ions remain securely in tetrahedral coordination within the microporous AlPO framework. Others have also shown that Co^{II} ions in framework sites may be raised to the Co^{III} state without loss of structural integrity of the AlPO framework.[201–203]

In a typical experiment, 0.25 g of catalyst, 20 g of the alkene, and an alkene:benzaldehyde (mole) ratio of 1:3 are used. The reaction mixture is loaded into a stainless steel, high-pressure catalytic reactor (Cambridge Reactor Design) lined with polyethyl ether ketone (PEEK) and equipped with a mechanical stirrer and liquid-sampling valve. Dry air is pressurized into the reaction vessel (30 bar), and the reactor heated typically for 8 h at a temperature of 323 K. The results are summarized in Table 6. Results obtained with comparable, larger-pore (MAlPO-5) and smaller-pore (MAlPO-18) redox molecular sieve catalysts, the shapes of which are 7.3 × 7.3 Å and 3.8 × 3.8 Å, respectively, are also tabulated. It is noteworthy that conversions are consistently higher for both the MnAlPO-36 and CoAlPO-36 catalysts than with those of their larger-pore (AlPO-5) analogues. Almost certainly, the reasons for the superior performance of the MAlPO-36 catalyst is because a greater fraction (ca. 0.5 compared with 0.25) of the Mn or Co can be raised to the +3 oxidation state, which is the root cause of the catalytic activity. Significantly MgAlPO-36 is totally inactive; there is no redox ion in the framework of the micropores in this case, and hence no means of initiating the free-radical reactions that lead to epoxidation.

Table 6. Catalytic aerobic partial oxidation of alkenes.[a]

Substrate	Catalyst	*t* [h]	Conv. [%]	Product selectivity [%] epoxide	diol	others[b]
cyclohexene	CoAlPO-36	8	54	69	27	4
	Co-AlPO-5	8	47	74	15	11
	MnAlPO-36	8	62	77	19	5
	MnAlPO-5	8	44	77	13	10
	MgAlPO-36	8		No reaction		
α(+)-pinene	CoAlPO-36	8	54	84	–	16[c]
	CoAlPO-5	8	32	55	–	46
	MnAlPO-36	8	59	91	–	9
	MnAlPO-5	8	42	66	–	34
R-(+)-limonene	CoAlPO-36	8	46	78	–	23
	CoAlPO-5	8	28	39	–	61
	MnAlPO-36	8	51	87	–	13
	MnAlPO-5	8	30	51	–	49
styrol	CoAlPO-36	4	46	34	58.6	8
	MnAlPO-36	4	55	27	61.3	12
	MnAlPO-5	4	32	49	50.0	1
1-hexene[c]	CoAlPO-18	24	37	87	–	13
	MnAlPO-18	24	43	91	–	9

[a]Reaction Conditions: $T = 323$ K; 30 bar dry air; 35 g substrate; substrate: benzaldehyde mole ratio 1:3; solid catalyst 0.25 g. [b] These other products were mainly 2-cyclohexen-1-ol and 2-cyclohexen-1-one from cyclohexene; verbenol and verbenone from α-(+)-pinene; carveol, carvone and *trans*-carveyl acetate from (*R*)-(+)-limonene; and 1-phenyl-1,2-ethanediol from styrol. [c] hexanal was used instead of benzaldehyde.

Benzaldehyde molecules may freely enter the large (ca. 650 $m^2 g^{-1}$) internal surfaces of both MAlPO-36 and MAlPO-5 catalysts, thereby generating[203, 204] first PhCO· and then the PhCOOO· radicals, which, from the sequence of steps shown in Scheme 2, lead to the formation of benzoic acid and cyclohexene oxide. In this sequence, reaction 5 is known[205, 206] to proceed much faster than 6. This free-radical based epoxidation of cyclohexene (and the other alkenes listed in Table 6) is mechanistically quite distinct from the radical-free epoxidation of alkenes using alkylhydroperoxides and titanosilicate catalysts (which is discussed in Section 7.4.2).

1. $PhCHO + Mn^{III} \longrightarrow PhCO^{\cdot} + H^{+} + Mn^{II}$
2. $PhCO^{\cdot} + O_2 \longrightarrow PhCOOO^{\cdot}$
3. $PhCOOO^{\cdot} + PhCHO \longrightarrow PhCOOOH + PhCO^{\cdot}$
4. $PhCOOOH + PhCHO \longrightarrow 2\ PhCOOH$
5. $PhCOOO^{\cdot} + C_6H_{10} \longrightarrow C_6H_{10}O + PhCOO^{\cdot}$
6. $PhCOOOH + C_6H_{10} \longrightarrow C_6H_{10}O + PhCOOH$
7. $PhCOO^{\cdot} + PhCHO \longrightarrow PhCOOH + PhCO^{\cdot}$
8. $PhCOOOH + Mn^{II} \longrightarrow PhCOO^{\cdot} + OH^{-} + Mn^{III}$

Scheme 2. Probable mechanism of the transformations summarized in Table 6.

Other aldehydes may also be used as sacrificial oxidants provided they are small enough to gain access to the active sites situated at the inner surface of the molecular-sieve catalyst. Benzaldehyde is itself too large to enter Mn- or CoAlPO-18, but hexanal is not. Although it diffuses less rapidly into the MAlPO-18 structure than benzaldehyde does in AlPO-36, it nevertheless functions efficiently in epoxidizing hex-1-ene (Table 6).

Figure 36 is a composite representation of the versatility of a CoAlPO-36 (and MnAlPO-36) molecular-sieve catalyst in the aerobic oxidation of cyclohexane and in the aerobic (Baeyer–Villiger) lactonization of ketones (Mukaiyama

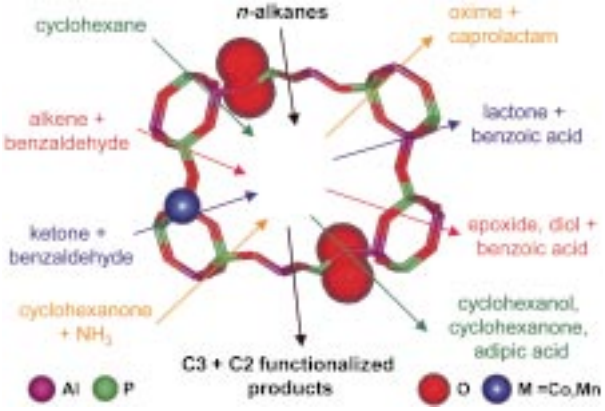

Figure 36. The AlPO-36 microporous structure with either Mn^{III} or Co^{III} ions at framework sites gives rise to excellent catalysts for the various processes.

conditions). For completeness, the ability of this engineered catalyst to effect ammoximation of cyclohexanone to yield the corresponding oxime and caprolactam, is also included.

7.4.2. Epoxidation using Alkylhydroperoxides

Epoxidation using a sacrificial oxidant, especially alkylhydroperoxides (such as tertiary butylhydroperoxide TBHP, cumene hydroperoxide CuHP, 2-methyl-1-phenyl-2-propyl hydroperoxide MPPH,[207] or ethylbenzene hydroperoxide EBHP, the latter being the reagent of choice in the Shell process for the epoxidation of propylene), is much easier to effect (in the presence of an appropriate catalyst) than doing so with molecular oxygen.[197, 198] One of the most widely used catalysts, certainly on a commercial scale, for the epoxidation of propylene with alkylhydroperoxides is the Ti^{IV}/SiO_2 heterogeneous catalyst that is utilized in the Shell process.[208]

With the arrival of the M41S family of mesoporous silicas, Corma et al.[209] were quick to realize that the larger pores of these mesoporous silicas opened up new possibilities for the epoxidation of larger alkenes, provided Ti^{IV} ions could be satisfactorily "placed" at the walls of the silica. In 1995 my colleagues and I embarked[210] on an extensive study of the preparation with a titanocene precursor of a uniquely powerful alkene epoxidation catalyst by using Ti^{IV} ions grafted on to MCM-41 mesoporous silica. By using the preparative and in situ characterizing techniques described earlier in this review, we established the following facts:

- all the Ti^{IV} centers are isolated (single site) surface species, spatially well-separated (when the Ti loading of the catalyst is low) from one another
- the atomic architecture of these Ti^{IV}-centered catalytically active sites is quantitatively defined
- effectively they are titanol groups tripodally linked through Ti-O-Si bonds to the surfaces of the mesoporous silica support
- numerous additional spectroscopic studies (in addition to X-ray absorption spectroscopy,[25, 210] including diffuse reflectance,[211] and UV/Vis photoluminescence[212] measurements) leave[146] no doubt concerning the precise structure of the Ti(IV) centered active site, which is shown, along with its mode of creation, in Figure 37.

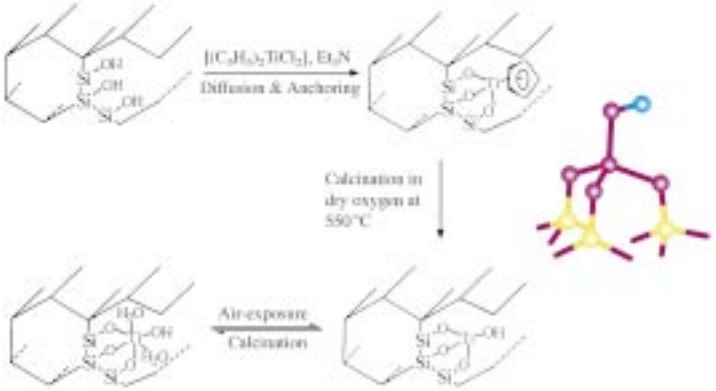

Figure 37. In situ X-ray absorption (XRA) measurements reveal that both the half-sandwich and calcined materials (derived from anchoring titanocene to the inner walls of MCM-41[210]) are tripodally attached to the silica.[146]

Combined in situ XRA and XRD investigations (as outlined in Section 6.3 and Figure 25) reveal how, from the changes in the X-ray absorption spectra in proceeding from the calcined state to the catalytically active form of the catalyst, the O-Ti bond lengths and the coordination number of the titanium active site is determined (Figure 38). We see clear evidence of the expansion of the coordination sphere of the active site during catalysts.

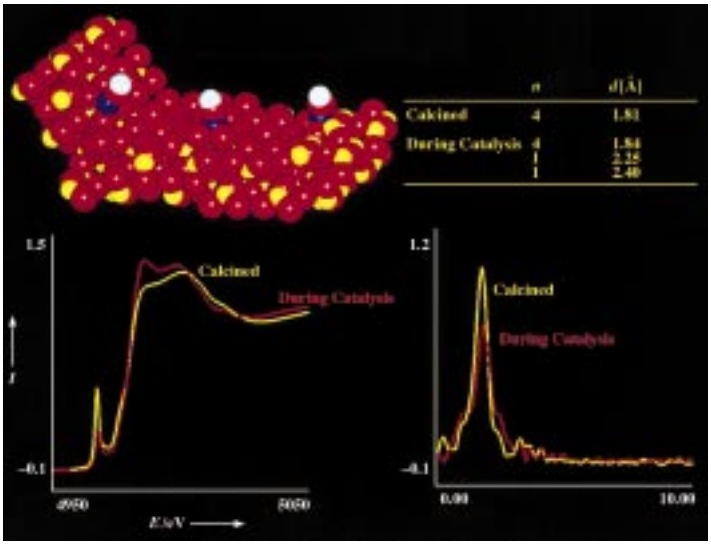

Figure 38. In situ XRA spectra of reacting epoxidation catalysts Ti↑MCM-41 (where the pendant OH groups attached to tripodally bound Ti^{IV} ions stand proud of the surface) reveal an expansion of the Ti coordination number from four to six.[25] EXAFS analysis corroborated by the observed changes in pre-edge absorption intensities, yield quantitative data pertaining to the reaction sphere of the active site. (The XRA evidence shows no change in valence of the Ti^{IV} ion. Cyclic-voltammetry studies with titanosilsesquioxane analogues (which are soluble) also show no sign of valence change of the Ti^{IV} during the course of catalytic epoxidation). The spectra here (bottom left) were obtained by in-situ X-ray measurements.

Computational studies,[213] using nonlocal density functional theory, reveal two interesting insights (Figure 39).

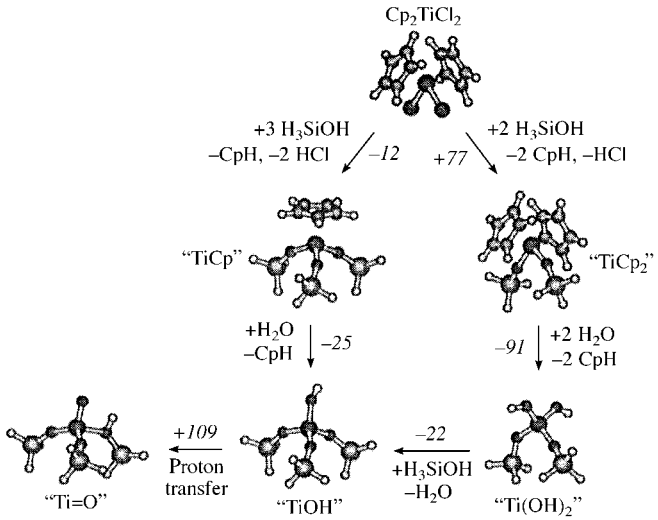

Figure 39. Results of DFT calculations[213] shows the structure of the active site of the Ti↑MCM-41 epoxidation catalyst; for further information see the text.

First, the "half-sandwich" intermediate formed during the preparation of the catalyst (see left part of the second row of Figure 39) is, as observed experimentally, much more stable than the butterfly-shaped intermediate shown on the right.[214, 215] Second, it predicts that as well as the TiOH active site, it is energetically almost as feasible to have a "diol" active site, in which the Ti^{IV} ion is bipodally bound to the siliceous surface, but with two, rather than one, OH groups attached to the active site. (Some experimental evidence for the occurrence of a small amount of this closely-related active site has been uncovered).[21, 212, 213]

Deeper analysis into the fundamentals of Ti^{IV}-centered catalytic epoxidation has revealed several other important facts which will be summarized in the next Section. These are:

- the enhancement (promotion) of catalytic performance by chemical modification of the active center
- proof that epoxidation of alkenes by alkylhydroperoxides is a radical-free and not a free-radical reaction
- the crucial importance of stereocongestion at, and hence access of reactant to, the active center.

7.4.2.1. Enhancing the Performance of a Supported Ti^{IV} Epoxidation Catalyst by Modifying the Active Center

In the epoxidation catalyst designated Ti↑MCM-41 (see Figure 38) the titanol group stands proud of the siliceous surface to which it is securely bonded owing to its manner of preparation (via a titanocene precursor). The Ti^{IV} active center is therefore much more accessible to the alkylhydroperoxide and alkene reactants than it is in the case of a Ti→MCM-41 catalyst[216] in which the Ti^{IV} centers are introduced during synthesis (Figure 40). This is borne out by

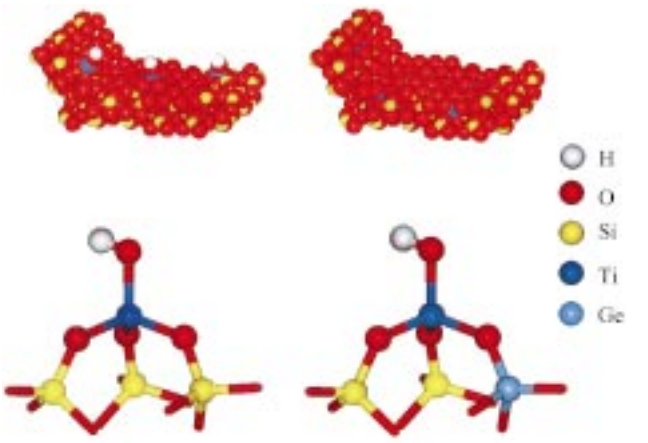

Figure 40. Top: Representation of parts of the epoxidation catalyst surface for (left) Ti↑MCM-41 and (right) Ti→MCM-41. Bottom: The $Ti^{IV}(OH)(OSi\equiv)_3$ active center is catalytically less powerful than the modified center $Ti^{IV}(OH)(OSi\equiv)_2(OGe\equiv)$. (See text and references [27] and [220].)

the more than tenfold enhancement in turnover frequency of conversion of cyclohexene by Ti↑MCM-41 over Ti→MCM-41 catalysts[217] (for both TBHP and MPPH). As we show in Section 7.4.2.3 it is much more convenient to explore the precise influence of accessibility to the Ti^{IV} active site by using titanosilsequioxane derivatives. But by using various strategies derived from organometallic chemistry[218] it is relatively straightforward to alter the immediate composition of the atoms to which the Ti^{IV} active center is attached. By using volatile Bu_4Ge in combination with in situ FTIR and X-ray absorption (Ge and Ti K-edge studies) and ex situ HREM (with X-ray emission imaging) it was possible to confirm the replacement of one of the three O-Si groups to which a Ti^{IV} active center is anchored (to a mesoporous silica) by a 0-Ge group (Figure 40).[219, 220] Given the great similarity in the chemistry of silicon and germanium, it is not clear where the source (electronic?) of this catalytic promotion lies. It has also been found that introducing tin (but in a rather less precise manner) to the vicinity of the Ti^{IV} active site diminishes the catalytic performance.

It is not simply the atoms in the immediate environment of the active site that govern the overall catalytic performance. In any reaction involving selective oxidation of alkenes or alkanes, hydrophobic/hydrophilic effects[221,222] may have a large effect, as is well testified by many studies.[223, 224] Epoxidations at active sites grafted on to the inner surfaces of MCM-41 mesoporous silica are no exceptions. We have shown[224] (admittedly using an engineered vanadyl active site rather than a titanol one) that "placing" methyl groups in the vicinity of the active site significantly enhances the catalytic performance in the epoxidation of cyclohexene, and this enhancement arises primarily because of facilitation of the approach of the reactants to the active site.

7.4.2.2. Mechanistic Considerations: Epoxidation with Alkylhydroperoxides is a Radical-Free Reaction

Several experiments that we have carried out in association with K. U. Ingold,[217] leave little doubt that no free radicals are implicated to any significant extent in the Ti^{IV}-catalyzed epoxidations of alkenes using alkylhydroperoxide as an oxidant. If radicals had been involved in these oxidations we would expect to obtain very little cyclohexene oxide relative to the yields of cyclohexenal, cyclohexenone, and (*tert*-alkyl)cyclohexenyl peroxide (Scheme 3). Likewise, by using MPPH in place of TBHP, products derived from benzyl radicals would be formed. These products were indeed produced when reactions were initiated by UV irradiation of the reactants in the absence of catalysts.

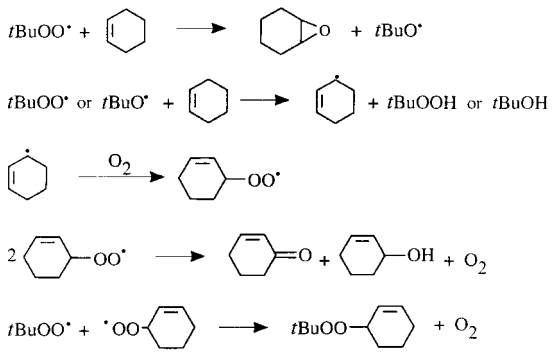

Scheme 3. Possible reaction between cyclohexene and TBHP under conditions that favor the formation of free radicals.

Another compelling argument for a radical-free mechanism comes from our oxidation studies of *cis*-stilbene with *tert*-butyl peroxyl radicals, generated by the thermal decomposition of di-*tert*-butyl hyponitrite in the presence of TBHP. Here, because of Reaction (8): we expect, and do indeed find,

$$t\mathrm{BuO{-}N{=}N{-}O}t\mathrm{Bu} \xrightarrow{\triangle} \mathrm{N_2} + 2\,t\mathrm{BuO}^{\bullet} \xrightarrow{2\,t\mathrm{BuOOH}} 2\,t\mathrm{BuOH} + 2\,t\mathrm{BuOO}^{\bullet} \quad (8)$$

benzaldehyde and *trans*-stilbene oxide in approximately equal amounts, together with a small quantity of *trans*-stilbene. However, reaction of *cis*-stilbene with TBHP or MPPH in the presence of our Ti^{IV}-centered epoxidation catalyst, gives *cis*-stilbene oxide as the only oxidation product. It is therefore clear that epoxidation proceeds by non-radical chemistry, and our experiments indicate that the alkene and the peroxide must both be coordinated to the Ti^{IV} center for reaction to ensue. This is borne out by the increased coordination number measurable from in situ EXAFS studies (see Figure 38).

7.4.2.3. Exploring the Influence of Steric Congestion on the Catalytic Performance of Ti^{IV} Active Centers using Soluble Titanosilsequioxane Analogues

The remarkable similarity in the local structures of the established active site in our Ti/silica epoxidation catalysts and that of the heteroatom vertex in a titanosilsesquioxane such as $R_7Si_7O_{12}TiOX$ (see Figure 4), studied earlier by Feher,[225] Roesky,[197] and others[226, 227] offers abundant scope for detailed investigations into the mode of operation of our (single-site) heterogeneous catalyst through the agency of a large range of soluble, strictly comparable, model compounds. Take, for example, the incompletely condensed silsesquioxane $[(cis\text{-}C_5H_9)_7Si_7O_9(OH)_3]$ with titanium isopropoxide $Ti(OiPr)_4$. Three of the four Ti(O*i*Pr) ligands will substitute for the three pendant OH groups on the incomplete silsesquioxane box (Scheme 4).[230] There is a tendency for the resulting $(C_5H_9)_7Si_7O_9TiOiPr$ to dimerize. When the same incompletely condensed silsesquioxane is treated with another titanium tetraalkoxide ($Ti(OR)_4$), the corresponding titanosilsesquioxane complexes $[(cis\text{-}C_5H_9)_7Si_7O_{12}TiOR]_n$ ($n = 1$, 2) are also formed (Scheme 4). The dimeric titanosilsesquioxanes ($n = 2$) may form yielding a situation in which the tripodally bound (to -O-Si) titanium atom becomes five-coordinated, one of the Ti-O links being (determined from X-ray crystallographic studies)[228] so long (ca. 2.25 Å) as to indicate the presence of a dative bond (compare with results shown in Figure 38). Detailed catalytic studies[229, 230] of the epoxidation of cyclohexene in $CDCl_3$ solution at 45 °C in the presence of each of the titanosilsesquioxanes enumerated above leave no doubt that steric accessibility to the Ti^{IV} active site is the principal determinant of catalytic performance.

Titanosilsesquioxanes also offer further scope to explore the relative importance in catalysts (through their Ti^{IV} active centers) of ions that are bipodally or monopodally attached, through an oxygen atom, to a tetrahedrally coordinated silicon atom. There is no doubt that, so far as durability and sustained activity of such catalysts go, a tripodally bound

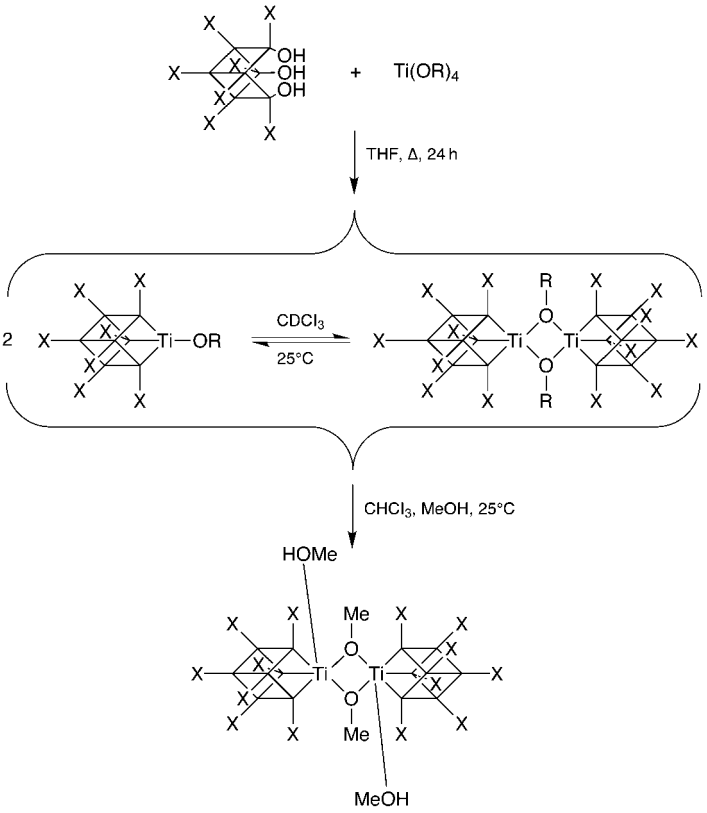

Scheme 4. Synthetic scheme and proposed structures for titanosilsequinone; the unlabeled corners are Si atoms, the edges O bridges. X = cyclopentyl, cyclohexyl; R = Me, Et, *n*Pr, *i*Pr, *n*Bu, *t*Bu, $Me_2CH_2CH_2CH_2$.

Ti^{IV} center is superior. Preliminary experiments[231] using silsesquioxanes in which the titano-vertex is as shown in Figure 4 (right), show that a Ti^{IV} ion juxtaposed to Ge (through oxygen) is, as seen in the case of the heterogenous catalysts,[219] the most powerful epoxidation catalyst.

7.4.2.4. Converting an Inactive Four-Coordinated Ti^{IV} Compound into an Active Epoxidation Catalyst by Grafting it to a Silica Surface

Deeper insights into the supreme importance of steric accessibility of the reactants to a central, potentially catalytically active four-coordinated titanium atom are well illustrated by the comparative behavior of the two entities schematized in Figure 41. The molecule on the left displays zero catalytic activity in the epoxidation of cyclohexene (under the same conditions as employed for the titanosilsesquioxanes described above). When, however, three of the $OSiPh_3$ groups are removed (by refluxing in THF) so as to yield the species on the right, this now exhibits catalytic activity some eighty per cent of that of the Ti↑MCM-41 catalyst in ref. [210]). Indeed, upon calcining this material so as to generate a tripodally bound titanol group, as in Figure 4 (left), the material has an activity as good as that of the titanocene-derived analogue.[231] Molecular dynamics calculations help to understand how an increase in the accessibility to the central titanium engenders catalytic activity (Figure 42).

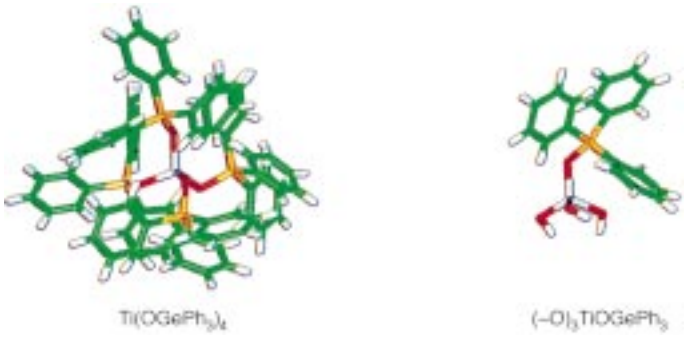

Figure 41. The tetrahedrally bonded Ti^{IV} center in the molecule on the left and also in its silico analogue $Ti(OSiPh_3)_4$ is inactive as a catalyst in cyclohexene epoxidation with alkyl hydroperoxides (such as THBP).[231] When, however, either of these is tripodally anchored to mesoporous silica so as to leave only one pendant $OGePh_3$ (or $OSiPh_3$) group (right) the Ti^{IV} ion becomes catalytically active (see Figure 42).

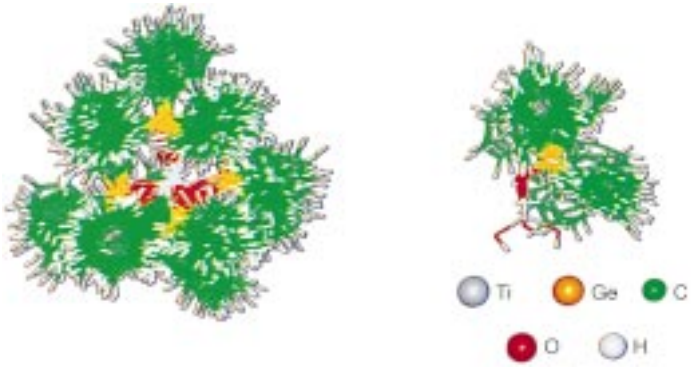

Figure 42. The molecular dynamic simulations for each of the clusters in Figure 41 were carried out at 500 K for a duration of 5 ps, using a 1 fs timestep. The Ti atom and the three anchoring oxygen atoms were kept fixed during the simulation for the surface-anchored cluster. These representations consist of superposition of frames from the simulation taken at 200 fs intervals. By comparing these two views it is clear that the access of the reactants is far greater for the right than for the left entity. The latter shows how effectively the four triphenyl groups shroud the central potentially catalytically active (and coordinatively unsaturated) Ti^{IV} ion.

7.5. Engineered, High-Area, Shape-Selective Solid Acid Catalysts

Ever since Weisz et al.[43, 44] demonstrated the power and widespread utility of ZSM-5 as a solid acid catalyst for the shape-selective dehydration of methanol to useful hydrocarbons, there have been intense research efforts on two fronts. First, the quest for new microporous solids that are engineered so as to limit (shape-selectively) the process of dehydration of methanol so as to favor the production of only light olefins (ethene, propene, and butene) rather than of benzene, toluene, and xylene. Second, the preoccupation with the mechanism of the dehydration, and, in particular, with the precise steps that lead to the formation of C-C bonds. Greater progress has been achieved in the first than in the second of these two efforts.

Considerable efforts have also been made to generate new, solid acid catalysts that favor the skeletal isomerization of 1-butene or 1-pentene into their branched chain analogues. For example, conversion of 1-butene into 2-methylpropene is of great value as a stepping stone towards the production of *tert*-butyl methyl ether (MTBE), a valuable (high-octane) constituent of petrol (gasoline).

In collaboration with K. I. Zamaraev and his associates, my colleagues and I established[232, 233] that the catalytic dehydration of all alcohols takes place over strong Brønsted acid sites, rather than over Lewis acid ones. Several different HZSM-5 catalysts (some of small, some of large crystallite size, and some partially ion-exchanged such as NaHZSM-5) were investigated and all compared with amorphous aluminosilicate specimens with larger pore diameters but with comparable acid strength. Detailed investigations of the catalytic dehydration of all four isomeric butanols were made and yielded an unambiguous answer (Figure 43). The catalytic activity of all the catalysts is directly proportional to the concentration of the bridging hydroxyl Al-O(H)-Si groupings (that is, the Brønsted acid sites) and does not correlate with the concentration of strong (or weak) Lewis acid sites. Further proof that Lewis acid sites are not catalytically active, whereas Brønsted ones are, comes from the fact that preadsorbed acetonitrile (which affects Lewis but not Brønsted sites) has no effect on the rate of dehydration, whereas increasing

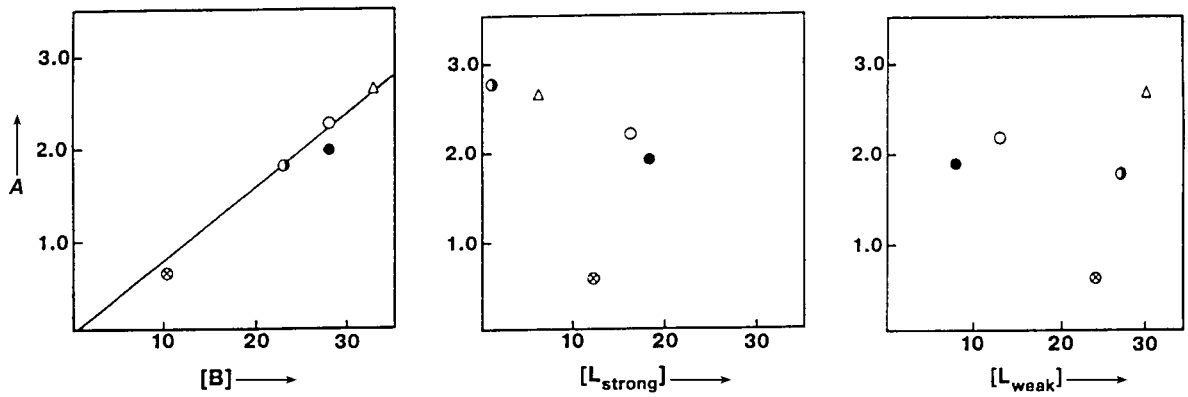

Figure 43. Observed[233] relation between the acid catalytic activity A (in 10^{17} molecules per second and per gram of catalyst) of a series of ZSM-5 samples (△ (NaHZSM-5, sample 2), ◑ (HZSM-5, sample 3, ● (HZSM-5, sample 4)) and an amorphous aluminosilicate (⊗) in the dehydration of 2-butanol to butene and the concentration of Brønsted (B) and Lewis acid (L) sites.

amounts of preadsorbed pyridine (which becomes attached to Brønsted sites) progressively decreases the rate of dehydration of 2-butanol. (The concentration of the Brønsted Al-O(H)-Si sites was measured by four disctinct methods: ^{1}H NMR spectroscopy, (quantitative) IR spectroscopy, by "poisoning" titration with pyridine, and from direct analysis of the Al content).

7.5.1. DAF-4 and STA-2: Catalysts that Generate Light Olefins in the Dehydration of Methanol

Success on this front consists of designing a microporous solid, the pore apertures and diameters of which function as constraints for the production of bulky hydrocarbons, but still favor the generation of the light olefins mentioned above. Much interest has been shown both academically and industrially in developing appropriate catalysts for such purposes.[234–236]

By careful choice of an organic template (as the structure-directing agent, see Section 5), my colleagues and I prepared a new shape-selective microporous solid acid catalyst that has a structure akin to that of the naturally occurring, zeolitic (aluminosilicate) mineral levyne[237] (idealized formula: $Ca_9[Al_{18}Si_{36}O_{108}]\cdot 50\,H_2O$), which is isotypic with the previously reported synthetic material ZK-20.[238] This new, designed catalyst, known as DAF-4,[62] is an aluminophosphate in which up to 20 % of the Al^{III} framework ions is replaced by Co^{II} (or other divalent) ones. Our aim in designing it was to arrive at a microporous solid acid catalyst in which the cavities were somewhat different from those in CoAlPO-18 and SAPO-18 (see Section 5).

We judged it desirable to "create" cavities that were slightly smaller in one direction than they are in CoAlPO-18, and larger in the other so as to secure the shape selectivity that would prevent the methanol yielding heavier alkenes upon dehydration. With the knowledge that a 1,4-diaminocyclohexane template gives rise to a porous layered $AlPO_4$ structure[239] we reasoned that 1,2-diaminocyclohexane would favor the formation of a microporous solid with 8-ring windows (that is, with eight oxygen atoms lining the window), as in the chabazitic materials SAPO-34, CoAlPO-18, and CoAlPO-44, but significantly different in its cavity shape. However, because 1,2-diaminocyclohexane was found to be unstable under the hydrothermal conditions of synthesis, we chose instead the more stable 2-methylcyclohexylamine as the template (these templates are spatially similar because the CH_3 group occupies almost the same space as a protonated NH_2 group). Crystallization from a gel of composition $xCoO_n$: $(1-x/2)Al_2O_3$:$ySiO_2$:$(1-y/2)P_2O_5$:$25\,H_2O$:$1.0\,C_7H_{15}N$, where $x = 0-0.4$ and $y = 0-0.2$, under autogenous pressure for 7 d at 200 °C resulted in the production of the desired solid. In its Co^{II} substituted form, DAF-4 transforms methanol with greater than 75 per cent conversion at 350 °C into ethene and propene, with a selectivity of about 60 % and about 20 % for the two alkenes, respectively.

Wright and his colleagues[64] have succeeded in producing another, well-defined microporous solid acid (AlPO) catalyst known as STA-2 (see Figure 8). In its Mg^{II}-substituted form this catalyst also converts methanol with high efficiency into ethene and propene. The similarity in cage dimensions and disposition of (protonic) acid sites in these two catalysts is illustrated in Figure 44. So far as the mechanistic details of methanol dehydration (leading to alkenes) is concerned, ingenious proposals have been made by van Santen et al.,[240] by Catlow et al.,[241] as well as by others.[242–244] One plausible explanation, which is backed up by reliable computational evidence, is shown in Scheme 5.

7.5.2. Skeletal Isomerization of 1-Butene: The Merits of Boron-Substituted Zeolite β

Here, the aim is to arrive at maximal amounts of 2-methylpropene (Figure 45). Previous work (see for example refs. [245, 246]) has shown that both aluminosilicate and aluminophosphate microporous acid catalysts are viable catalysts for this conversion. Recent work[247] has shown that, contrary to expectation, certain borosilicate microporous materials are very good catalysts for this isomerization. This fact again highlights how subtle is the dependence of Brønsted

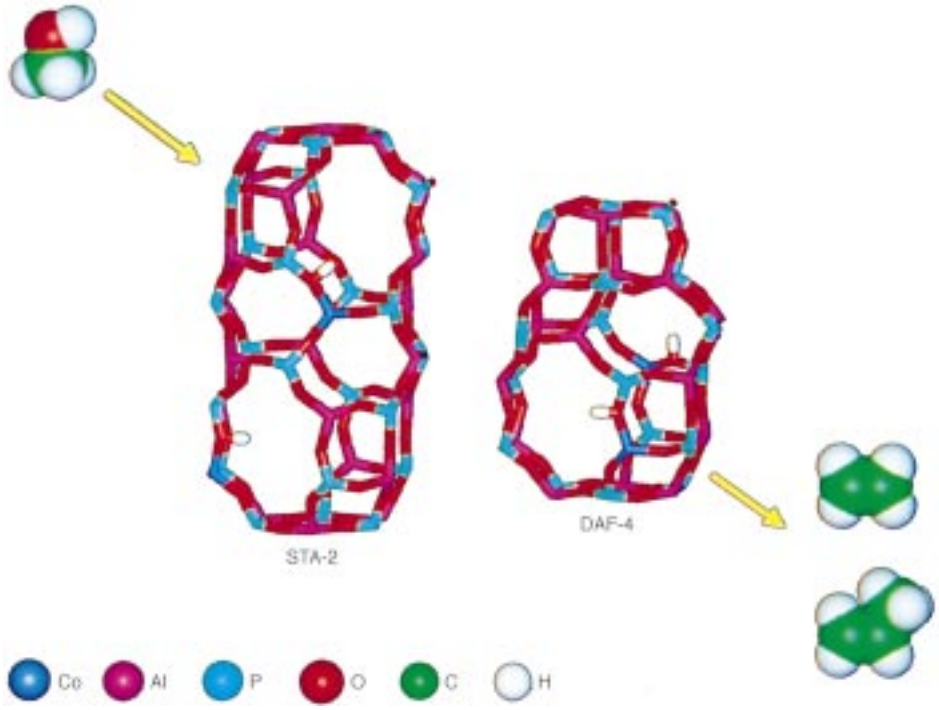

Figure 44. The solid acid, molecular sieve catalysts St. Andrews No. 2 (STA-2)[64] and Davy-Faraday No. 4 (DAF-4),[62] each with a cage diameter of ca. 3.8 Å function as excellent shape-selective catalysts in the preferential conversion of methanol into the light olefins ethene and propene.

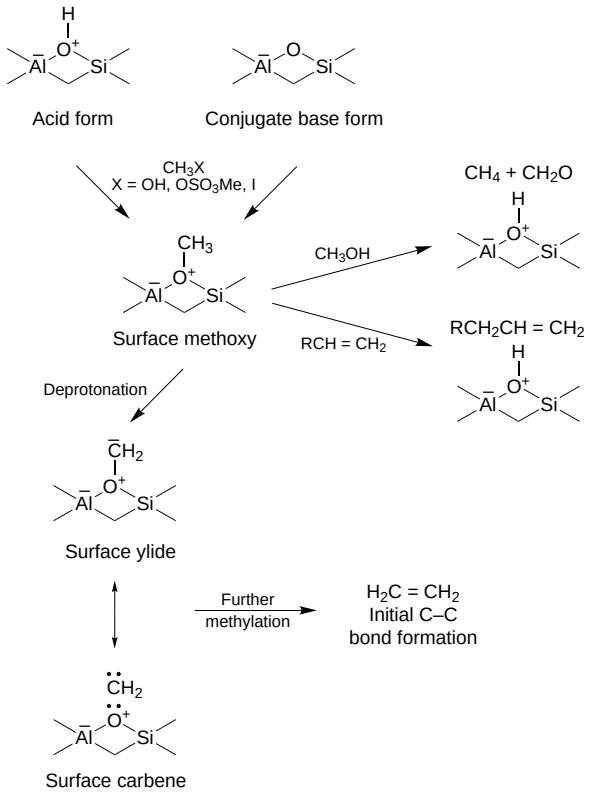

Scheme 5. Methyloxonium mechanism for the dehydration of methanol.[241]

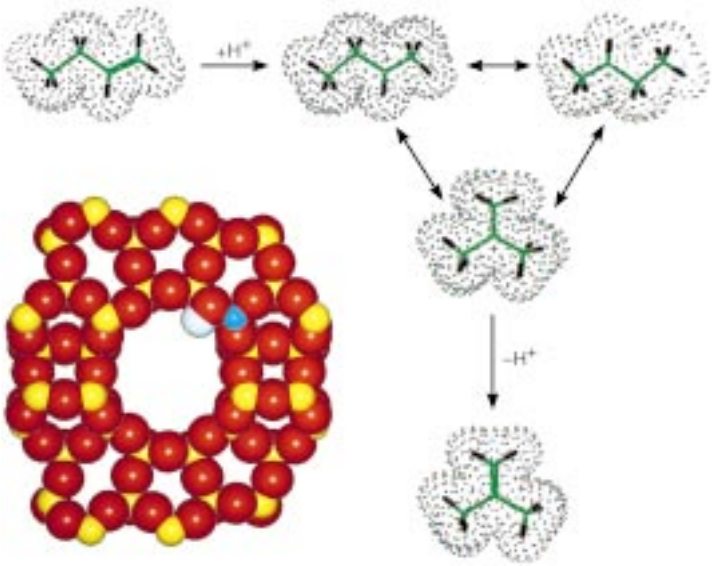

Figure 45. The acid-catalyzed isomerization of 1-butene (top left) to 2-methylpropene (bottom right) occurs rapidly on the inner walls (which provide protons) of microporous catalysts such as DAF-1[60] (see Figure 8) and boron-substituted zeolite β (shown schematically).[247]

acid strength (and hence catalytic performance) upon the precise structure of the microporous silicate into which the boron is incorporated (tetrahedrally). Work done jointly with P. A. Wright on a series of boro- and alumino-silicate structures (such as ZSM-12, ZSM-48, and zeolite β) with comparable values of Si/Al and Si/B ratios, strongly imply that long-range electrostatic effects profoundly influence the Brønstedt activity of certain sites.

7.6. Designing Durable, High-Performance Bimetallic Catalysts for the Hydrogenation of Alkenes

Bimetallic nanoparticles possess catalytic properties that differ sharply from those of solid solutions of the bulk metals. This was one of the key conclusions to emerge from the early work of Sinfelt, [248] and its veracity has been multiply attested. Among the many studies of bimetallic catalysts, some are of great technological importance (for example, Pt-Re, Pt-Ir, and Pt-Rh) in processes such as the reforming of naphtha and, to a lesser degree, in the control of autoemissions.[249] The current interest in the use of bimetallic catalysts is largely a consequence of the enhanced activity and selectivity that may be achieved by two metals working synergistically. However, despite considerable effort, the preparation of these systems by metal-salt deposition and subsequent calcination followed by reduction to the active, low-valent species is not always reliable and has many drawbacks, the greatest of which is the lack of control over size, morphology, and homogeneity of the resulting bimetallic nanoparticles. Preformed colloids however offer useful scope in these contexts. But there is a crucial practical factor: nanoparticles tend to migrate, coalesce, and sinter, thereby leading to drastic loss of active surface and hence of catalytic performance.

All these disadvantages are overcome if mixed carbonylmetalate clusters are used as the precursors of the dimetal nanocatalysts. Moreover, if one of the metals in the cluster is oxophilic, it will tend to be anchored securely to a siliceous (large-area) support. In our group[250–252] we have taken steps to circumvent all the above-mentioned disadvantages, and have indeed used a number of mixed carbonylmetalates as a means of producing well-dispersed, dimetal nanoparticles of composition Ag_3Ru_{10},[250] $Cu_4C_2Ru_{12}$,[251] and Pd_6Ru_6.[252] The strategy employed is schematized in Figure 46.

In situ X-ray absorption and FTIR spectroscopies as well as ex situ high-resolution electron microscopy (see Section 6) were used to chart the progressive conversion, by gentle thermolysis of the parent carbonylates into the derived, dimetal nanoparticle catalysts. Thus, for the anionic cluster carbonyl species $[Ru_6C(CO)_{16}Cu_2Cl]_2[PPN]_2$ —where PPN = bis(triphenylphosphane)iminium)—separate recorded copper and ruthenium K-edge X-ray absorption spectra yield a detailed structural picture (Figure 47) of the active, approximately 15 Å diameter catalyst. It is a rosette-shaped entity (Figure 48) in which twelve exposed Ru atoms are connected to a square base composed of relatively concealed Cu atoms. These, in turn, are anchored by four oxygen bridges to four Si atoms of the mesopore lining.

The dimetal catalysts prepared in this way exhibit no tendency to sinter, aggregate, or fragment into their component metals during use. The nanoparticles perform well in the catalytic hydrogenation of 1-hexene—a detailed kinetic study[251] at 373 K and 20 bar H_2 shows the maximum turnover frequency (TOF) [(mol_{substr}) per ($mol_{cluster}$) per hour] to be 51200, with an average value of 22400—and also in the hydrogenations at 65 bar H_2 and 373 K of diphenylacetylene, phenylacetylene, stilbene, *cis*-cyclooctene, and D-limonene, the average TOF being 17610, 70, 150, and 360, respectively.

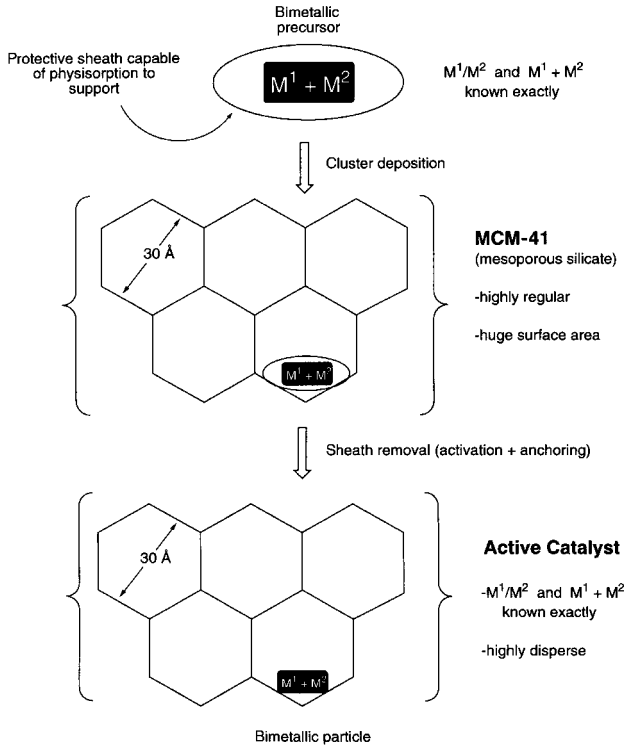

Figure 46. The strategic principles employed[250–252] to prepare high-performance, dimetal nanoparticle catalysts encapsulated within mesoporous silica (MCM-41).

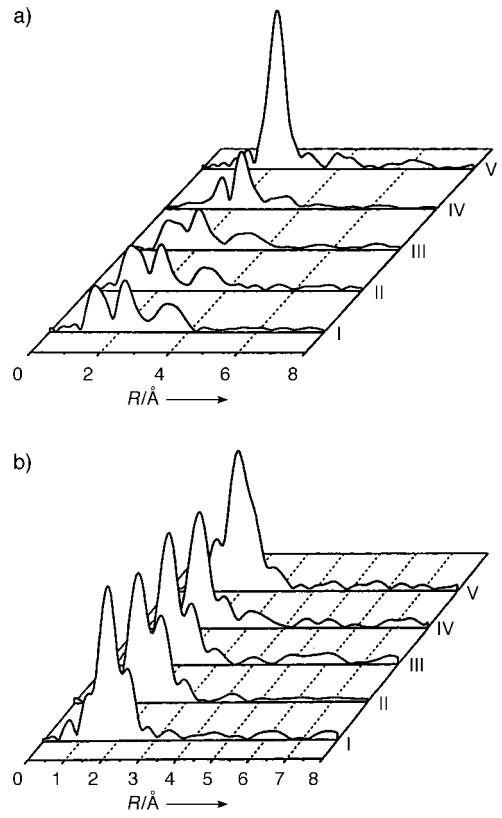

Figure 47. Fourier transforms of the EXAFS data taken during the gentle thermolysis of the mixed carbonylmetallate precursor $[Ru_6C(CO)_{16}Cu_2Cl]_2^{2-}$ (I) from its original state (II), through to the encapsulated and heat-treated product (III 80 °C, IV 130 °C) to yield the active $Cu_4C_2Ru_{12}$ nanocatalyst (V 180 °C).[251] a) Ru K-edge, b) Cu K-edge.

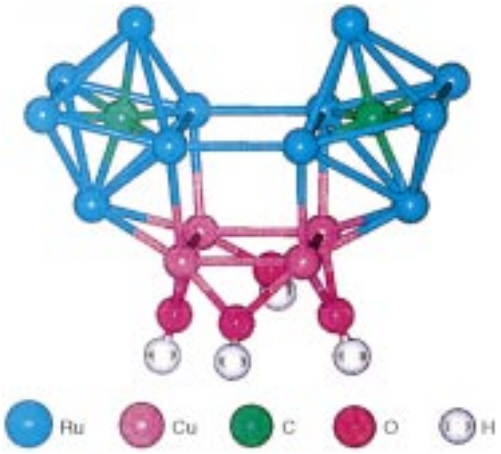

Figure 48. The EXAFS results lead to a picture of the active catalyst, which is ca. 15 Å in diameter, and which is rosette-shaped; for further information, see the text and Figure 49.

We now return to the structure shown in Figure 48. Bromley et al.[253] have recently used this as a starting model for various computational techniques to determine the energy-minimized structure. By applying molecular dynamics methods based on interatomic potentials to this "precursor" mixed-metal carbide nanocatalyst, the structure was optimized to find low-energy configurations. This procedure was carried out for both the cluster in free space, and for a number of silica-cluster bonding scenarios. Fully quantum mechanical ab initio density functional theory (DFT) was applied to each of a number of possible cluster structures, optimized by the molecular dynamics calculations. DFT single-point calculations were performed on each cluster so as to compare their total energies. With preference given to the lowest energy clusters, but also guided by our experimental EXAFS results, candidate clusters were chosen. These were then further energy-minimized and geometry optimized using DFT.[254] The resulting geometry of the cluster, especially when it is bound to a silica surface, agrees well with our EXAFS data (Figure 49). Significantly, it is seen that the carbon atoms,

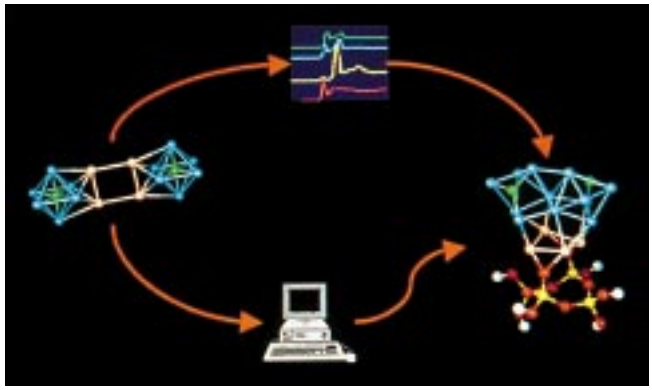

Figure 49. A combination of molecular dynamics energy minimization and density functional computations (shown here as a computer) on the "initial" $Cu_4C_2Ru_{12}$ cluster (left) leads to a new structure (right) in which the carbon atoms are situated at the surface of the silicon-anchored cluster.[253] The structure is in good agreement with that determined by experimental EXAFS data (top).

initially located at the centers of Ru_6 octahedra in the parent mixed carbonylmetalate tend to take up positions at the surface of the catalytically active nanoparticle catalyst. The precise significance of this fact, which would have been almost impossible to establish by any other technique, remains to be discovered.

7.7. Designing Constrained Chiral Catalysts: Heterogenized Organometallics For A Range of Organic Reactions

In the pharmaceutical and agrochemical industries, as well as in the expanding fields of fragrances and flavors, there is a growing demand for enantiomerically pure products. Not surprisingly, therefore, increased attention is now being given to the design of powerful enantioselective catalysts. After all, only a relatively minute amount of the requisite chiral catalyst is needed to generate large amounts of the targeted chiral product. But how does one set about designing the requisite catalyst? Leaving aside engineered enzymes and other biological, macromolecular chiral catalysts, the most popular procedure to date has been to "construct" the right homogeneous transition metal-based complex, which generally operates at low temperatures and at moderately high pressures.[14, 255–257]

To date homogeneous catalysts in which metal ion complexes are attached to carefully designed chiral ligands are still the most effective enantioselective catalysts. But it has been appreciated for some time—see, for example, the early review by Burwell[258]—that heterogeneous catalysts would be preferable owing to a variety of intrinsic practical advantages that are directly connected to such factors as ease of separation, handling, and recovery, not to mention their higher potential for regeneration and re-use. Awareness of such advantages prompted Schwab[259] several decades ago to modify metal surfaces such as Raney nickel with certain stereospecific adsorbents so as to confer enantioselectivity on the resulting catalyst. Much later, Akabori and co-workers[260] in Japan reported the first reasonably reliable metal-catalyzed asymmetric hydrogenation. Their preparation consisted of metallic Pd supported on silk and this was successful in the hydrogenations of oximes and ketones.

As Swiss workers have recently emphasized,[261, 262] there are only a limited number of possible approaches to the design of enantioselective heterogeneous catalysts. One of these seeks to find (or prepare) solids in which the active sites are located in a chirally discriminating environment. To be precise, this approach encompasses (but is not restricted to) the use of chiral solids (that is those that exhibit a chiral space group, such as $P2_12_12_1$, so that an active site in any one of the three mutually perpendicular crystallographic screw axes is intrinsically prochiral). Stratagems of this kind were used in early work on photoactive prochiral molecular crystals.[263, 264]

Another approach entails the phenomenon of chiral leaching, in which a cavity may be created in a solid by a stereospecific etchant (such as that which occurs when D- or L-tartaric acid attacks the sites of screw dislocations at the cleavage surfaces of calcite[265]). Related to this is the recent ingenious achievement of Gellman et al.[266] in creating chiral kinks (produced when monatomic terraces interact) on single crystal faces of metallic Ag. However, neither of these two approaches seem particularly well-suited for routine use or scale-up. Chiral imprinting, which involves the interaction of a chiral template with a solid such that, upon removal of the template, a chiral imprint or "footprint" is left, might prove to be a powerful technique for the preparation of enantiomerically discriminating catalysts, but is still in its very early stages.

In contrast, the last family of approaches to be considered here, namely the *creation of a chiral environment for the active sites* has already been shown to be viable for a range of reactions. One way forward, therefore, is to graft a chiral ligand/modifier (which exerts stereochemical control) to a catalytically active (but not itself stereoselective) solid, a classic example being the use of adsorbed cinchona alkaloid on a Pt surface for hydrogenation. Another is to graft an "ordinary" active site to a chiral solid support. Yet another entails the heterogenization (or immobilization) of chiral homogeneous transition metal complexes on a large-area solid support. We have focused on the last of these three options.

7.7.1. The strategy

As mentioned earlier, the availability of a large range of materials in well-defined, mesoporous forms unlocks new possibilities in solid-state catalysis as they provide uniquely advantageous supports for the development of new chiral catalysts. Indeed, the large diameter channels (see Figures 9 and 10) of the MCM-41 family of mesoporous silica permit the direct grafting of complete chiral metal complexes and organometallic moieties on to the inner walls of these large surface solids by a variety of ways that include functionalizing the pendant surface silanol with organic groups such as alkyl halides, amines, carboxylates, and phosphanes. This opens routes to the preparation of novel catalysts consisting of quite large concentrations of accessible, well-spaced, and structurally well-defined active sites. One may, therefore, expect, and we do indeed find (as shown below), that such heterogeneous solids catalysts behave at least as efficiently as their homogeneous counterparts and sometimes with far superior enantio- or regioselectivity.

Various kinds of organometallic, chiral catalysts may be tethered to the inner walls of a mesoporous host employing the strategy adumbrated in Figure 50. The key features here

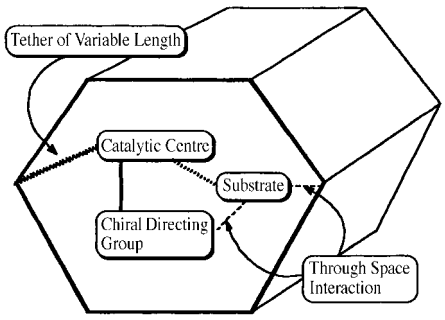

Figure 50. Schematic representation of the confinement concept in which the substrate is incarcerated in the cavity of a chiral modified mesoporous host and leads to chiral heterogeneous catalysis.[269]

are the reactant's (substrate's) interaction with both the pore wall and the chiral directing group. The confinement of the reactant (substrate) within the mesoporous channel should lead to a larger influence of the chiral directing group on the orientation of the substrate (reactant) relative to the reactive catalytic center when compared to the situation in solution. (This is not only the case for enantioselective reactions but also for regioselective ones).

The chiral chelate ligands based on 1,1′-bis(diphenylphosphanyl)ferrocene (dppf) are particularly attractive for tethering into MCM-41 for several reasons: first, their planar chirality never undergoes racemization; second, they are synthetically very accessible;[267] and third, they possess functionalities suitable for reaction with pore-bound tethers. The opportunities for variations of the groups attached to an adjacent nitrogen atom and hence the steric/electronic characteristics for both metal complexation and tailoring of the chiral environment, chural catalysts offer great scope for the designer of constrained chiral catalysts.

The homogeneous transition metal complexes of dppf derivatives are active for a large variety of stereoselective reactions, such as cross-coupling of organometallic reagents with alkenyl of aryl halides, aldol-type reactions, substitutions of allylic substrates with nucleophiles, hydrogenation and hydrosilylation of olefins and ketones, and hydroboration. Thus, with the chiral MCM-41 derivatives, catalytic regio- and enantioselective syntheses (that is, the altered selectivity of the chiral complexes tethered in siliceous MCM-41 versus that of their homogeneous analogues) might, for example, be explored in the fashion typified by Corma et al.[268] in the rhodium/USY system, where an increase in the enantiomeric selectivity from 75 to 95 % could be achieved. (This is thought to have been caused by the additional substrate-pore wall interaction as shown above.)

7.7.2. Designing a Chiral Catalyst Confined Within Mesoporous Silica: Its Superior Performance Relative to its Homogeneous Analogue in Allylic Amination

We have demonstrated[269, 270] that a chiral ligand derived from dppf bonded to an active metal center (in this case Pd^{II}) and tethered, through a molecular link of appropriate length, to the inner walls of a mesoporous support (MCM-41, ca. 30 Å diameter) yields a degree of catalytic regioselectivity as well as enantiomeric excess that is far superior to either the homogeneous counterpart or the Cabosil-bound catalyst (Cabosil is a nonporous, large-area siliceous material).

Our conceptual methodology was to take a homogeneous system of known catalytic behavior and perform suitable modifications prior to tethering this catalyst within the mesopore. Care is taken to ensure that all activity is confined to the internal surface of the MCM-41 channels. This is achieved by selectively deactivating the external surface of the support. (We have shown previously by electron microscopy on functionalized mesopores stained with Ru_6-based clusters that this is a reliable and satisfactory method).

Our approach to the preparation of our catalytic system is shown schematically in Figure 51. The mesoporous framework was first treated with Ph_2SiCl_2 under nondiffusive conditions to deactivate the exterior walls of the material. The interior walls of this same material were then derivatized with 3-bromopropyltrichlorosilane to give the activated MCM-41 (**1**). The ferrocenyl-based ligand **2** was prepared from ferrocene by literature methods.[271] Treatment of the activated MCM-41 (**1**) with an excess of **2** yields the chiral catalytic precursor **4**, which, on reaction with $PdCl_2$/MeCN, gives the required catalyst **6**. In a separate experiment the closely

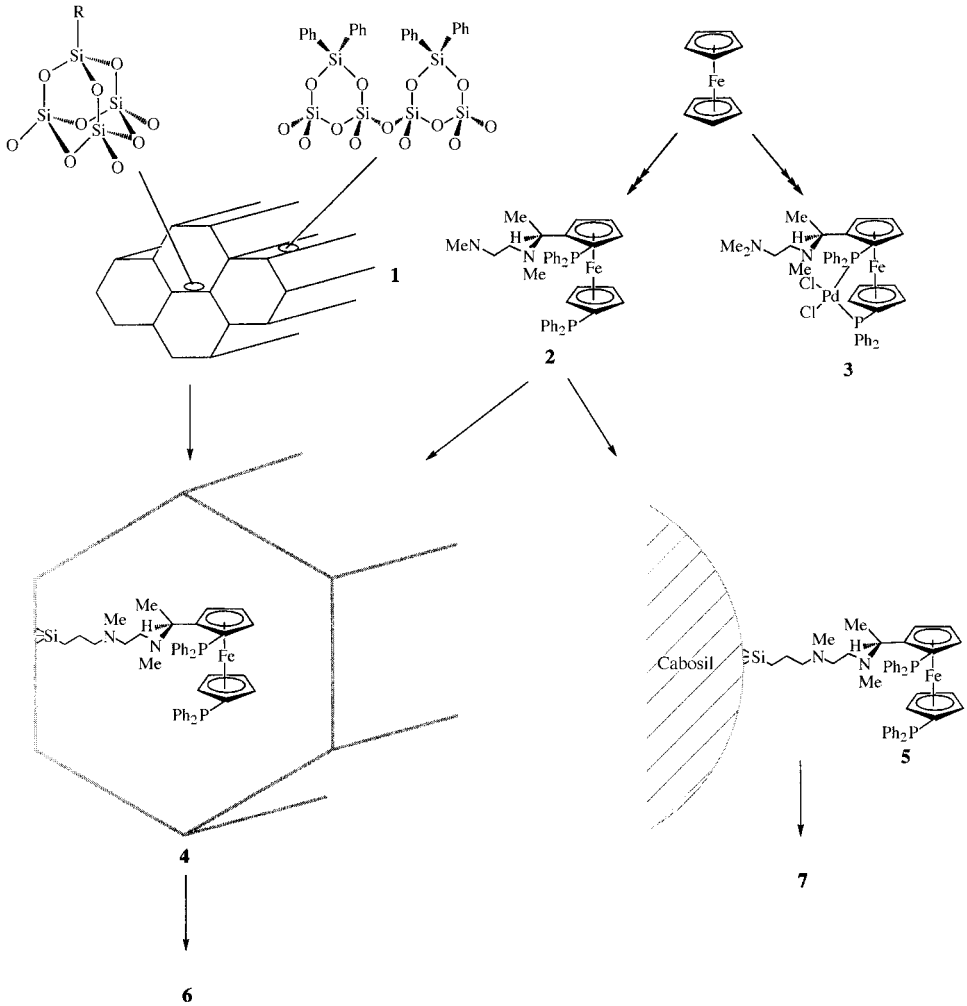

Figure 51. Sequence of steps showing the immobilization of *N*-[1′,2-bis(diphenylphosphanyl)ferrocenyl]-ethyl-*N*,*N*′-dimethylethylenediamine (**2**) in its chirally constrained and unconstrained (**5**) states.[270] R = $(CH_2)_3Br$.

related cabosil-supported catalyst **7** was prepared in a similar manner from surface-activated Cabosil and **2** followed by addition of the required Pd^{II} salt.

The catalyst **6** was fully characterized by a range of techniques. First, the structural integrity of the MCM-41 catalytic precursor **4** was established by MAS NMR and EXAFS spectroscopy. The presence of the tethered ferrocenyl catalysts was confirmed by comparison of the ^{13}C MAS NMR spectrum of **4** with that of the unattached precursor **2**. Apart from the additional signals arising from the propyl tethering unit, the spectra were essentially the same. Examination of the ^{31}P MAS NMR spectra of **2** and **4** showed identical chemical shift values. Significant changes in the aliphatic region of the ^{13}C MAS NMR and in the ^{31}P MAS/NMR spectra were noted on incorporation of the Pd^{II} ion to yield the active catalyst **6**. Two ^{31}P resonances at $\delta = 15.9$ and 34.4 were recorded, which clearly indicates two different phosphorous environments, these have been assigned as one being *trans* to a nitrogen atom and the other being *trans* to a chloride ion.[272] The change in the aliphatic region of the ^{13}C MAS NMR spectrum corresponds to changes in the methyl resonances of the amines, further corroborating the assignment of the ^{31}P spectrum. This entire arrangement was borne out by a detailed EXAFS analysis of **6**. The coordination environment of the cationic species within the mesopore is depicted in Figure 52.

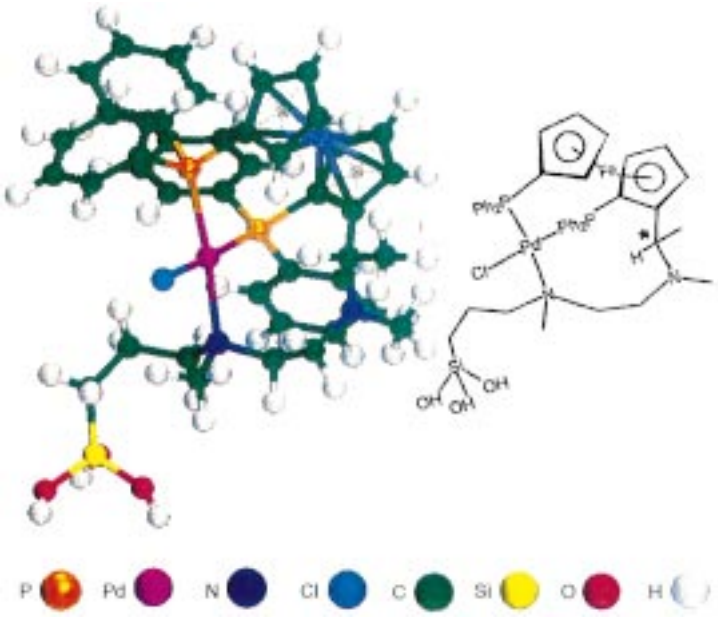

Figure 52. The structure of the organometallic "dppf"-Pd^{II} entity (labeled A in Figure 53) used for the allylic amination of cinnamyl acetate described in the text.

To test our catalysts we used an allylic amination (Tsuji–Trost) reaction between cinnamyl acetate and benzylamine. This reaction has two possible products: a straight-chained product (which is favored as a result of the retention of the delocalized π system) and a chiral-branched product (Figure 53). The aim of the reaction is to produce the greatest possible yield of the branched product with the highest possible enantiomeric excess (*ee*). Three catalysts were

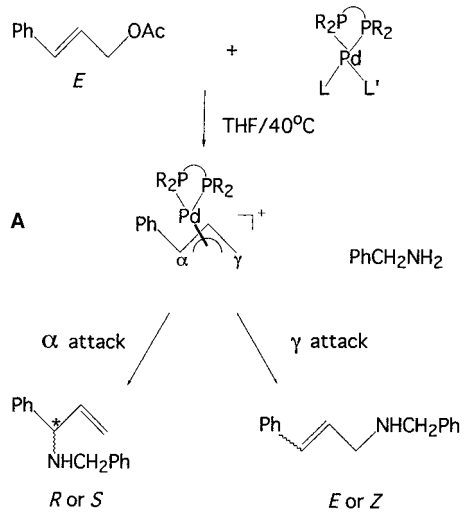

Figure 53. The allylic amination of cinnamyl acetate with benzaldehyde in the presence of a Pd^{II} complex as a catalyst. See also Table 7.

examined: the homogeneous **3** (see Figure 51), the Cabosil-supported one **7**, and that attached within the mesoporous material **6**. Preliminary results of the studies are listed in Table 7. With the homogeneous catalyst **3** the reaction is directed solely towards the straight-chain product whereas

Table 7. Catalytic performance of entities **3**, **6**, and **7**—see ref. [270], and Figures 51 and 53—in the allylic amination of cinnamyl acetate.

Catalyst[a]	Conversion [%][b]	Straight chain product[%][c]	Branched [%]	% *ee*
3 (*S*)	76	99+	–	–
7 (*S*)	98	98	2	43
6 (*S*)	99+	49	51	>99
6 (*R*)	99+	50	50	93

[a] Symbols in brackets denote the chirality of the directing group. [b] Conversion is stated relative to the use of benzylamine. [c] Regioselectivity and enantiomeric excess determined by chiral GC-MS.

catalyst **7** showed some of the desired regioselecticity by producing 2% of the branched product. However, the enantioselectivity of the reaction is relatively low being 43% *ee*. But the use of the mesopore-confined catalyst **6** promotes a dramatic change in the regioselectivity of the reaction, producing 51% of the branched product. The enantioselectivity of the confined catalyst (compare Figures 51, 52, and 54) is also greatly improved relative to the Cabosil-bound catalyst, with the *ee* value now approaching 100%. These results indicate that the control exercized by the MCM-41 on the activity of the palladium–ferrocenyl catalyst is considerable. The profound changes in the regio- and enantioselectivity are clearly apparent from the data listed in Table 7.

It requires little imagination to see that, in addition to Pd, a range of other platinum group metals (Ru, Rh, Os, Ir, Pt), placed strategically within appropriate chiral organic drapery on the inner walls of mesoporous silica (and other oxides), may be used to design a rich variety of other chirally constrained catalysts. Rhodium, platinum, and other ions,

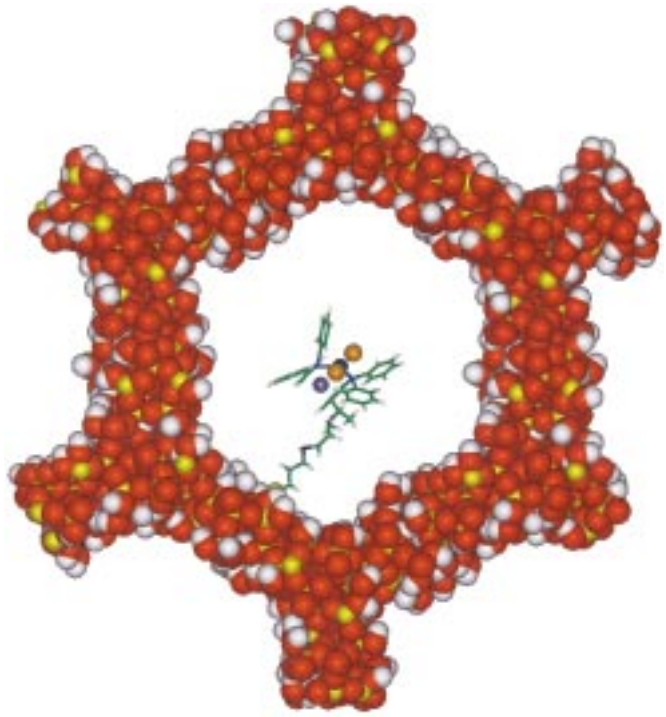

Figure 54. Scalar model of the "dppf"-Pd^{II} chirally constrained catalyst that exhibits superior performance both in regard to regioselectivity and enantiomeric excess in the allylic amination of cinnamyl acetate. Color scheme as in Figure 55.

including those like gold outside the platinum group offer the possibility of enabling the strategy established above to be harnessed in such processes as aldol cyclizations and hydroformylations. There is also abundant scope, not only systematically to modify the ferrocenylphosphane ligand, but also to utilize quite distinctly different kinds of ligands such as those derived from semicorrine and bisoxazoline (as utilized so effectively in other contexts by Pfaltz et al.[273] and Evans et al.,[274] respectively).

7.7.3. Quantitative Comparisons of Heterogeneous and Homogeneous Catalysts

The fact that we may now routinely design (using the strategies described above) soluble homogeneous, catalytic single-site, entities that are strictly comparable to designed, single-site, insoluble heterogeneous catalysts, places us in a uniquely powerful position to compare the catalytic performance of the same engineered active site in the homogeneous (freely dispersed, unconstrained, and accessible) state with that of the heterogeneous, spatially constrained state. Figures 54 and 55 summarize in a visual fashion how this comparison is made in the case of the dppf-based catalyst used for the allylic amination process described in the preceding section.

The stage is set to enable many other strictly comparable homogeneous and heterogeneous catalysts to be investigated, the targets being: to assemble and to modify desired catalytically active sites, to explore the subtleties in their mode of

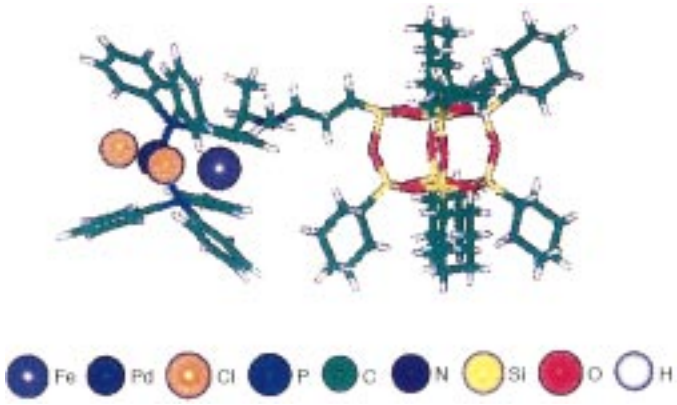

Figure 55. The soluble, unconstrained, cyclohexylsilsesquioxane analogue of the chirally confined "dppf"-Pd^{II} catalyst shown in Figure 54.

action, and to determine the precise atomic architecture of the sites under operating conditions.[*]

7.8. Concluding Remarks: Biomimetic Catalysts and Beyond

Our aim, which in some measure has been achieved, is to make those attributes of catalysis that are important measurable, rather than be tempted to make those that are readily measurable important. The deliberate choice of microporous and mesoporous solids facilitates the successful design, synthesis, and detailed characterization of many new catalysts covering a wide range of important organic reactions. All the catalysts described here have the active sites located at, or tethered to, the inner surfaces of these large-area solids. There is abundant scope, however, to construct yet a further kind of catalyst also using porous solids. The diameter of the cages of the pores must be so designed as to facilitate the in situ assembly (and testing) of well-defined "homogeneous" organometallic catalysts locked (or rattling) inside the inorganic container. These are akin to the "tea bag"[24] or "ship-in-bottle"[169] catalysts described previously.

An important example of "ship-in-bottle" catalysts is the one consisting of dimeric copper oxysalts so constrained within an appropriate zeolitic cage as to alter significantly the electronic properties of bound dioxygen molecules. The bound oxygen molecule is known[275] to be perpendicular to the Cu-Cu axis. It is also known[276] from incarceration, in a judicious matter, of the dimeric copper compounds inside the "right" inorganic cage, that scission of the O-O bond is facilitated, thereby yielding catalysts that mimic enzymes such as tyrosinase, which converts L-tyrosine to L-DOPA. The challenges here are obvious: to achieve the best synthesis of the "ship-in-bottle" catalyst, and to monitor, by in situ techniques the precise changes in catalytic performance consequent upon incarceration. Computational work, incorporating density functional and molecular dynamics procedure of the kind described above, will have an increasingly im-

[*] Note added in proof (November 18, 1999): Our comparison of the catalytic performance of homogeneous engineered Ti^{IV}-centered active sites in $[(c\text{-}C_5H_9)_7Si_7O_{12}TiOXPh_3]$, where X = Si, Ge, or Sn with their heterogeneous analogues (see ref. [220]) has now been published (ref. [231]).

portant interpretative and predictive role to play. In addition, there is a considerable range of possibilities emerging from the chiral confinement concept summarized in Figure 51.

The term inorganic enzyme has been used[277] to describe the kind of catalyst that has been discussed here. This term seems justified, since our catalysts exhibit several of the cardinal features of enzymes: a well-defined catalytic site (or pocket), and the element of molecular selectivity (shape-, regio- or enantioselectivity). And just as the assembly and modification of active sites in mutant[8, 9, 278] and maquette[47] enzymes play key roles in protein engineering, so likewise does the fashioning and functioning of active sites in engineering their inorganic analogues. Time-resolved structural studies are indispensable techniques for both.

I acknowledge with gratitude continued financial support from the Engineering and Physical Sciences Research Council of the U.K. and the cooperation of the staff of the Daresbury Synchrotron Laboratory. I am also indebted to all my colleagues and international collaborators for their constructive cooperation. Dr. Markus Dugal critically assessed the first draft of my manuscript. The continued helpful input of Dr. I. E. Maxwell over the years is much appreciated.

Received: May 17, 1999 [A 343 IE]
German version: *Angew. Chem.* **1999**, *111*, 3800 – 3843

[1] J. M. Thomas, *Michael Faraday and the Royal Institution: The Genius of Man and Place*, Institute of Physics, Bristol, **1991**.
[2] Inscribed on the enormous tombstone of Karl Marx in Highgate Cemetery, London, is the quotation from his work: "Philosophers have only interpreted the world. The point, however, is to change it". It is disputable whether, bearing in mind the far-reaching and wide-ranging discoveries[1] made by Faraday, whose tombstone is also in Highgate Cemetery and on which is simply inscribed his name and dates (1791 – 1867), the changes to the world wrought by Marx can compare in their permanent effects with those that flowed from the work of Faraday and of Ziegler.[3–5]
[3] L. P. Williams, *Michael Faraday*: *A Biography*, Chapman and Hall, London, **1965**.
[4] It has often been remarked that, by his discovery of the dynamo with its consequential production of continuous electricity, that Faraday freed more people from hard labor and slavery than political geniuses such as Abraham Lincoln.
[5] It is hard to picture modern daily life without polyethene and polypropene!
[6] J. J. Berzelius, quoted by G. M. Schwab in *Katalyse*, Macmillans, London, **1955**; see also Jan Trofast, *Bz. Årsber*, Academy of Sciences, Lund, **1979**, ISBN 91-7190-005-5.
[7] G. P. Winter, A. R. Fersht, A. J. Wilkinson, M. Zöller, M. Smith, *Nature* **1982**, *299*, 756.
[8] M. Smith in *Science and Society* (Ed.: M. Moskovits), Anansi, Concord, Ontario, **1995**, p. 69; see also A. R. Fersht, J.-P. Shi, A. J. Wilkinson, D. M. Blow, P. Carter, M. M. Y. Waye, G. P. Winter, *Angew. Chem.* **1984**, *96*, 455; *Angew. Chem. Int. Ed. Engl.* **1984**, *23*, 467.
[9] J. B. Jones, G. De Santis, *Acc. Chem. Res.* **1999**, *32*, 99; see also *Enzyme Catalysis in Organic Synthesis* (Eds.: K. Drauz, H. Waldmann), VCH, Weinheim, **1995**.
[10] V. M. Cornish, D. Mendel, P. G. Schultz, *Angew. Chem.* **1995**, *107*, 677; *Angew. Chem. Int. Ed. Engl.* **1995**, *34*, 621.
[11] *Acc. Chem. Res.* **1993**, *26* (7) (Eds.: R. A. Lerner, P. G. Schultz); see also P. G. Schultz, *Angew. Chem.* **1999**, *111*, 37; *Angew. Chem. Int. Ed.* **1999**, *38*, 37.
[12] F. H. Arnold, *Acc. Chem. Res.* **1998**, *31*, 125.
[13] M. T. Reetz, K.-E. Jaeger, *Trends Biotechnol.* **1998**, *16*, 396.
[14] *Applied Homogeneous Catalysis with Organometallic Compounds* (Eds.: B. Cornils, W. A. Herrmann), VCH, Weinheim, **1996**.
[15] B. Cornils, W. A. Herrmann, *Angew. Chem.* **1997**, *109*, 1074; *Angew. Chem. Int. Ed. Engl.* **1997**, *36*, 1048.
[16] G. A. Somorjai, *MRS Bull.* **1998**, *23*, 11.
[17] In other words, their Debye – Waller factors are larger than those of atoms in the bulk. There are other subtleties at work here, which devolve upon the differences between so-called structure-senstivite and structure-insensitive reactions (see refs. [20 – 23] for a full discusssion of such definitions). For structure-sensitive reactions (exemplified by the hydrogenation of ketoesters with Pt/cinchona/Al_2O_3) catalytic activity may be at its optimal with bigger rather than with smaller crystallites, depending upon which crystallographic face of the crystallite is most conducive for reaction. For the hydrogenation mentioned above Pt crystallites of 5 nm diameter exhibit the highest activity.
[18] J. M. Bassett, J. P. Candy, A. Choplin, B. Didillon, P. Quignand, A. Theolier in *Perspectives in Catalysis* (Ed.: J. M. Thomas, K. I. Zamaraev), Blackwells, Oxford, **1992**, p. 125.
[19] J. Evans, *Chem. Soc. Rev.* **1997**, 11.
[20] *Handbook of Heterogeneous Catalysis* (Eds.: G. Ertl, H. Knözinger, J. Weitkamp), Wiley-VCH, **1997**.
[21] R. A. van Santen, *Theoretical Heterogeneous Catalysis*, World Scientific, Singapore, **1999**; *Introduction to Zeolite Science and Practice* (Eds.: H. van Bekkum, E. M. Flanigen, J. C. Jansen), Elsevier, Amsterdam, **1991**.
[22] M. Che, C. Louis in *Handbook of Heterogeneous Catalysis* (Eds.: G. Ertl, H. Knözinger, J. Weitkamp), Wiley-VCH, **1997**, p. 207.
[23] J. M. Thomas, W. J. Thomas, *Principles and Practice of Heterogeneous Catalysis*, Wiley-VCH, **1997**.
[24] J. M. Thomas, *Philos. Trans. R. Soc. London A* **1990**, *333*, 173.
[25] J. M. Thomas, *Faraday Discuss. R. Soc. Chem.* **1996**, *105*, 1.
[26] P. J. Maddox, J. Stahurski, J. M. Thomas, *Catal. Lett.* **1988**, *1*, 67.
[27] J. M. Thomas, *Chem. Eur. J.* **1997**, *3*, 1557.
[28] M. Klunduk, T. Maschmeyer, J. M. Thomas, B. F. G. Johnson, *Chem. Eur. J.* **1999**, *4*, 1481.
[29] T. Bein, *Angew. Chem.* **1999**, *111*, 335; *Angew. Chem. Int. Ed.* **1999**, *38*, 323.
[30] P. G. Schultz, R. A. Lerner, *Science* **1995**, *269*, 1835.
[31] C. L. Hill, R. D. Gall, *J. Mol. Catal. A* **1996**, *114*, 103.
[32] A. Holzwarth, H.-W. Schmidt, W. F. Maier, *Angew. Chem.* **1998**, *110*, 2788; *Angew. Chem. Int. Ed.* **1998**, *37*, 2644.
[33] W. F. Maier, S. Klein, *Angew. Chem.* **1996**, *108*, 2376; *Angew. Chem. Int. Ed. Engl.* **1996**, *35*, 2230.
[34] M. T. Reetz, M. H. Becker, K. M. Kühling, A. Holzwarth, *Angew. Chem.* **1998**, *110*, 2792; *Angew. Chem. Int. Ed.* **1998**, *37*, 2647.
[35] E. Reddignton, A. Sapienza, B. Gurau, R. Viswanathan, S. Sarangapani, E. S. Smotkin, T. E. Mallouk, *Science* **1998**, *280*, 1735.
[36] S. M. Senken, *Nature* **1998**, *394*, 350.
[37] P. Cong, R. D. Doulen, Q. Fary, D. M. Giaquinta, S. Guan, E. W. McFarlad, D. M. Poojany, K. Self, H. W. Turner, W. H. Weinberg, *Angew. Chem.* **1999**, *111*, 507; *Angew. Chem. Int. Ed.* **1999**, *38*, 483.
[38] R. Schlögl, *Angew. Chem.* **1998**, *110*, 2467; *Angew. Chem. Int. Ed.* **1998**, *37*, 2333.
[39] G. J. Britovsek, V. C. Gibson, D. F. Wass, *Angew. Chem.* **1999**, *111*, 448; *Angew. Chem. Int. Ed.* **1999**, *38*, 428.
[40] In their recent account of the "Search for New-generation Olefin Polymerization Catalysts: Life Beyond Metallocenes", Brtiovsek et al.[39] state that "…the speed of catalyst discovery is likely to be limited only by the flair and imagination of the synthetic organometallic and coordination chemist for ligand design."
[41] D. J. Berrisford, C. Bolm, K. B. Sharpless, *Angew. Chem.* **1995**, *107*, 1159; *Angew. Chem. Int. Ed. Engl.* **1995**, *34*, 1059.
[42] M. T. Reetz, S. R. Waldvogel, *Angew. Chem.* **1997**, *109*, 870; *Angew. Chem. Int. Ed. Engl.* **1997**, *36*, 865.
[43] P. B. Weisz, *Pure Appl. Chem.* **1980**, *52*, 2091.
[44] P. B. Weisz, W. O. Haag, R. M. Lago, *Nature* **1984**, *309*, 589.
[45] M. Taramasso, G. Perego, B. Notari, US-Pat. 4410501, **1983**.
[46] B. Notari, *Adv. Catal.* **1996**, *41*, 253.
[47] F. Rabanal, B. R. Gibney, W. F. DeGrado, C. C. Moser, P. L. Dutton, *Inorg. Chim. Acta.* **1996**, *243*, 213.

[48] All the structures shown in Figure 8 were synthesized (and solved) in the author's laboratory or in those of his former colleagues.
[49] R. Szostak, *Handbook of Molecular Sieves*, van Nostrand Reinhold, New York, **1992**.
[50] J. T. Ying, C. P. Mehnert, M. S. Wong, *Angew. Chem.* **1999**, *111*, 58; *Angew. Chem. Int. Ed.* **1999**, *38*, 56.
[51] P. Behrens, *Angew. Chem.* **1996**, *108*, 561; *Angew. Chem. Int. Ed. Engl.* **1996**, *35*, 515.
[52] C. T. Kresge, M. E. Leonowicz, W. J. Roth, J. C. Vartuli, J. S. Beck, *Nature* **1992**, *359*, 710.
[53] Q. Huo, D. I. Margalese, U. Ciesla, P. Feng, T. E. Geir, P. Sieger, R. Leon, P. M. Petroff, F. Schüth, G. D. Stucky, *Nature* **1994**, *368*, 317.
[54] J. M. Thomas, *Nature* **1994**, *368*, 289.
[55] A. Corma, *Chem. Rev.* **1995**, *95*, 559.
[56] J. C. Vartuli, J. S. Beck, *Curr. Opin. Solid State Mater. Sci.* **1997**, *2*, 98.
[57] M. J. MacLauchlan, N. Coombs, G. A. Ozin, *Nature* **1999**, *397*, 681.
[58] F. Rey, G. Sankar, J. M. Thomas, T. Maschmeyer, G. N. Greaves, *Top. Catal.* **1996**, *3*, 121.
[59] P. A. Wright, R. H. Jones, S. Natarajan, R. G. Bell, J. Chen, M. B. Hursthouse, J. M. Thomas, *J. Chem. Soc. Chem. Commun.* **1993**, 633.
[60] S. Natarajan, P. A. Wright, J. M. Thomas, *J. Chem. Soc. Chem. Commun.* **1993**, 1863.
[61] J. Chen, R. H. Jones, S. Natarajan, M. B. Hursthouse, J. M. Thomas, *Angew. Chem.* **1994**, *106*, 667; *Angew. Chem. Int. Ed. Engl.* **1994**, *33*, 639.
[62] P. A. Barrett, R. H. Jones, J. M. Thomas, G. Sankar, I. J. Shannon, C. R. A. Catlow, *Chem. Commun.* **1996**, 2001.
[63] P. A. Wright, G. W. Noble, P. Lightfoot, R. E. Morris, K. J. Hudson, A. Kuick, H. Graafsma, *Angew. Chem.* **1997**, *109*, 76; *Angew. Chem. Int. Ed. Engl.* **1997**, *36*, 81.
[64] G. W. Noble, P. A. Wright, A. Kuick, *J. Chem. Soc. Dalton Trans.* **1997**, 4485.
[65] S. A. I. Barri, G. W. Smith, D. White, D. Young, *Nature* **1984**, *312*, 533.
[66] R. H. Jones, J. M. Thomas, J. Chen, R. Xu, Q. Huo, S. Li, Z. Ma, A. M. Chippindale, *J. Solid State Chem.* **1993**, *102*, 204.
[67] V. Alfredsson, M. W. Anderson, *Chem. Mater.* **1996**, *8*, 1141.
[68] W. Zhou, H. M. A. Hunter, P. A. Wright, Q. Ge, J. M. Thomas, *J. Phys. Chem. B* **1998**, *102*, 6933.
[69] D. Ozkaya, W. Zhou, J. M. Thomas, P. A. Midgeley, V. J. Keast, S. Hermans, *Catal. Lett.* **1999**, *60*, 101.
[70] J. Chen, J. M. Thomas, *J. Chem. Soc. Chem. Commun.* **1994**, 603.
[71] J. Chen, J. M. Thomas, R. P. Townsend, C. M. Lok, GB-Pat. 93186443, **1993**.
[72] D. W. Lewis, C. M. Freeman, C. R. A. Catlow, *J. Phys. Chem.* **1995**, *99*, 11194.
[73] D. W. Lewis, C. R. A. Catlow, J. M. Thomas, *Chem. Mater.* **1996**, *8*, 1112.
[74] D. W. Lewis, D. J. Willock, G. J. Hutchings, C. R. A. Catlow, J. M. Thomas, *Nature* **1996**, *382*, 604.
[75] J. S. Chen, P. A. Wright, J. M. Thomas, S. Natarajan, L. Marchese, S. M. Bradley, G. Sankar, C. R. A. Catlow, P. L. Gai-Boyes, R. P. Townsend, C.-M. Lok, *J. Phys. Chem.* **1994**, *98*, 10216.
[76] a) *Computer-Aided Molecular Design*, *Applications to Agrochemicals*, *Materials and Pharmaceuticals* (Eds.: C. H. Reynolds, M. K. Holloway, H. K. Cox), Am. Chem. Soc., Washingon, **1995**; b) R. S. Bohacek, C. McMartin in Ref. [76a].
[77] V. Gillet, A. P. Johnson, P. Mata, S. Sike, P. J. Williams, *J. Comput. Aided Mol. Des.* **1993**, *7*, 127.
[78] T. I. Oprea, C. M. W. Ho, G. R. Marchall in ref. [76a], p. 65.
[79] R. S. Bohacek, C. J. McMartin, *J. Am. Chem. Soc.* **1994**, *116*, 5560.
[80] H. J. Bohn, *J. Comput. Aided Mol. Des.* **1992**, *6*, 61.
[81] R. A. Lewis, P. M. Dean, *Proc. R. Soc. B* **1989**, *236*, 125.
[82] C. Verlinde, G. Rudenko, W. Hol, *J. Comput. Aided Mol. Des.* **1992**, *6*, 131.
[83] A. Miranker, M. Karplus, *Proteins Struct. Funct. Genet.* **1995**, *23*, 472.
[84] H. Gies, *Stud. Surf. Sci. Catal.* **1994**, *85*, 295.
[85] A. Stewart, *Zeolites* **1989**, *9*, 140.
[86] D. H. Olson, W. M. Meier, *Atlas of Zeolite Structure Types*, Butterworths – Heinemann, London, **1992**.
[87] L. B. McCusker, *Mater. Sci. Forum* **1993**, *133 – 136*, 423.
[88] D. W. Lewis, G. Sankar, J. K. Wyles, J. M. Thomas, D. J. Willock, *Angew. Chem.* **1997**, *109*, 2791; *Angew. Chem. Int. Ed. Engl.* **1997**, *36*, 2675.
[89] G. Sankar, J. M. Thomas, J. K. Wyles, W. Clegg, C. R. A. Catlow, D. W. Lewis, *Chem. Commun.* **1998**, 117.
[90] D. J. Willock, D. W. Lewis, C. R. A. Catlow, G. J. Hutchings, J. M. Thomas, *J. Mol. Catal. A* **1997**, *199*, 415.
[91] Chabazite, a naturally occurring zeolitic (aluminosilicate) has (in its dehydrated state) an ideal formula: $Ca_6[Al_{12}Si_{24}O_{72}]$, and the diameter of the essentially circular pore openings is 3.8 Å. Its framework is isotypic with the silicoaluminophosphate SAPO-34 and with CoAlPO-44.
[92] P. W. Werner, L. Eriksson, M. Westdahl, *J. Appl. Crystallogr.* **1985**, *18*, 367.
[93] G. Cheetham, M. M. Harding, *Zeolites* **1996**, *16*, 245.
[94] G. W. Noble, P. A. Wright, P. Lightfoot, R. E. Morris, K. J. Hudson, A. Kvick, H. Graafsma, *Angew. Chem.* **1997**, *109*, 76; *Angew. Chem. Int. Ed. Engl.* **1997**, *36*, 81.
[95] D. W. Lewis, C. R. A. Catlow, J. M. Thomas, *Faraday Discuss. Chem. Soc.* **1997**, *106*, 451.
[96] D. A. Jefferson, J. M. Thomas, R. F. Egerton, *Chem. Br.* **1981**, *17*, 514.
[97] J. M. Thomas, *Proceedings of Joint ACS*, *RSC and Canadian IC Symposium*, Bloomington, Indiana, USA, May **1982**; ACS Symp. Ser. **1993**, 211 (*Inorganic Chemistry*: *Towards the 21st Century* (Ed.: M. H. Chisholm)), 445 – 472.
[98] J. M. Thomas, B. G. Williams, T. G. Sparrow, *Acc. Chem. Res.* **1985**, *18*, 324 – 330.
[99] Z. L. Wang, J. Bentley, N. D. Evans, *J. Phys. Chem. B* **1999**, *103*, 751.
[100] L. A. Bursill, E. A. Lodge, J. M. Thomas, *Nature* **1980**, *286*, 111.
[101] L. A. Bursill, J. M. Thomas, *J. Phys. Chem.* **1981**, *85*, 3007.
[102] J. M. Thomas, G. R. Millward, S. Ramdas, L. A. Bursill, M. Audier, *Faraday Discuss. Chem. Soc.* **1981**, *72*, 345.
[103] J. M. Thomas, G. R. Millward, *J. Chem. Soc. Chem. Commun.* **1982**, 1380.
[104] O. Terasaki, J. M. Thomas, G. R. Millward, *Proc. R. Soc. London A* **1984**, *395*, 153.
[105] O. Terasaki, J. M. Thomas, G. R. Millward, D. Watanabe, *Chem. Mater.* **1989**, *1*, 158.
[106] O. Terasaki, *J. Elec. Microsc.* **1994**, *43*, 337.
[107] O. Terasaki, T. Ohsuna, N. Ohnishi, K. Hiraga, *Curr. Opin. Solid State Mater. Sci.* **1997**, *2*, 94.
[108] M. M. J. Treacy, *Ultramicroscopy* **1994**, *23*, 411.
[109] J.-O. Bovin, V. Alfredsson, G. Karlsson, A. Carlsson, Z. Blum, O. Terasaki, *Ultramicroscopy* **1996**, *62*, 297.
[110] D. Ozkaya, W. Zhou, J. M. Thomas, P. A. Midgeley, V. J. Keast, S. Hermans, *Catal. Lett.* **1999**, *60*, 113.
[111] G. R. Millward, S. Ramdas, J. M. Thomas, M. T. Barlow, *J. Chem. Soc. Faraday Trans. 2* **1983**, *79*, 1075.
[112] W. Zhou, J. M. Thomas, D. S. Shephard, B. F. G. Johnson, D. Ozkaya, T. Maschmeyer, R. G. Bell, Q. Ge, *Science* **1998**, *280*, 705.
[113] M. Pan, P. A. Crozier, *Ultramicroscopy* **1993**, *48*, 332.
[114] N. Ohnishi, K. Hiraga, *J. Elec. Microsc.* **1996**, *45*, 85.
[115] A. Klug, *Les Prix Nobel en 1982*, The Nobel Foundation, Stockholm, **1983**, 93.
[116] a) *The Electron* (Eds.: A. Kirkland, P. D. Brown), Inst. of Materials, London, **1998**; b) R. Henderson in ref. [116a], p. 183.
[117] B. Böttcher, S. A. Wynne, R. A. Crowther, *Nature* **1997**, *386*, 88.
[118] S. Nikopoulos, J. M. Gonzales-Calbet, M. Vallet-Regi, A. Corma, C. Corell, J. M. Guil, J. Patiente, *J. Am. Chem. Soc.* **1995**, *117*, 9947.
[119] P. Wagner, O. Terasaki, M. E. Davis, *J. Phys. Chem. B*, in press.
[120] For the solving of the structure of a metal-substituted aluminum phosphate catalyst by electron microscopy, computer simulation, and X-ray powder diffraction, see P. A. Wright, S. Natarajan, J. M. Thomas, R. G. Bell, P. L. Gai-Boyes, R. H. Jones, J. Chen, *Angew. Chem.* **1992**, *104*, 1526; *Angew. Chem. Int. Ed. Engl.* **1992**, *31*, 1472 – 1475.
[121] Real-space imaging of molecular sieves composed of aluminum phosphates and their metal-substituted analogues are described in P. L. Gai-Boyes, J. M. Thomas, P. A. Wright, R. H. Jones, S. Natarajan, J. Chen, R. Xu, *J. Phys. Chem.* **1992**, *96*, 8206.
[122] A. Howie, *J. Microsc. Oxford* **1979**, *177*, 1.
[123] S. J. Pennycook, *Ultramicroscopy* **1989**, *30*, 58.
[124] M. M. J. Treacy, A. Howie, *J. Catal.* **1980**, *63*, 265.
[125] D. Ozkaya, J. M. Thomas, D. S. Shephard, T. Maschmeyer, B. F. G. Johnson, G. Sankar, R. Oldroyd, *Elec. Microsc. Anal. Proc.* **1997**, 403.

[126] P. L. Gai, *Adv. Mater.* **198**, *10*, 1259.
[127] E. D. Boyes, P. L. Gai, *Ultramicroscopy* **1997**, *67*, 219.
[128] *In Situ Microscopy in Materials Research* (Ed.: P. L. Gai), Kluwer, Dordrecht, **1997**.
[129] J. M. Thomas, J. Klinowski, *Adv. Catal.* **1985**, *33*, 199.
[130] G. Engelhardt, D. Michel, *High-Resolution Solid State NMR of Silicates and Zeolites*, Wiley, **1984**.
[131] C. A. Fyfe, J. M. Thomas, J. Klinowski, G. C. Gobbi, *Angew. Chem.* **1983**, *95*, 257; *Angew. Chem. Int. Ed. Engl.* **1983**, *22*, 259.
[132] C. A. Fyfe, G. C. Gobbi, J. Klinowski, J. M. Thomas, S. Ramdas, *Nature* **1982**, *296*, 530.
[133] J. M. Thomas, J. Klinowski, S. Ramdas, B. K. Hunter, D. T. B. Tennakoon, *Chem. Phys. Lett*. **1983**, *102*, 158.
[134] L. A. Villaescusa, P. A. Barrett, M. A. Camblor, *Chem. Commun.* **1998**, 2329.
[135] E. Lippmaa, E. Mägi, M. Samoson, M. Tarmak, G. Engelhardt, *J. Am. Chem. Soc.* **1981**, *103*, 4992.
[136] E. Lippmaa, P. Sarv, T. Tuhern, K. Keskinen, A. Root, *J. Phys. Chem.* **1995**, *99*, 13763.
[137] I am grateful to Dr. J. Klinowski for preparing these simplified versions of the more detailed spectra published in ref. [136].
[138] J. F. Haw, J. B. Nicholas, T. Xu, L. W. Beck, D. B. Ferguson, *Acc. Chem. Res.* **1996**, *29*, 259.
[139] S. Vasudevan, J. M. Thomas, C. J. Wright, C. Sampson, *J. Chem. Soc. Chem. Commun*. **1982**, 418.
[140] J. M. Thomas, W. J. Thomas, *Principles and Practice of Heterogeneous Catalysis*, Wiley-VCH, **1997**, p. 221.
[141] A. K. Cheetham, M. M. Eddy, J. M. Thomas, *J. Chem. Soc. Chem. Commun.* **1984**, 1337.
[142] P. A. Wright, J. M. Thomas, A. K. Cheetham, A. K. Nowak, *Nature* **1986**, *318*, 611.
[143] J. E. Enderby, *Chem. Soc. Rev.* **1995**, *25*, 159.
[144] J. F. C. Turner, W. I. F. David, C. Benmore, C. Barker, N. Kaltsoyannis, G. Sankar, J. M. Thomas, C. R. A. Catlow, *J. Phys. Chem. B*, submitted.
[145] J. F. C. Turner, R. Dove, J. Dreyer, W. I. F. David, C. R. A. Catlow, *Rev. Sci. Instrum.* **1999**, in press.
[146] J. M. Thomas, *Chem. Eur. J.* **1997**, *3*, 1557.
[147] J. W. Couves, J. M. Thomas, G. N. Greaves, R. H. Jones, D. Waller, A. J. Dent, G. E. Derbyshire, *Nature* **1991**, *354*, 465.
[148] J. M. Thomas, G. N. Greaves, *Science* **1994**, *265*, 1675.
[149] G. Sankar, J. M. Thomas, *Top. Catal.* **1999**, *8*, 1. The principal initiator of the three-element detector described in Figure 26a is my colleague, Dr. G. Sankar, to whom I am most grateful.
[150] B. J. Clausen, H. Topsøe, R. Frahm, *Adv. Catal.* **1998**, *42*, 3.
[151] I. J. Shannon, G. Sankar, T. Maschmeyer, J. M. Thomas, R. D. Oldroyd, M. Sheehy, D. Madill, A. Waller, R. P. Townsend, *Catal. Lett.* **1997**, *44*, 23.
[152] R. Raja, J. M. Thomas, *Chem. Commun.* **1998**, 1841.
[153] J. M. Thomas, R. Raja, G. Sankar, R. G. Bell, *Nature* **1999**, *398*, 227.
[154] *Activation and Functionalisation of Alkanes* (Ed.: C. L. Hill), **1989**, Wiley-VCH, chap. 6 – 8.
[155] T. Tatsumi, M. Nakamura, S. Negishi, H. Tominaga, *J. Chem. Soc. Chem. Commun.* **1990**, *476*, 177.
[156] J. A. Smegal, C. L. Hill, *J. Am. Chem. Soc.* **1983**, *105*, 3515.
[157] B. R. Cook, T. J. Reinert, T. S. Suslick, *J. Am. Chem. Soc.* **1986**, *108*, 7281.
[158] N. Herron, C. A. Tolman, *J. Am. Chem. Soc.* **1987**, *109*, 2837.
[159] D. Mansuy, *Pure Appl. Chem.* **1987**, *59*, 759.
[160] J. F. Lyons, P. E. Ellis, Jr., W. K. Myers, Jr., *J. Catal.* **1995**, *155*, 59.
[161] R. Raja, P. Ratnasamy, US-Pat. 5767320, **1998**.
[162] R. Raja, P. Ratnasamy, *Stud. Surf. Sci. Catal.* **1996**, *101*, 181.
[163] T. Maschmeyer, J. M. Thomas, G. Sankar, R. D. Oldroyd, A. F. Masters, J. K. Beattie, J. A. Klepetko, I. J. Shannon, *Angew. Chem.* **1997**, *109*, 1713; *Angew. Chem. Int. Ed. Engl.* **1997**, *36*, 1639.
[164] J. M. Thomas, G. N. Greaves, G. Sankar, P. A. Wright, J. Chen, A. J. Dent, L. Marchese, *Angew. Chem.* **1994**, *106*, 1922; *Angew. Chem. Int. Ed. Engl.* **1994**, *33*, 1871.
[165] P. A. Barrett, G. Sankar, C. R. A. Catlow, J. M. Thomas, *J. Phys. Chem.* **1996**, *100*, 8977.
[166] L. E. Iton, I. Choi, J. A. Desjardins, V. A. Maroni, *Zeolites* **1989**, *9*, 535.
[167] S. S. Lin, H. S. Weng, *Appl. Catal. A* **1994**, *118*, 21.
[168] H. Krauschaar-Czarnetzki, W. G. M. Hoogervoest, W. H. J. Stork, *Stud. Surf. Sci. Catal.* **1994**, *84*, 1869.
[169] C. A. Tolman, J. D. Droliner, M. J. Nappa, N. Herron in *Activation and Functionalisation of Alkanes* (Ed.: C. L. Hill), Wiley, Chichester, **1989**, p. 303.
[170] J. M. Thomas, W. J. Thomas, *Introduction to the Principles of Heterogeneous Catalysts*, Academic Press, London, **1967**, 383.
[171] G. Sankar, R. Raja, J. M. Thomas, *Catal. Lett.* **1998**, *55*, 15.
[172] J. T. Groves, *Nature* **1997**, *389*, 329.
[173] M. L. Ludwig, A. L. Metzger, K. A. Pattridge, W. C. Stallings, *J. Mol. Biol.* **1991**, *219*, 335.
[174] P. A. Barrett, G. Sankar, R. H. Jones, C. R. A. Catlow, J. M. Thomas, *J. Phys. Chem.* **1997**, *101*, 9555.
[175] T. Maschmeyer, J. M. Thomas, A. F. Masters, J. K. Beattie, G. Sankar, R. D. Oldroyd, J. A. Klepetko, *Angew. Chem.* **1997**, *109*, 1713; *Angew. Chem. Int. Ed. Engl.* **1997**, *36*, 1639.
[176] J. K. Kochi, R. T. Tang, T. Bernath, *J. Am. Chem. Soc.* **1973**, *95*, 7114.
[177] S. Uemura, A. Spencer, G. Wilkinson, *J. Chem. Soc. Dalton Trans.* **1973**, 2565.
[178] C. E. Sumner, G. R. Steinmetz, *Inorg. Chem.* **1989**, *28*, 4290.
[179] J. K. Beattie, T. W. Hambley, J. A. Klepetko, A. F. Masters, P. Turner, *Polyhedron* **1997**, *16*, 2109.
[180] J. K. Beattie, T. W. Hambley, J. A. Klepetko, A. F. Masters, P. Turner, *Polyhedron* **1998**, *17*, 1343.
[181] J. K. Beattie, T. W. Hambley, J. A. Klepetko, A. F. Masters, P. Turner, *Chem. Commun.* **1998**, 45; also M. Dugal, R. Raja, G. Sankar, J. M. Thomas, unpublished results.
[182] R. Raja, P. Ratnasamy, US-Pat. 5767320, **1998**.
[183] P. Ratnasamy, R. Raja, EP 0784045, **1998**.
[184] P. A. Wright, S. Natarajan, J. M. Thomas, R. G. Bell, P. L. Gai-Boyes, R. H. Jones, J. S. Chen, *Angew. Chem.* **1992**, *104*, 1526; *Angew. Chem. Int. Ed. Engl.* **1992**, *31*, 1472.
[185] G. Sankar, R. Raja, J. M. Thomas, *Catal. Lett.* **1998**, *55*, 15.
[186] R, Raja, G. Sankar, J. M. Thomas, *J. Am. Chem. Soc.*, in press.
[187] A. Baeyer, V. Villiger, *Ber. Dtsch. Chem. Ges.* **1899**, *32*, 3625.
[188] G. Strukul, *Angew. Chem.* **1998**, *110*, 1256; *Angew. Chem. Int. Ed.* **1988**, *37*, 1198.
[189] K. Kaneda, S. Ueno, T. Imanaka, *J. Chem. Soc. Chem. Commun.* **1994**, 797.
[190] M. Hamamota, N. Nakayama, Y. Nishiyama, Y. Ishii, *J. Org. Chem.* **1993**, *58*, 6421.
[191] P. A. Barrett, G. Sankar, C. R. A. Catlow, J. M. Thomas, *J. Phys. Chem.* **1996**, *100*, 8977.
[192] T. Yamada, O. Rhode, T. Takai, T. Mukaiyama, *Chem. Lett.* **1991**, 5.
[193] M. T. Reetz, K. Töllner, *Tetrahedron Lett.* **1995**, *36*, 9461.
[194] W. A. Herrmann, F. E. Kühn, R. W. Fischer, W. R. Thiel, C. C. Romao, *Inorg. Chem.* **1992**, *31*, 4431.
[195] J. M. Thomas in ref. [116a], p. 158.
[196] R. Criegee, *Justus Liebigs Ann. Chem.* **1948**, *560*, 127.
[197] R. Murugavel, H. W. Roesky, *Angew. Chem.* **1997**, *109*, 491; *Angew. Chem. Int. Ed. Engl.* **1997**, *36*, 477.
[198] R. A. Sheldon, M. Wallou, I. W. C. E. Arendo, U. Schuchardt, *Acc. Chem. Res.* **1998**, *31*, 485.
[199] T. Mukayiama in *The Activation of Dioxygen and Homogeneous Catalytic Oxidation* (Eds.: D. H. R. Barton, A. E. Martell, D. T. Sawyer), Plenum, New York, **1993**, p. 133.
[200] G. Sankar, R. Raja, J. M. Thomas, *Proc. 12th Int. Congr. Catalysis, Granada*, **2000**, in press.
[201] B. Kraushaar-Czarnetski, W. G. M. Hoogeroost, C. Ameis, W. H. J. Stork, *J. Chem. Soc. Faraday Trans.* **1991**, *87*, 891.
[202] L. E. Iton, I. Choi, J. A. Desjardins, V. A. Moroni, *Zeolites* **1989**, *9*, 535.
[203] H. F. W. J. van Breukelen, M. E. Gerrisen, V. M. Ummels, J. S. Broes, J. H. C. van Hoof, *Stud. Surf. Sci. Catal.* **1996**, *105*, 1029.
[204] M. P. J. Peters, M. Basio, P. Leijton, *Appl. Catal. A* **1994**, *118*, 51.
[205] T. C. Chou, G. C. Lee, *Ind. Eng. Chem. Fundam.* **1985**, *24*, 32.
[206] S. A. Masloo, E. A. Blymberg, *Russ. Chem. Rev.* **1976**, *45*, 155.
[207] I. W. C. E. Arends, K. U. Ingold, D. D. M. Wayner, *J. Am. Chem. Soc.* **1995**, *117*, 4710.
[208] H. P. Wulff (Shell Oil), GB-Pat. 1249079, **1971**.
[209] T. Blasco, A. Corma, M. T. Navarro, J. Perez-Pariente, *J. Catal.* **1995**, *156*, 65.

[210] T. Maschmeyer, F. Rey, G. Sankar, J. M. Thomas, *Nature* **1995**, *378*, 159.
[211] L. Marchese, T. Maschmeyer, E. Gianotti, S. Coluccia, J. M. Thomas, *J. Phys. Chem.* **1997**, *101*, 8836.
[212] L. Marchese, E. Gianotti, V. Dellarocca, T. Maschmeyer, F. Rey, S. Coluccia, J. M. Thomas, *Phys. Chem. Chem. Phys.* **1999**, *1*, 585.
[213] P. E. Sinclair, G. Sankar, C. R. A. Catlow, J. M. Thomas, T. Maschmeyer, *J. Phys. Chem. B* **1997**, *101*, 4232.
[214] The "butterfly shaped" intermediate is the stable entity when molybdenocene replaces titanocene.[25, 215]
[215] I. J. Shannon, T. Maschmeyer, R. D. Oldroyd, G. Sankar, J. M. Thomas, H. Pernot, J-P. Balikdjian, M. Che, *J. Chem. Soc. Faraday Trans.* **1998**, *94*, 10, 1495.
[216] In Ti →MCM-41 the Ti^{IV} ions are incorporated into the framework of the mesoporous silica during synthesis, and are in the walls. In Ti ↑ MCM-41 the ions are introduced, post synthesis, on to the surface and the titanol groups stand proud.
[217] R. D. Oldroyd, J. M. Thomas, T. Maschmeyer, P. A. MacFaul, D. W. Snelgrove, K. U. Ingold, D. D. M. Wayner, *Angew. Chem.* **1996**, *108*, 2966; *Angew. Chem. Int. Ed. Engl.* **1996**, *35*, 2787.
[218] C. Nedez, A. Choplin, J. M. Bassett, *Inorg. Chem.* **1994**, *33*, 1094.
[219] R. D. Oldroyd, J. M. Thomas, G. Sankar, *Chem. Commun.* **1997**, 2025.
[220] R. D. Oldroyd, G. Sankar, J. M. Thomas, D. Ozkaya, *J. Phys. Chem. B* **1998**, *102*, 1849.
[221] K. U. Ingold, D. W. Snelgrove, P. A. MacFaul, R. D. Oldroyd, J. M. Thomas, *Catal. Lett.* **1997**, *48*, 21.
[222] C. H. Berke, A. Kiss, P. Kleinschmidt, J. Weitkamp, *Chem. Ing. Tech.* **1991**, *63*, 623.
[223] S. Klein, S. Thorimbert, W. F. Maier, *J. Catal.* **1996**, *163*, 476.
[224] R. D. Oldroyd, G. Sankar, J. M. Thomas, M. Huinnius, W. F. Maier, *J. Chem. Soc. Faraday Trans.* **1998**, *94*, 3177.
[225] F. J. Feher, S. L. Gonzales, J. W. Ziller, *Inorg. Chem.* **1988**, *27*, 3440.
[226] T. Maschmeyer, C. M. Lindall, A. F. Masters, L. D. Field, *Aust. J. Chem.* **1994**, *47*, 1127.
[227] T. Maschmeyer, J. M. Thomas, A. F. Master in *New Trends in Materials Chemistry* (NATO ASI Ser. **1997**, *55*) p. 461.
[228] T. Maschmeyer, M. Klunduk, C. M. Martin, J. M. Thomas, B. F. G. Johnson, *Chem. Commun.* **1997**, 1847.
[229] M. Klunduk, J. M. Thomas, G. Sankar, B. F. G. Johnson, C. M. Martin, T. Maschmeyer, *J. Organomet. Chem.*, in press.
[230] M. Klunduk, T. Maschmeyer, J. M. Thomas, B. F. G. Johnson, *Chem. Eur. J.* **1999**, *5*, 1481.
[231] J. M. Thomas, G. Sankar, M. Klunduk, B. F. G. Johnson, M. P. Attfield, T. Maschmeyer, R. G. Bell, *J. Phys. Chem. B* **1999**, *103*, 8809.
[232] C. Williams, M. A. Makerova, L. V. Malysheca, E. A. Paukshtis, K. I. Zamaraev, J. M. Thomas, *J. Chem. Soc. Faraday Trans.* **1990**, *86*, 3473.
[233] K. I. Zamaraev, J. M. Thomas, *Adv. Catal.* **1996**, *41*, 335.
[234] J. A. Rabo, *Proc. 10th Int. Congr. Catalysis Part A*: *New Frontiers in Catalysis* (Eds.: L. Guczi, F. Solymosi, P. Tetanyi), Elsevier, New York, **1993**, p. 1.
[235] L. Marchese, J. M. Thomas, P. A. Wright, J. S. Chen, *J. Phys. Chem.* **1993**, *97*, 8109.
[236] Y. Xu, C. R. A. Catlow, J. M. Thomas, J. W. Couves, *Mater. Chem.* **1991**, *3*, 667.
[237] R. M. Barrer, I. S. Kerr, *Trans. Faraday Soc.* **1959**, *55*, 1915.
[238] G. T. Kerr, US-Pat. 34596765, **1969**.
[239] P. A. Barrett, R. H. Jones, *J. Chem. Soc. Chem. Commun.* **1995**, 1979.
[240] G. J. Kramer, R. A. van Santen, C. A. Emeis, A. K. Nowak, *Nature* **1993**, *363*, 529.
[241] P. E. Sinclair, C. R. A. Catlow, *J. Chem. Soc. Faraday Trans.* **1997**, *93*, 333.
[242] G. J. Hutchings, R. Hunter, P. Johnston, L. L. van Tensburg, *J. Catal.* **1993**, *60*, 142.
[243] C. M. Zicovich-Wilson, P. Viruela, A. Corma, *J. Phys. Chem.* **1995**, *99*, 13224.
[244] R. Shah, M. C. Payne, M.-H. Lee, J. D. Gale, *Science* **1996**, *271*, 1395.
[245] S. Natarajan, P. A. Wright, J. M. Thomas, *J. Chem. Soc. Chem. Commun.* **1993**, 1861.
[246] I. E. Maxwell, J. E. Naber, *Catal. Lett.* **1992**, *12*, 105.
[247] P. A. Wright, J. M. Thomas, in preparation.
[248] J. H. Sinfelt, *Bimetallic Catalysts*, Wiley, New York, **1983**.
[249] J. H. Sinfelt, *Int. Rev. Phys. Chem.* **1988**, *7*, 281.
[250] D. S. Shephard, T. Maschmeyer, B. F. G. Johnson, J. M. Thomas, G. Sankar, D. Ozkaya, W. Zhou, R. D. Oldroyd, *Angew. Chem.* **1997**, *109*, 2337; *Angew. Chem. Int. Ed. Engl.* **1997**, *36*, 2242.
[251] D. S. Shephard, T. Maschmeyer, G. Sankar, J. M. Thomas, D. Ozkaya, B. F. G. Johnson, R. Raja, R. D. Oldroyd, R. G. Bell, *Chem. Eur. J.* **1998**, *4*, 1214.
[252] R. Raja, S. Hermans, S. Bromley, G. Sankar, J. M. Thomas, B. F. G. Johnson, D. S. Shephard, T. Maschmeyer, *Chem. Commun.* **1999**, in press.
[253] S. T. Bromley, C. R. A. Catlow, J. M. Thomas, G. Sankar, unpublished results.
[254] All the density functional calculations were done using a double numeric polarized basis and a gradient corrected functional.
[255] R. Noyori, *Chem. Soc. Rev.* **1989**, *18*, 187.
[256] R. A. Sheldon, *Chirotechnology*, Dekker, New York, **1993.**
[257] G. W. Parshall, S. D. Ittel, *Homogeneous Catalysts*, Wiley, New York, **1992**.
[258] R. L. Burwell, *Chem. Rev.* **1952**, *57*, 1034.
[259] G. M. Schwab, *Catalysis from the Standpoint of Chemical Kinetics*, Macmillans, London, **1936**.
[260] S. Akabori, Y. Izumi, Y. Fuju, S. Sakurzi, *Nature* **1956**, *178*, 323.
[261] A. Baiker, H. U. Blaser in *Handbook of Heterogeneous Catalysis vol. 5* (Eds.: G. Ertl, H. Knözinger, J. Weitkamp), VCH, Weinheim, **1996**, *5*, 2422.
[262] A. Baiker, *Curr. Opin. Solid State Mater. Sci.* **1998**, *3*(*1*), 86; see also T. Maschmeyer, *Curr. Opin. Solid State Mater. Sci.* **1998**, *3*(*1*), 71.
[263] G. M. J. Schmidt, B. S. Green, *Tetrahedron Lett.* **1970**, 4249.
[264] J. M. Thomas, *Philos. Trans. R. Soc. A* **1974**, *277*, 251.
[265] J. M. Thomas, G. D. Renshaw, C. Roscoe, *Nature* **1964**, *203*, 72.
[266] C. F. McFadden, P. S. Cremer, A. J. Gellman, *Langmuir* **1996**, *12*, 2483.
[267] *Ferrocenes* (Eds.: A. Togni, T. Hayashi), VCH, Weinheim, **1995**, chap. 2.
[268] A. Corma, M. Iglesias, C. del Pino, F. Sanchez, *J. Organomet. Chem.* **1992**, *431*, 233.
[269] J. M. Thomas, T. Maschmeyer, B. F. G. Johnson, D. S. Shephard, *J. Mol. Catal. A* **1999**, *141*, 139. I am grateful to T. Maschmeyer for Figure 50.
[270] B. F. G. Johnson, S. Raynor, D. S. Shephard, T. Maschmeyer, J. M. Thomas, G. Sankar, S. Bromley, R. Oldroyd, L. Gladden, M. D. Mantle, *Chem. Commun.* **1999**, 1167.
[271] T. Hayashi, T. Mise, M. Fukishima, M. Kagatoni, N. Nagashuna, Y. Hamada, A. Matsumato, S. Kawakami, M. Korishi, K. Yamamoto, M. Kumada, *Bull. Chem. Soc. Jpn.* **1980**, *53*, 1138.
[272] T. Suzuki, M. Kita, K. Kashiwabara, J. Fujita, *Bull Chem. Soc. Jpn.* **1990**, *63*, 3434.
[273] D. Müller, G. Umbricht, B. Weber, A. Pfaltz, *Helv. Chim. Acta* **1991**, *74*, 232.
[274] D. A. Evans, K. A. Woerpel, M. J. Scott, *Angew. Chem.* **1992**, *104*, 439; *Angew. Chem. Int. Ed. Engl.* **1992**, *31*, 430.
[275] E. I. Solomon, M. D. Lowery, *Science* **1993**, *259*, 1575.
[276] R. Raja, P. Ratnasamy, *J. Mol. Catal. A* **1995**, *100*, 93.
[277] By the Editor of *Nature* on the cover of the issue that contain the paper by Wright et al.[142] on the atomic structure of zeolite L-pyridine complexes.
[278] S. S. Ghosh, S. C. Bock, S. E. Rokita, E. T. Kaiser, *Science* **1986**, *231*, 145.